

TALLINN UNIVERSITY OF TECHNOLOGY  
DOCTORAL THESIS  
75/2018

# **Alumina-graphene Hybrid Materials for Electrochemical Sensing of Bio-analytes**

MASOUD TALEB



TALLINN UNIVERSITY OF TECHNOLOGY

School of Engineering

Department of industrial Engineering

This dissertation was accepted for the defence of the degree 28/11/2018

**Supervisor:**

Prof. Irina Hussainova  
School of Engineering  
Tallinn University of Technology  
Tallinn, Estonia

**Opponents:**

Prof Michael Gasik,  
AALTO University Foundation  
Helsinki, Finland

Prof Kaupo Kukli  
Institute of Physics, University of Tartu  
Tartu, Estonia

**Defence of the thesis:** 19/12/2018, Tallinn

**Declaration:**

Hereby I declare that this doctoral thesis, my original investigation and achievement, submitted for the doctoral degree at Tallinn University of Technology, has not been previously submitted for doctoral or equivalent academic degree.

Masoud Taleb

-----  
signature



European Union  
European Social Fund



Investing in your future

Copyright: Masoud Taleb, 2018

ISSN 2585-6898 (publication)

ISBN 978-9949-83-371-9 (publication)

ISSN 2585-6901 (PDF)

ISBN 978-9949-83-372-6 (PDF)

TALLINNA TEHNIKAÜLIKOOL  
DOKTORITÖÖ  
75/2018

**Alumiiniumoksiid-  
grafeenhübriidmaterjalid biovedelike  
elektrokeemiliseks tuvastamiseks**

MASOUD TALEB



# Contents

<b>List of Publications .....</b>	<b>7</b>
<b>Author's Contribution to the Publications .....</b>	<b>8</b>
<b>INTRODUCTION .....</b>	<b>9</b>
<b>List of Abbreviations.....</b>	<b>11</b>
<b>1 REVIEW OF THE LITERATURE .....</b>	<b>12</b>
1.1 Introduction.....	12
1.2 Electrochemical sensors .....	13
1.3 Nanoparticle-based electrochemical sensors.....	15
1.4 Graphene.....	15
1.4.1 Graphene: properties and production .....	16
1.4.2 Potential of graphene in sensing applications .....	16
1.4.3 Electrochemistry of graphene .....	17
1.4.4 Objectives of the study .....	17
<b>2 EXPERIMENTAL AND MATERIALS .....</b>	<b>19</b>
2.1 Materials, reagents and glassware.....	19
2.2 Synthesis of catalyst.....	19
2.3 Fabrication of sensor.....	20
2.4 Synthesis of Cu modified catalyst.....	20
2.5 Preparation of electrolyte solution.....	20
2.6 Characterization of materials.....	21
2.6.1 Physical characterization methods .....	21
2.6.2 Electrochemical characterization methods.....	21
<b>3 DEVELOPMENT OF SENSORS .....</b>	<b>26</b>
3.1 Morphologic characterization of hybrid materials.....	26
3.2 Optimization of experiments.....	28
3.2.1 Powder preparation parameters.....	28
3.2.2 Effect of pH.....	28
3.2.3 Effect of scan rate .....	29
3.3 Electrochemical characterization of hybrid materials.....	30
3.3.1 Surface area study.....	30
3.3.2 Electrocatalytic behaviour of sensors .....	30
3.3.3 Electrochemical determination of bio analytes .....	32
3.3.4 Interface properties of sensors .....	34

3.4 Performance characteristic of sensors .....	35
3.4.1 Stability and reproducibility of developed sensors .....	35
3.4.2 Interference and reproducibility study .....	35
<b>4 CONCLUSIONS .....</b>	<b>37</b>
<b>List of Figures .....</b>	<b>38</b>
<b>List of Tables .....</b>	<b>39</b>
<b>References .....</b>	<b>40</b>
<b>Acknowledgements .....</b>	<b>43</b>
<b>Abstract .....</b>	<b>44</b>
<b>Kokkuvõte .....</b>	<b>46</b>
<b>Appendix.....</b>	<b>49</b>
<i>Publication I.....</i>	<i>49</i>
<i>Publication II.....</i>	<i>61</i>
<i>Publication III.....</i>	<i>71</i>
<i>Publication IV .....</i>	<i>79</i>
<b>Curriculum vitae.....</b>	<b>90</b>
<b>Elulookirjeldus .....</b>	<b>91</b>

## List of Publications

The list of author's publications, on the basis of which the thesis has been prepared:

- I **M. Taleb**, Alumina/graphene/Cu hybrids as highly selective sensor for simultaneous determination of epinephrine, acetaminophen and tryptophan in human urine, *Journal of Electroanalytical Chemistry*, 2018, 823, 184-192.
- II **M. Taleb**, Roman Ivanov, Sergei Bereznev, Sayed Habib Kazemi, Irina Hussainova, Ultra-sensitive voltammetric simultaneous determination of dopamine, uric acid and ascorbic acid based on a graphene-coated alumina electrode, *Microchimica Acta*, 2017, 184 (12) 4603-4610.
- III **M. Taleb**, Irina Hussainova, Roman Ivanov, Iwona Jasiuk, Graphenated ceramic nanofibers for highly sensitive simultaneous detection of dopamine, uric acid and ascorbic acid, *Advanced Materials Letters*, 2017, 8 (12) 1178-1183.
- IV **M. Taleb**, Roman Ivanov, Sergei Bereznev, Sayed Habib Kazemi, Irina Hussainova, Graphene-ceramic hybrid nanofibers for ultrasensitive electrochemical determination of ascorbic acid, *Microchimica Acta*, 2017, 184 (3) 897-905.

## **Author's Contribution to the Publications**

Contribution to the papers in this thesis is:

- I Design of the experiments; Electrode fabrication; Electrochemical and physical characterization of electrode material; Drafting the manuscript.
- II Design of the hybrid material with a varied carbon flake density; Optimization of the process parameters; Analysis and choosing optimum parameters; Drafting the manuscript.
- III Design of the experiments for determination AA, DA and UA in mixture; Analysis of the results; Drafting the manuscript.
- IV Deposition of Cu nanoparticles onto the fabricated sensor; Characterization of the synthesized materials; Optimization of the process parameters; Determination of EP, AP and Trp; Analysis of the results; Drafting the manuscript.

## INTRODUCTION

Human body may represent a periodic table, in which elements and compounds regulate the function of organs by chemical or physiological processes. Each element plays a crucial role in human metabolism. Unbalanced number of compounds may lead to severe diseases and serious issues in our daily life [1]. Biosensors are devices to monitor our bodily fluids and their composition regarding chemical or physiological processes. Historically, data generated from these devices was either analogue in nature or aggregated in a fashion that was not conducive to critical secondary or tertiary analysis [2]. However, in recent years much attention has been paid to these devices. In 2017, \$15.4 Billion was devoted to develop biosensors, usage of which is continuously growing due to a rise of demand in diagnostics and monitoring combined with aging of the population with its concomitant increase in the prevalence of chronic disease, increasing healthcare costs and unmet healthcare needs [3]. Therefore, looking for a cost-effective, highly sensitive and selective sensor to determine the specific molecules is highly demanding.

A wide variety of carbon-based materials such as graphene, carbon nanotubes (CNTs), crystalline diamond, and diamond-like carbon have been applied for sensor fabrication [4]. Except the choice of material, many researchers have used various techniques such as spectrophotometry [5], high performance liquid chromatography [6], chemiluminescence [7], fluorometry [8] for precise measurements. Among them, electrochemical sensors satisfy the main requirements due to their relative simplicity of production, high selectivity and sensitivity, and fast response [9]. The only issue with electrochemical sensors is restricted number of materials suitable for electrochemical detection with the high sensitivity and selectivity. Therefore, efforts have been done to develop materials that work in varied analytes and have ability to determine the low concentration of compounds in a mixture [9].

In the recent years, graphene and graphene-based materials have attracted much attention because of its unique structure and properties. Graphene has large surface-to-volume ratio, excellent electrical conductivity, high carrier mobility and density, which can be greatly beneficial for sensor functions [10]. Having a large surface area gives huge number of the active sites and enhances the loading of desired biomolecules. Excellent conductivity and a narrow band gap of graphene can be beneficial for conducting electrons between biomolecules and electrode surface [4].

The use of graphene in any application begins with the challenge of producing graphene with the maximum active surface area. The quality, surface area, and structure of graphene layers vary in dependence on foreseen applications. One of the best ways to increase the surface area is to use an effective substrate. A three-dimensional structured substrate can host more graphene sheets and possibly more sites for electron transfer [11]. Number of active sites can further be increased by functionalization of the graphene using abrasive acids such as concentrated sulfuric and nitric acid [12].

On the other hand, metal nanoparticles (NPs) have shown very promising results catalysing the reaction on the graphene electrode due to their fascinating physical and chemical properties, such as, size- and shape dependent interatomic bond distances, nanoscale electrochemical processes to be probed, which are significantly different from those of the bulk materials [13]. Among them, copper nanoparticle with great catalytic activities can facilitate the reactions on the electrode surface by decreasing the over-potentials when applied to the sensors [14].

In this work, multi-layered graphene sheets were deposited onto a network of aluminium oxide nanofibers ( $\text{Al}_2\text{O}_3$ ) using a chemical vapour deposition (CVD) procedure. The hybrid materials of graphene-alumina were examined as the sensor materials and tested for their sensing ability on simultaneous determination of ascorbic acid (vitamin C), dopamine acid, and uric acid in a ternary mixture of compounds. Obtained results were promising; thus, function of sensor was studied by further deposition of transitional metal nanoparticles i.e. copper NPs on the structure. Fabricated sensor was successfully tested for electrochemical determination of epinephrine, acetaminophen and tryptophan in human urine samples. Final results were evaluated by interference study and standard addition technique in human urine sample.

## List of Abbreviations

AA	Ascorbic Acid, $C_6H_8O_6$
ANF	Alumina Nanofiber
ANF-C	Alumina Nanofibers coated by Carbon
AP	Acetaminophen, $C_8H_9NO_2$
CuNPs	Copper Nanoparticles
CV	Cyclic Voltammetry
CVD	Chemical Vapour Deposition
DA	Dopamine, $C_8H_{11}NO_2$
DPV	Differential Pulse Voltammetry
EDX	Energy-Dispersive X-ray (spectroscopy)
EIS	Electrochemical Impedance Spectroscopy
EP	Epinephrine, $C_9H_{13}NO_3$
GAIN	Graphene Augmented Inorganic Nanofibers
GCE	Glassy Carbon Electrode
GO	Graphite Oxide
HRSEM	High Resolution Scanning Electron Microscopy
HRTEM	High Resolution Transmission Electron Microscopy
LoD	Limit of Detection
SCE	Saturated Calomel Electrode
SEM	Scanning Electron Microscopy
TEM	Transmission Electron Microscopy
3D	Three-dimension
2D	Two-dimension
1D	One-dimension
0D	Zero-dimension
Trp	L-Tryptophan, $C_{11}H_{12}N_2O_2$
UA	Uric Acid, $C_5H_4N_4O_3$
WC	Tungsten Carbide

# 1 REVIEW OF THE LITERATURE

## 1.1 Introduction

The word “sensor” originates from the Latin word “sentire” which basically means ‘to identify’ anything. In general definition, sensors are devices which detect and respond to some variable quantity of physical, chemical or biological changes in their specified environment. These changes are further converted into signals that are human-readable for further processing [1]. They are Generally classified in two main groups as physical sensors and chemical sensors. Physical sensors mainly are used for collecting physical responses such as temperature, magnetic field, pressure and force; however, chemical sensors deal with particular analyte and chemical reactions and can be used for determination of qualitative and quantitative determination of analyte. Some of the important chemical sensors are optical mass sensitive and electrochemical sensors.

The history of chemically sensitive sensors back to as early as 1906, when the concentration of an acid was associated to the electric potential generated between parts of the fluid located on two sides of a glass membrane. Three years later, the concept of pH was introduced by Søren Peder Lauritz Sørensen and an electrochemical determination approach for pH measurements was implemented in 1922 [15]. In 1956, Leland C. Clark Jnr fabricated first ‘true’ biosensor for oxygen detection and was called as ‘father of biosensors’ [16]. He further developed an amperometric enzyme electrode for detection of glucose in 1962. His invention was followed by other researchers such as Guilbault and Montalvo leading to the first potentiometric sensor for detection of urea. Eventually, first commercial sensor was developed in 1975 by Yellow Spring Instruments for glucose detection [17].

In recent decades, chemical sensor-related research has even experienced explosive growth. According to the annual reports, sensor related research has been spread in different sectors such as pharmaceutical, environmental, food, biomedical, clinical, and etc. Among them, sensors with ability to detect the chemical compounds in human bodily fluids such as urine and blood samples have received much attention. The main reason can be the steep increase in the cost of healthcare that makes it necessary to monitor patient’s health status in fast and easy way. Having appropriate feedback in real time from the life-threatening compounds enables doctors to deliver the necessary medications in case of health threatening conditions. Additionally, such sensors have ability to monitor tiny fluctuations of importance bio molecules and other health parameters that can lead to fast diagnosis and cheap treatment.

There are number of properties that define ability of biosensor in detecting bio compounds in an analyte:

- 1. Selectivity:**

Selectivity is perhaps the most important feature of a sensor. In our body, different compounds and elements are mixed together affecting others functions. Therefore, a sensor should be capable to distinguish desired compounds in bodily fluids, produce unique signal for it and visualize it for further analysis.

- 2. Reproducibility:**

Reproducibility defines the sensing ability to produce the same responses while the measurement conditions altered and repeat.

- 3. Repeatability:**

When all operating and environmental conditions remain constant, repeatability defines the system's sensing ability to produce the same response for successive measurements. Repeatability in both long-term and short-term estimates the sensor precision.

**4. Stability:**

Stability of the sensor is another important challenge for sensor development. Stability is to produce the same output value over a period of time.

**5. Sensitivity:**

Sensitivity is the ratio of magnitude of output signal to the magnitude of input signal. The slope of the calibration curve of current versus analyte concentration can be used to calculate the sensor's sensitivity.

**6. Linearity:**

Linearity of the biosensor is described by the closeness of the calibration curve to a specified straight line. When a system is linear, concentration of the analyte can be estimated in linear range.

## 1.2 Electrochemical sensors

Electrochemistry is a field of chemistry that investigates reactions happening at the surface of electrical conductors (electrodes). These reactions mainly involve exchange of electrons and provide valuable information regarding the energy levels of the system since exchange of electrons is generally dependent on the potential applied at the surface of the electrode. Therefore, flow of electrons is measured proportional to the rate of reaction and, under transport limited conditions is described as a function of bulk concentration of the reacting species.

Having above background, electrochemical sensors were built and developed to determine the concentrations of specific species in an analyte. Very soon, electrochemical sensors attracted attentions and were believed to be promising sensors due to their low cost, ease of use, simplicity, high sensitivity, low limit of detection, and selectivity [18].

At first, electrochemical sensors were developed for fuel cells, composed of noble metal electrodes in an electrolyte to detect gases [19]. In gas sensors, electrolyte is normally an aqueous solution of strong inorganic acids that generates a small current while detecting gas.

Later, development of electrochemical sensors made them more applicable to study the minute fluctuations of species in analytes. Number of electrons, potential or conductivity transmits between the analyte and receptor is measured and result is used to determine the analyte concentration in the whole system. Electrochemical sensors are classified in three different sub-classes [9]:

- Amperometric sensors
- Potentiometric sensors
- Conductometric electrochemical sensors

Although in all of these sensors measurement of change on the electrochemical property is the main function to recognize the reaction, the measured electrochemical property is different. An amperometric sensor, for example, measures the current of the working electrode to determine the concentration; however, a conductometric sensor measures the change in the conductance of the sensing surface. On the other type,

potentiometric sensors, monitors the potential of the working electrode to estimate the concentration of compound.

Before discussing the details of graphene electrochemistry, it is useful to consider the basics of electrochemistry in the commonly used carbon-based electrodes that have been utilized for many years in industrial and academic settings.

Electrochemistry is the study of charge transference between an electrode and solution, where a reduction and oxidation reactions occur and monitored. A typical three electrode electrochemical cell may be used to perform such measurements (Fig. 1). Three electrodes are usually needed in order to obviate the passage of current through the reference electrode, which otherwise may result in changes in the activities of the various species.

In this method, redox reaction (oxidation-reduction) happens at the working electrode and the potential is externally controlled between the working and reference electrodes. The necessary second electrode reaction takes place at the counter electrode but since generated current is large in respect to the working electrode, the current is limited by processes happening at the latter. This current is proportional to the rate of reaction at the working electrode that can be employed to quantify species at the working electrode.

O: the oxidized species,  
R: the reduced species,  
 $e^-$ : a single electron,  
 $k_o$ : the oxidation reaction rate constant,  
 $k_R$ : the reduction reaction rate constant.

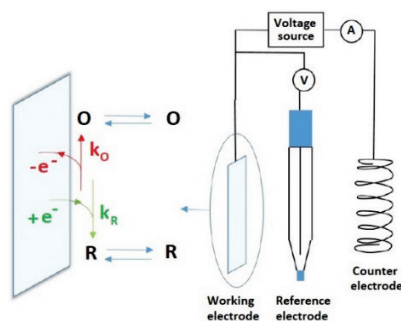


**Figure 1.** Three-electrode electrochemical cell and a scheme of a redox reaction [20].

Electron transference between solution species and an electrode depends on various factors such as diffusion coefficient of substance in analyte, intrinsic properties of the solution species i.e. density, and other adsorbed species on the electrode surface that may affect the reaction by passivating the active surface of the electrode. This passivation effect enables one to quantify the amount of the adsorbed species passivating the electrode surface.

In electrochemical systems, if a reaction is kinetically slow, more energy is required as compared to diffusion limited case before the oxidation and reduction peak appear further away from the equilibrium potential. Therefore, the current response recorded in a system in such a condition provides details about kinetics of the system and the concentrations of the oxidized and reduced species of the redox couple. This is used in voltammetry techniques like cyclic voltammetry and differential pulse voltammetry. Then in such system, one can study the concentration of analyte by using voltammetry technique and analyzing the peak currents.

The diffusion rate of the reaction increases with the scan rate since there is less time for a concentration profile to extend into solution and therefore, the height of the peak current increases. However, more increase in scan rate pushes the current peaks further away from the equilibrium potential because more energy is required to reduce the oxidized species.

### 1.3 Nanoparticle-based electrochemical sensors

Recently, the use of varied nanoparticles in analytical chemistry has gained much attention with new developments in nanotechnology [21, 22]. Nanoparticles provide unique chemical, physical, and electronic properties which rarely can be seen in their bulk counterparts. Therefore, using nanoparticles can add valuable properties and enable us to construct novel electrochemical sensors with better selectivity, higher sensitivity, wide linear dynamic range, low cost, and stability [23].

Numerous nanoparticle including metal, metal oxide, mixed metal oxide, composite nanoparticles and polymers have been tested for their unique properties such as electrical conductivity, stability, electronic, magnetic, and optical properties [21, 23].

Since nanoparticles own large specific surface area and high surface energy, the implementation of nanoparticles into electrochemical sensors creates higher active sites for the reactions and electron exchange between the electrode and analyte. Additionally, presence of nanoparticles can enhance the stability of sensor by providing effective physical or chemical bonds between the electrode and target species [24].

Modification of the electrode surface using nanoparticles was found to be a useful approach to enhance the sensitivity and selectivity of the sensor. In general, electrocatalytic activity of the nanoparticles decreases the over-potential required for catalytic reactions and thus enhance the overall performance [13].

To develop electrochemical biosensors with a high performance, the electron transport properties between the active sites of the electrode and target compounds should be improved. By exploiting the conductivity of nanoparticles, the electron mobility can be enhanced profoundly resulting to higher sensitivity [25].

When the nanoparticle interact with analyte, target molecules react on the surface and generate electrical signals which can define the concentration of the target species [24].

Among various metal nanoparticles, copper has gained much attention due to its high conductivity, intrinsic properties and wide potential applications. Copper nanoparticles (CuNPs) as an important semiconductor with a band gap of 2.1 eV, and large surface-to volume ratio is considered promising material to be used in optics, electronics, gas sensor and electrochemical sensors [14, 26]. The surface area-to-volume ratio of particles depends on different factors such as shape and size of nanoparticles. The characteristic properties including the electronic transitions, phase transition temperature and the electronic energy levels are also modulated by the change in surface area. Electrochemical deposition of CuNPs as an effective technique to deposit tiny nanoparticles over carbon based electrode, may assist one to reach higher surface area of the CuNPs over the substrate and benefit the catalytic effect of Cu in electrochemical sensors [27].

### 1.4 Graphene

Graphene as a monoatomic two-dimensional structure of carbon atoms discovered in 2004 by Geim et.al [28] has drawn huge research interests due to its extraordinary properties and potential applications in nanotechnology. Numerous layers of graphene can be attached together to form graphite, one-dimension (3D) structure of carbon atoms or can simply rolled to form carbon nanotube, a one-dimension (1D) structure of

carbon atoms. Graphene atoms can also be seen as a zero-dimension (0D) structure by wrapping to form fullerenes [28, 29].

The two-dimension (2D) nature of graphene coupled with delocalized  $\pi$  electrons from  $sp^2$  hybridization in C-C bond enables analyte molecules to adsorb on the electrode surface, exchange charge with it or change surface properties which make it suitable material for sensing applications.

#### **1.4.1 Graphene: properties and production**

Graphene as a hot research material owns not only unusual properties regarding extreme mechanical strength [30], thermal conductivity [31], but also peculiar high charge carrier mobility [32], optical transparency [33], superior intrinsic carrier velocity, and chemical inertness in room temperature. Graphene owns highest possible surface area to volume ratio at  $2600 \text{ m}^2 \text{ g}^{-1}$  and electron mobility rate of up to  $230000 \text{ cm}^2 \text{ V}^{-1} \text{ s}^{-1}$  [34] which is considered as an important factor in electrochemical applications. Ability to provide unique combination with all these characteristics made graphene as a promising material for electronic and sensor applications.

In addition to monolayer graphene, few-layer graphene has been extensively investigated in various applications. There is a lot of debate over the correct name of graphene like materials due to variation from the 2D lattice structure of pure graphene with the introduction of defects, increased oxygen content and multiple layers [35-37].

Different techniques have been employed for preparation of graphene sheets including exfoliating, thermal decomposition and reduction of graphene oxide. Exfoliation represents a repeated peeling process of graphene layers in oxygen plasma [38]. However, the size and crystalline quality cannot be easily controlled and graphene layers have been widely distributed in thickness. In other way, exfoliation can be performed in liquid phase and using graphite oxide in ultrasonic bath.

Recently, novel techniques such as mechanical exfoliation technique; a microwave-assisted exfoliation and exfoliation of single sheets employing gases are introduced.

Although exfoliation techniques potentially are cheaper and commercially interesting, there are several limitation factors, such as impurities and defects causing by application of either aggressive solvents or mechanical loads.

Chemical vapor deposition (CVD) of graphene on transition metals is another promising approach to produce graphene. CVD introduces an inexpensive way to deposit graphene layers on the surface of substrate by decomposing inserted gas to carbon radicals [39]. The chosen substrate (metal) works as a catalyst to decrease energy barrier of reaction and growth of the graphene layers on the substrate.

Among above techniques, a catalyst-free CVD growth of few-layered graphene on dielectric substrates of nanofibers has been developed by I. Hussainova's group [11, 40, 41]. Highly foliated graphene contains high surface area which is coupled with the high edge density of the 3D nanostructures.

#### **1.4.2 Potential of graphene in sensing applications**

Graphene has widely been studied for sensing applications. In some works, noticeable applications of graphene have been discussed [10, 35, 42]. Excellent electrical conductivity combined with large surface area of the graphene has made it an ideal material as an electrode in electrochemical applications. Main challenge to use a material

as an electrode in electrochemical sensing system is to have a reduction or oxidation reaction possibility on the electrode surface. In this case, electrochemical reaction may lead a change in current, voltage or impedance that can be recorded and further analyzed. Generally, monolayer graphene with edges and defected sites is considered as a promising electrode material which allows the surface exchange, but it is also common to increase the surface exchange by adding functional groups [43]. Very extensive reviews covering the role of graphene in electrochemistry and biosensors have been published in recent years from the leading electrochemistry and graphene groups [2, 10, 35].

### **1.4.3 Electrochemistry of graphene**

Working electrode, at which redox reactions occur, can be fabricated using various electrically conductive materials. Generally, metals such as gold and platinum are ideal conductors but are not suitable for mass production of biosensors due to their high price [18, 44, 45]. Instead, carbon-based electrodes have been shown to be promising candidates due their lower costs and tailorable surface structure affecting the performance. Carbon based materials such as basal plane pyrolytic graphite [46], glassy carbon electrodes and screen printed carbon electrodes [47] have been widely used for sensing applications. Although they all considered as carbon materials, they own different structure and electrochemical performance attributed to both functional groups and overall conductivity of the material.

Graphene as a conductive, environmental friendly and inexpensive material is considered very attractive material for bio-sensing devices utilising electrochemical methods [37]. Graphene has a wide stable electrochemical window, in which having oxygen functional groups results in a relatively slow electron transfer rate; however, as the oxygen content declines, the heterogeneous electron transfer rate increases gradually [48]. The surface of graphene is heterogeneous in which the electron transfer occurs at the edges and defected planes where contain higher density of electronic states [36].

In graphene produced by CVD technique, graphitic islands were detected implying major roles in the electron transfer; however, several studies showed some evidence of high activity on highly oriented pyrolytic graphite. This means that graphene can be assumed to be a model for the base plane of graphite where faster electron transfer may not be dominated by the edge planes [49].

### **1.4.4 Objectives of the study**

The main objective of the work was to development of the electrochemical sensors by a few layers of highly foliated graphene and to apply this system for simultaneous determination of biomolecules in clinical and food studies. To achieve this goal, a metal oxide – graphene hybrid material with different but tailorable architectures were developed and thoroughly characterized. The study was progressed with functionalization and further activation of the synthesized materials. Electrochemical activity of the materials was challenged by electrochemical deposition of Cu nanoparticles onto the structure using various surface treatment techniques. Thereafter, to optimize the performance, the parametric studies were carried out. The produced sensors were used for determination of Ascorbic Acid, Dopamine, Uric acid as well as

Epinephrine, Acetaminophen and Tryptophan in phosphate buffer solution and human urine samples.

To achieve the objective of the study the following activities were considered:

- Structural characterization and morphology studies of the hybrid material using physical and chemical approaches;
- Fabrication of an electrochemical sensor for simultaneous determination of ascorbic acid, dopamine and uric acid in human urine samples;
- Enhancement of electrochemical properties sensor material by optimizing powder preparation technique and applying chemical functionalization approach;
- Increase of catalytic activity of the structure by depositing Cu nanoparticles
- Further development of a highly selective sensor for simultaneous determination of epinephrine, acetaminophen and tryptophan in human urine;
- Optimization of the sensor working conditions including pH studies and effect of scan rate.

## 2 EXPERIMENTAL AND MATERIALS

### 2.1 Materials, reagents and glassware

All chemicals and reagents were of analytical grade and used as received without any purification. Ascorbic acid (AA), uric acid (UA), epinephrine (EP), acetaminophen (AP), tryptophan (Trp),  $\text{NaH}_2\text{PO}_4$  and Nafion<sup>®</sup> were purchased from Sigma-Aldrich.  $\text{Na}_2\text{HPO}_4$  was purchased from VWR chemicals and dopamine (DA) was acquired from Alfa Aesar. The Copper (II) sulfate pentahydrate salt ( $\text{CuSO}_4 \cdot 5\text{H}_2\text{O}$ ) was received from Fluka (Buchs, Switzerland).

All data of the current study were collected using clean and fully wet able glassware. To achieve reproducible results and minimize the errors, sulfuric acid made by Sigma-Aldrich (concentrated 95 % - 97 %, puriss. p.a, ACS reagent) was used to wash the glassware. Thereafter, test sells and sampling equipment were dried in oven (80 °C).  $\text{H}_2\text{O}_2$  (hydrogen peroxide 30 %) was used to increase the oxidative properties of the concentrated sulfuric acid while cleaning lab ware.

### 2.2 Synthesis of catalyst

The graphene augmented inorganic nanofibers was synthesized with the help of a direct catalyst-free chemical vapour deposition (CVD) technique at a treatment temperature of 1000 °C. Carbon foliates were grown along the dielectric surface of alumina nanofibers by flowing methane ( $\text{CH}_4$ ) and hydrogen ( $\text{H}_2$ ) gas through a CVD chamber at a rate of  $50 \text{ cm}^3 \text{ min}^{-1}$ . Carbonization process prolonged either for 60 min and 120 min resulting in the carbon weight gain of 300 % and 700 % compared to initial fibers' weight, respectively [Papers II– IV]. The optimized graphene-augmented network material was synthesized in the same chamber (1000 °C, 120 min) under methane ( $\text{CH}_4$ ) and hydrogen ( $\text{H}_2$ ) gas flow of  $200 \text{ cm}^3 \text{ min}^{-1}$  and  $100 \text{ cm}^3 \text{ min}^{-1}$ , respectively. In case of reference paper I, ANF-C400 synthesized and was immersed into severe oxidizing mixture of  $\text{H}_2\text{SO}_4/\text{HNO}_3$  (3:1, v/v) at 70 °C for 48 hours for purification of  $-\text{COOH}$  functionalized material. Thereafter, sample was washed with distilled water and dried in a vacuum (80 °C, 8 h). Obtained  $-\text{COOH}$  modified material was crashed in mortar, and powdered using  $\text{KM}^{-1}$  ball milling machine for 3 h. Resulting particles were additionally treated using Hielscher UP200Ht ultrasonic homogenizer for 20 min in 50 ml of water. Obtained materials were denoted as ANF-C300, ANF-C700 and ANF-C400, respectively (Fig. 2).

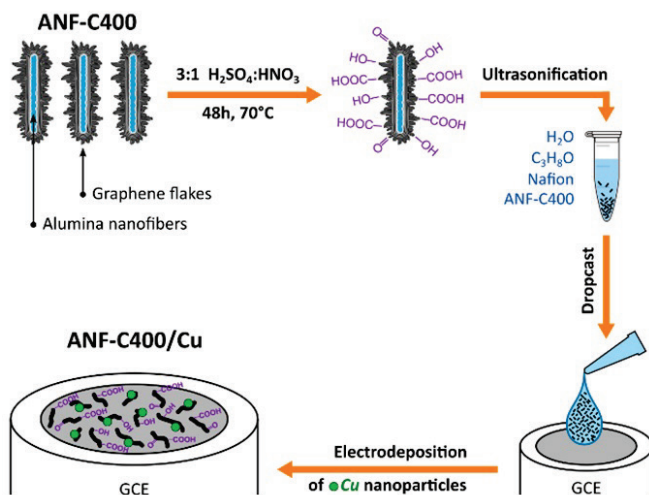


**Figure 2.** Scheme of electrode fabrication (ANF-C400 is called GAIN in reference Paper I)

### 2.3 Fabrication of sensor

A GCE electrode pressed into a Teflon holder of 5 mm in diameter was chosen as the substrate of synthesized materials due to its wide potential window, low background currents and chemical stability. Prior to modification, GCE was polished using  $0.05\ \mu\text{m}$  alumina slurry to end up a mirror like surface. Polished electrode was rinsed in Millipore water 3 times (each time for 1 min) while ultrasound bath was removing the adsorbed substances of the surface. Then, the GCE electrode was dried under  $\text{N}_2$  gas flow.

An electrode modifier ink was prepared by suspending 5 mg of synthesised material (ANF-C300, ANF-C700) in  $178\ \mu\text{L}$  Millipore water,  $25\ \mu\text{L}$  isopropanol and nafion® dispersion solution in a way that achieve 5 wt. % nafion in final catalyst layer. Catalyst suspension was sonicated 30 min to give uniform slurry. As prepared homogeneous slurry was spin-casted on the polished GCE and dried in room temperature (Fig. 2).

### 2.4 Synthesis of Cu modified catalyst

CuNPs were deposited electrochemically on the surface of fabricated sensor detailed in section 2.3. Prior to deposition, GCE covered ANF-C400 was cycled for 30 min to obtain reproducible cyclic voltammetric diagrams. Then calculated amount of  $\text{CuSO}_4 \cdot 5\text{H}_2\text{O}$  was dissolved in  $0.1\text{M}$   $\text{H}_2\text{SO}_4$  in a way that final concentration of Cu was achieved in solution [Paper I]. Electrochemical deposition procedure was performed by cycling the potential in the range between  $-0.1$  to  $0.4\ \text{V}$  vs. SCE at a scan rate of  $10\ \text{mV s}^{-1}$  for 10 cycles.

### 2.5 Preparation of electrolyte solution

$0.1\ \text{M}$  phosphate buffer solution was chosen as the analyte throughout the analytical measurements. Phosphate buffer is a water-based non-toxic solution that simulates physiological condition in this work. Needed amount of  $0.1\ \text{M}$  phosphate buffer was

prepared by mixing stock solutions of  $\text{Na}_2\text{HPO}_4$ ,  $\text{NaH}_2\text{PO}_4$  in a supporting electrolyte of 0.1 M KCl. The pH of the buffer solution was monitored and adjusted by addition of NaCl to a desired value as described in “optimization of experiments”.

Stock solutions of AA, DA, UA, EP, AP and Trp were prepared daily by dissolving a suitable amount of reagents in a 0.1 M phosphate buffer to achieve concentration in the range of nano molar (nM) to micro molar ( $\mu\text{M}$ ).

## **2.6 Characterization of materials**

### **2.6.1 Physical characterization methods**

Surface morphology and microstructural features of the synthesized materials were studied using a high-resolution transmission electron microscope (HRTEM JEOL JEM-2200FS, Japan) and further examined by a high-resolution scanning electron microscopy (HR-SEM) Zeiss HR Gemini FESEM Ultra 55 equipped with Bruker EDX system for energy-dispersive X-ray measurements.

Characterization of carbon layers were studied by a high resolution Raman spectrometer using Horiba LabRam HR800 spectrometer equipped with a green Nd:YAG laser ( $\lambda = 532.1 \text{ nm}$ ), a red He-Ne laser ( $\lambda = 632.8 \text{ nm}$ ), and a multichannel CCD detection system in the backscattering configuration.

XPS analysis was performed using an X-ray photoelectron spectroscopy (XPS) with an Omicron Multi probe XPS system (base pressure of  $2 \times 10^{-10}$  mbar) and an EA125 U5 analyzer at a  $45^\circ$  takeoff angle. Wide and core level spectra were collected at 50 and 20 eV pass energy, respectively.

### **2.6.2 Electrochemical characterization methods**

Electrochemical and sensing measurements including cyclic voltammetry (CV), differential pulse voltammetry (DPV), chronoamperometry (CA), and electrochemical impedance spectroscopy (EIS) were conducted in a potentiostat/galvanostat Autolab PGSTAT30 with FRA2 in a standard three-electrode electrochemical cell (Fig. 3). A Pt wire was used as the counter electrode; a saturated calomel electrode (SCE) was employed as the reference electrodes and a GCE covered synthesized material served as the working electrode (preparation details in 2.3 and 2.4). Prior to measurements and to achieve stable response, solution was deoxygenated by purging  $\text{N}_2$  gas into the solution. Additionally, all working electrodes were cycled for several times from  $-0.3$  to  $0.9 \text{ V}$  vs. SCE until depicting stable voltammograms.

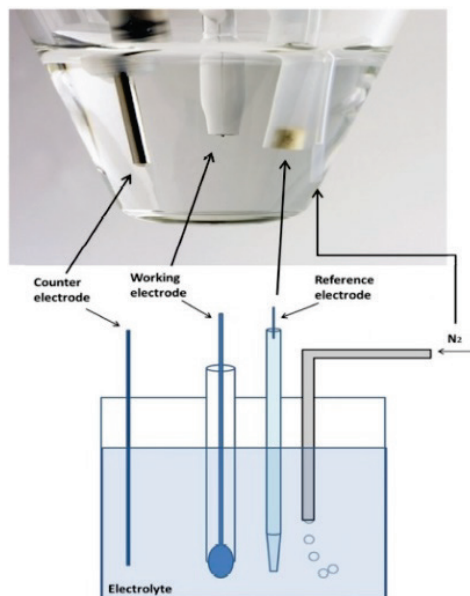


**Figure 3.** Scheme of a three-electrode compartment electrochemical cell including working, reference and counter electrodes.

### Cyclic voltammetry (CV)

Cyclic voltammetry (CV) is an electrochemical technique where the potential of the working electrode is ramped linearly versus time. Once the end potential on the triangular excitation potential ramp is reached, it begins a scan in the reverse direction (Fig. 4a) [20].

Cyclic voltammetry is considered as advantages technique due to a wide dynamic range, extreme sensitivity to low concentrations of ionic species, and ease of use. Additionally, CV is a non-destructive method for characterizing electron transfer mechanisms. Using CV, one can study redox processes, understand reaction intermediates and reaction products by varying the applied potential on the working electrode and measuring the current [1].

Important parameters of a CV voltammogram including peak potentials ( $E_{pc}$ ,  $E_{pa}$ ) and peak currents ( $I_{pc}$ ,  $I_{pa}$ ) form the basis for the analysis of the cyclic voltammetry response to the analyte. The shape and place of the peaks depend on the concentration of a reactant and a product at the electrode surface during the scan. In ideal case, the scan begins at a potential where analyte is neither oxidized nor reduced and negligible current flow can be monitored (Fig. 4b).

As soon as potential is ramped linearly, electron starts to transfer between the working electrode and the analyte which leads to an accumulation of product and a depletion of the reactant (oxidation / reduction of species).

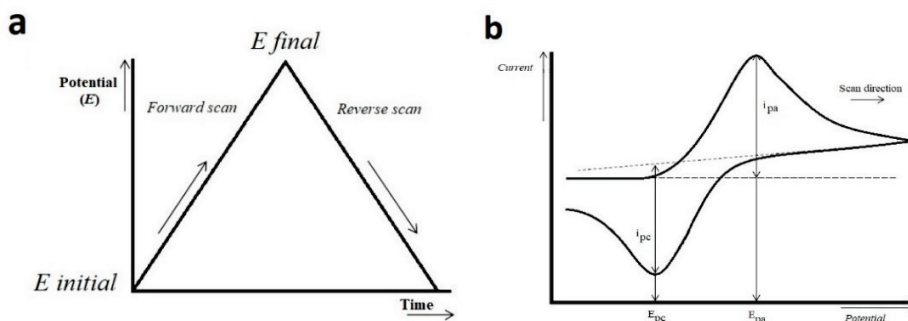


**Figure 4.** Scheme of cyclic voltammetry input waveform (a), and a sample of reversible cyclic voltammogram response (b).

If the electron transference between the working electrode and analyte is faster than diffusion, the reaction called as electrochemically reversible and anodic and cathodic peak separation can be calculated using equation 1 [20]:

$$\Delta E_p = E_{pa} - E_{pc} = 2.303 RTnF \quad (1)$$

In irreversible reactions, a reverse peak would not appear and voltammogram presents in a different shape. In irreversible reactions, electrode kinetics is slower than the rate of diffusion. The peak currents for irreversible system can be found using equation 2 [50]:

$$I_{p,c} = -2.99 \times 10^5 n(\alpha_c n')^{\frac{1}{2}} A C D^{\frac{1}{2}} \nu^{\frac{1}{2}} \quad (2)$$

where  $\alpha_c$  is cathodic electrochemical charge transfer coefficient,  $n'$  is the number of electrons transferred in rate determining step,  $A$  is the geometrical surface area ( $\text{cm}^2$ ),  $C$  the analyte concentration ( $\text{mol}/\text{cm}^3$ ),  $D$  the diffusion coefficient ( $\text{cm}^2/\text{s}$ ), and  $\nu$  the scan rate ( $\text{V s}^{-1}$ ).

### Differential pulse voltammetry (DPV)

Differential pulse voltammetry is another important technique to study electrode kinetics. In DPV, a small pulse is superimposed onto a single linear forward scan, without applying reverse scan. The current is measured just before the application of the pulse ( $i_a$ ) and the second at the end of the pulse ( $i_b$ ). The resultant difference in current ( $i_b - i_a$ ) is plotted versus the base potential (Fig. 5). The current peaks in resulting differential pulse voltammogram are directly proportional to the concentration of the corresponding analyte, while the peak potential ( $E_p$ ) correspond to the identity of the species, as it occurs near the polarographic half-wave potential (equation 3) [51]:

$$E_p = E_{1/2} - \Delta E/2 \quad (3)$$

DPV cannot study the reversibility of the reactions but can be used for measuring trace levels of organic and inorganic species at the very low concentrations of nM to  $\mu\text{M}$ .

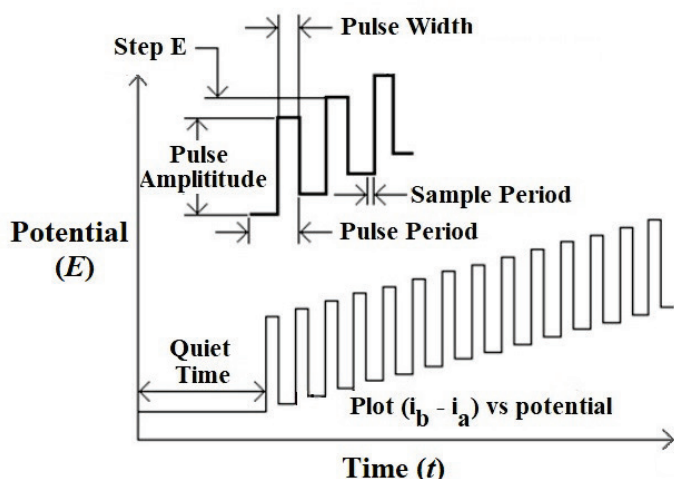


Figure 5. Differential Pulse Voltammetry

### Electrochemical impedance spectroscopy (EIS)

Electrochemical impedance spectroscopy has long been used to investigate the electrochemical systems. In this technique, a small sinusoidal AC voltage probe (typically 2 – 10 mV) is applied, and the current response is measured. The in-phase current response corresponds to the resistive (real) component of the impedance, while the out-of-phase current response implies the capacitive (imaginary) component.

To achieve a linear response and simple equivalent circuit analysis, a very small AC probe voltage applies to the electrode and response being recorded. Thereafter, obtained response being fitted to equivalent circuits of resistors and capacitors i.e. the Randles circuit shown in Fig. 6a. This equivalent circuit yields the Nyquist plot and provides a visual insight into the system dynamics (Fig. 6b) [52]:

$$R_s(C_d [R_{ct} Z_w])$$

where  $R_{ct}$  is the charge-transfer resistance,  $C_d$  is the double-layer capacitance;  $R_s$  is the solution-phase resistance and  $Z_w$  is the Warburg impedance, which appears from mass-transfer limitations.

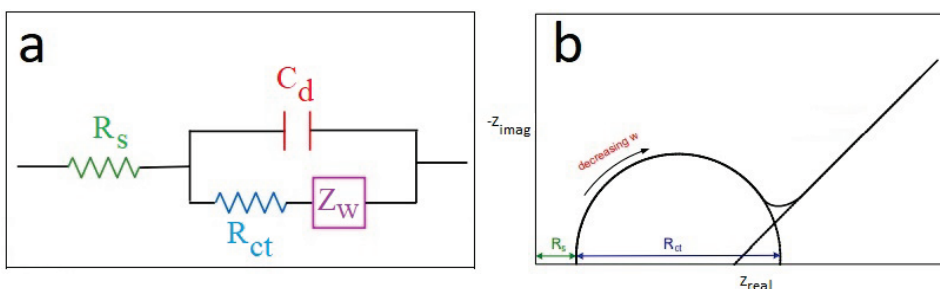
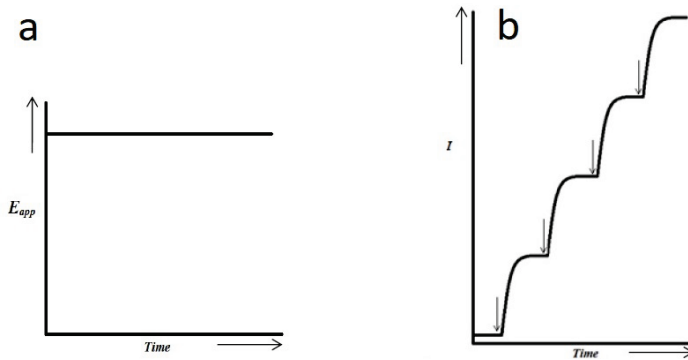


Figure 6. sample scheme of a Randles equivalent circuit (a) and Nyquist plot arising from the Randles circuit (b).

## Chronoamperometry (CA)

Chronoamperometry is the most common electrochemical technique utilized due to ease in result interpretation. Moreover, the technique requires minimal instrumentation to implement. In CA, a fixed potential is applied to an electrode until a steady state current is achieved. Stirring can ensure a constant concentration gradient of the analyte at the working electrode surface. After achieving a steady current on the electrode, addition of the analyte of interest is being started to the electrochemical cell. The addition of varied analytes results in increase in current, Fig. 7a-b. In CA plots, the magnitude of the current is proportional to the concentration of the analyte, which in turn is proportional to the rate of the redox reaction at the working electrode surface [20].



**Figure 7. a)** Current wave form for amperometry experiments **b)** A typical amperometry plot in stirred solution.

## 3 DEVELOPMENT OF SENSORS

### 3.1 Morphologic characterization of hybrid materials

The electrode materials have been thoroughly characterised by physical structural techniques. Surface morphology and structure of the synthesized materials were described in papers [I to IV]. Here, the most important properties and aspects are discussed.

HRTEM data collected from the synthesized samples clearly show that the core-shell type nanostructures are developed representing graphene layers wrapped around alumina nanofibers (ANFs) along a longitudinal axis. The layers' interspace was estimated to be 3–4Å. Therefore, the morphology of the hybrids of alumina and graphene-like nanostructures may be roughly represented by a filled multiwall carbon nanotube. The development of flakes or foliates on the fibers is demonstrated in Figure 8; these foliates consist of 2 - 3 graphene layers. Therefore, this corrugated graphene can be successfully utilized for the catalyst immobilization for providing more electrochemical active sites to catalyse reactions. The nanostructures of the ANF-C material and the surface of the ANFs after graphene synthesis are schematically shown in reference papers I to IV.

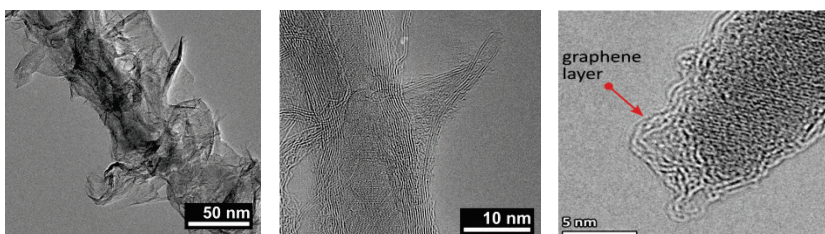


**Figure 8.** HRTEM images of the foliated hybrid nanostructures

Data from HRSEM approved the formation of micrographs of the three-dimensional arrays of graphenated alumina nanofibers graphene flakes on the fibers. Density of foliates of the samples depended to the CVD treatment time in a way that increased from  $30 \pm 5$  to  $50 \pm 10$  (per micron) in ANF-C300 and ANF-C700 materials. Simultaneously, the core diameter of the graphenated fibers increased from  $20 \pm 5$  nm to  $50 \pm 10$  for the ANF-C300 and ANF-C700, respectively. As shown in figure 9a-b and in agreement to the HRTEM data, carbon layers with lots of admixture of the graphitic flakes has formed on the nanofibers and has developed closed shell of graphene multi-layers and nano-flakes with controlled density.

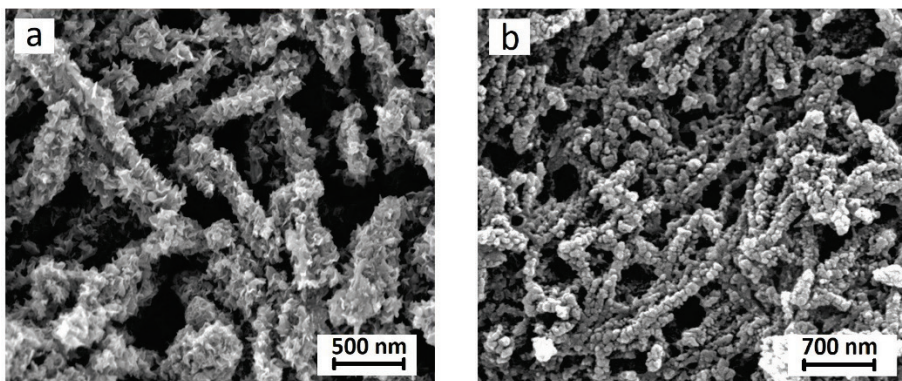


**Figure 9.** HRSEM image of the **a)** ANF covered graphene **b)** ANF-C400/Cu after milling

The Raman spectrum of the ANF decorated graphene (Fig. 10) presents a strong G band peak at around  $1596\text{ cm}^{-1}$ . This peak is considered as the evidence of the graphitized structure of material. The D peak observed at  $1340\text{ cm}^{-1}$  proves the appearance of the graphitic carbon formation. This band is often refers to the disordered defected edge-induced peak. The proportion of the D band the G peak (denoted as  $I_D / I_G$ ) is used as a measure of the quality of carbon nanostructures. In this work this calculated as 1.45 defining the degree of carbon graphitization. Additional 2D, D + D' peaks detected at  $2685$  and  $2929\text{ cm}^{-1}$  interpreted as characteristic of few-layers of graphene, respectively.

The chemical composition of the synthesized materials were analysed by XPS. Obtained data showed that surface of graphenated fibers was mainly composed of carbon and small amount of oxygen in both materials. The amount of carbon was higher in ANF-C700 as compared to ANF-C300. Further analysis, demonstrated a lower concentration of oxidized carbon centres in ANF-C700 as compared to ANF-C300. Oxidized centres may have formed due to the physical adsorption of oxygen or vapour mainly on the edge defects at room temperature after exposure of the sample to air. The surface area BET measurements revealed very close values of  $125\text{ m}^2\text{ g}^{-1}$  and  $119\text{ m}^2\text{ g}^{-1}$  for ANF-C300 and ANF-C700, respectively.

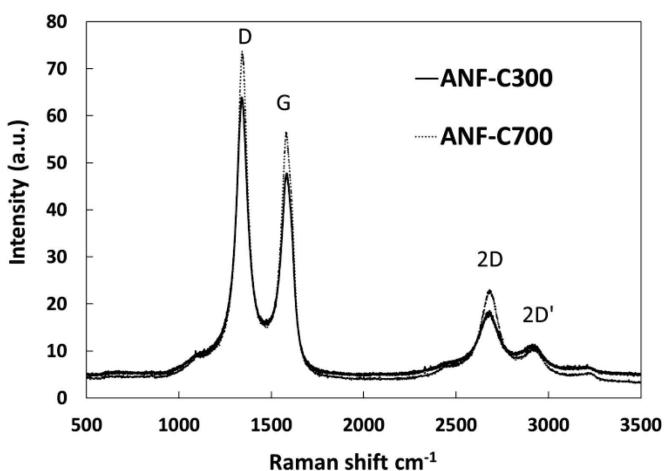


**Figure 10.** Raman spectra of the precursor ANF-C700

## 3.2 Optimization of experiments

The functional potential and electrochemical response of the developed sensors depend on number of factors including pH, scan rate and particle size of the synthesized material. Each of these factors are discussed in details in this section.

### 3.2.1 Powder preparation parameters

To obtain a stable signal from the sensor, an array of the graphenated fibers was powdered with the help of several techniques listed in Table 1. Due to the importance of electrochemical response, each sample was probed in 1 M KCl + 5 mM  $K_3Fe(CN)_6$  system. Electrochemical signals obtained from the prepared powders were analysed (reference paper III) and the optimum way of powder preparation was chosen for the rest of the experiments.

**Table 1.** Optimization of experiments by varying powder preparations techniques.

Sample No.	Mortar	Ball milling	Presence of WC	Ultrasound treatment	Microwave treatment	Strong Acid treatment
1	√	-	-	10 min in water	-	-
2	√	-	√	10 min in water	-	-
3	√	30 min	√	10 min in water	-	-
4	√	30 min	-	10 min in water	-	-
5	√	180 min	-	30 min in isopropanol	-	-
6	√	180 min	-	30 min in isopropanol	-	-
7	√	180 min	-	10 min in water	2 min	-
8	√	180 min	-	30 min in isopropanol	-	√

Thus, an approach used for sample 8 has been applied for paper I and approach 5 was used for rest of the reference publications.

### 3.2.2 Effect of pH

The pH of the supporting electrolyte has significant effect on the oxidation peak of the studied compounds on manufactured sensors. The pH range studied by using cyclic voltammetry at various pH values ranging from 4 to 9 (Fig. 11a-b). Experimental results for oxidation of EP, AP and Trp showed that oxidation and reduction potentials were pH dependent. An increase in analyte pH values shifted both anodic and cathodic peaks to more negative values. This behaviour was explained by a deprotonating step involved into all oxidation processes which is facilitated at the higher pH values [53]. According to maximum current from the CV measurements, the pH value of 6.0 was chosen for the further experiments for detecting EP, AP and Trp. This value was set as 7.0 for the electrochemical determination of AA, DA and UA as the analyte molecules were positively charged; therefore, an electrostatic attraction facilitated their movement towards the electrode surface.

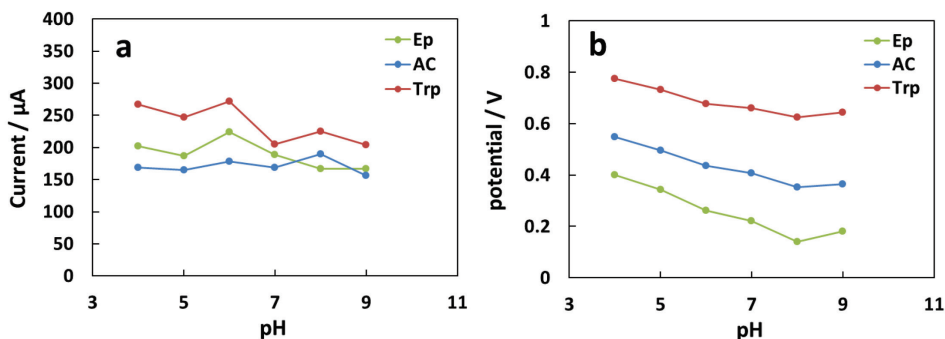


**Figure 11.** Effect of pH on **a)** the peak current and **b)** the peak potential for the oxidation of 200  $\mu\text{M}$  EP, 150  $\mu\text{M}$  AP and 100  $\mu\text{M}$  Trp in 0.1 M phosphate buffer (scan rate = 50  $\text{mVs}^{-1}$ ).

### 3.2.3 Effect of scan rate

Effect of scan rate on the cyclic voltammetry response was studied in the scan rates from 10 up to 200  $\text{mV s}^{-1}$ . The oxidation peak currents showed that by increasing the scan rate, the anodic and cathodic peak currents increased. Meanwhile, anodic peak potentials moved to more positive potential values; while cathodic peak potentials shifted to more negative values (Fig. 12). From the plotting, relation between the anodic peak current and square root of scan rate was described (insets in Fig. 12). It was found that the peak current is proportional to the square root of scan rate. The CV results approved that ANF-C700 was able to determine each of AA, DA, and UA in ternary mixture demonstrating the negligible interfering effect from interactions among AA, DA and UA.

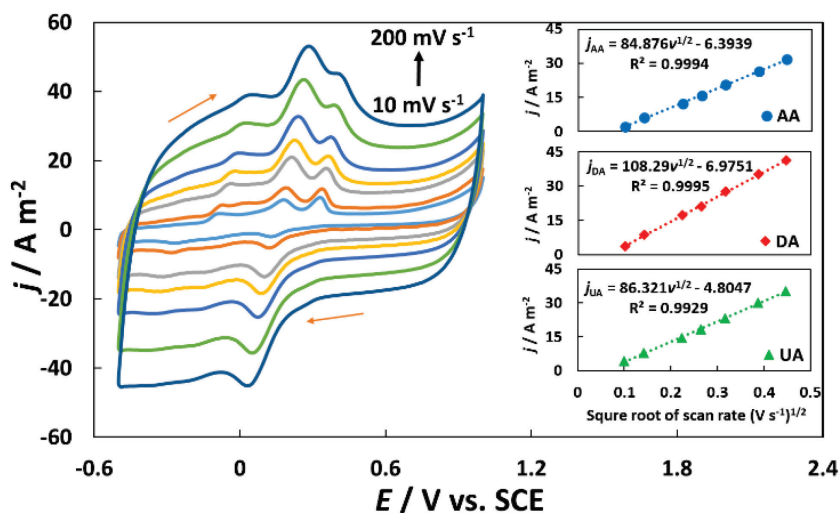


**Figure 12.** Effects scan rate at ANF-C700 modified electrode in 0.1 M phosphate buffer (pH 7.0) containing 5 mM AA, 1mM DA, and 1mM of UA at different scan rates (10, 20, 40, 70,100,150, 200  $\text{mV s}^{-1}$ ). Insets: plots of peak current versus square root of the scan rate for individual AA, DA and UA as noted in graph.

### 3.3 Electrochemical characterization of hybrid materials

#### 3.3.1 Surface area study

To investigate the kinetic of electrons transfer at an electrode/solution interface, a standard redox reaction of 0.5 mM  $\text{Fe}(\text{CN})_6^{3-/4-}$  in 0.1 M KCl was employed. Cyclic voltammetry data collected for ANF-C300 and ANF-C700 showed a set of improved reversible reactions. The separation between reduction and oxidation peak potentials for AA ( $\Delta E_p$ ) was around 70 mV for both samples at the scan rate of 10  $\text{mV s}^{-1}$  (Fig.13a). Peak currents intensities enhanced and peak positions shifted to more positive values with an increase in the scan rate from 10 to 200  $\text{mV s}^{-1}$  (Fig.13b). A linear dependency was observed between the peak currents and a square root of the potential scan rate implying a semi-infinite diffusion-controlled reaction on the electrode interface [54]. The electroactive surface areas of the ANF-C300 and ANFC700 electrodes were calculated as 0.333 and 0.426  $\text{cm}^2$  using the Randles–Sevcik equation (equation 4) [20]:

$$i_p = (2.69 \times 10^5)n^{3/2}ACD^{1/2}\nu^{1/2} \quad (4)$$

where  $i_p$  is the peak current (A),  $n$  is number of transferred electrons ( $n = 1$ ),  $A$  is the surface area of the electrode ( $\text{cm}^2$ ),  $C$  is the concentration of  $\text{Fe}(\text{CN})_6^{3-/4-}$  in analyte ( $\text{mol cm}^{-3}$ ),  $D$  is the ferricyanide diffusion coefficient ( $6.67 \times 10^{-6} \text{ cm}^2 \text{ s}^{-1}$ ) and  $\nu$  is the potential scan rate ( $\text{V s}^{-1}$ ).

From the above calculations, a higher surface area of the graphenated nanofibers accompanied by the highly porous 3D structure of the electrode material provides a relatively high electrochemically accessible surface area. This result shows an enhanced electrochemical activity and an excellent suitability of the ANF-C electrode for the electrochemical determination of small organic molecules and electrochemical sensing.

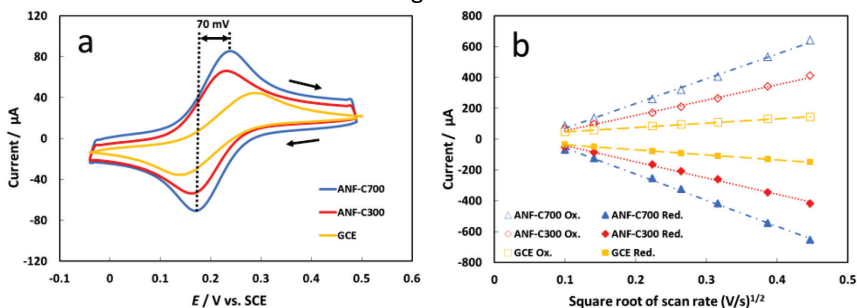


**Figure 13.** (a) CVs of ANF-C300, ANF-C700 and GCE electrodes recorded in 5mM  $\text{Fe}(\text{CN})_6^{3-/4-}$ +0.1M KCl solution at a scan rate of 10  $\text{mV s}^{-1}$ ; (b) anodic and cathodic peak currents of the electrodes vs. the square root of potential scan rates in the range of 10 to 200  $\text{mV s}^{-1}$ .

#### 3.3.2 Electrocatalytic behaviour of sensors

Electrocatalytic behaviour of ANF-C300, ANFC700 and GCE electrodes were studied in phosphate buffer solution ( $\text{pH} = 7.0$ ) and in ternary mixture of AA, DA and UA at the scan rate of 50  $\text{mV s}^{-1}$ . Oxidation peaks of DA and UA were very wide and in lower intensity in ANF-C300 sensor; however, very sharp pronounced oxidation peaks were observed using ANFC700 sensor at the potentials of -70 mV, 210 mV and 320 mV for individual compounds of AA, DA and UA, respectively (Fig. 14a-c). Therefore, ANF-C700 material

was challenged in ternary mixture of AA, DA and UA. The CV response recorded for the ternary mixture solution is presented in Fig. 14d. The ANF-C700 modified electrode clearly separated the oxidation peaks appeared at  $-80$  mV,  $190$  mV, and  $340$  mV for AA, DA and UA, respectively. Potential peak positions were nearly unchanged with reference to the peaks recorded for individually examined analytes by voltammetry technique. This clearly shows that ANF-C700 modified electrode is highly selective toward simultaneous determination of three components under consideration.

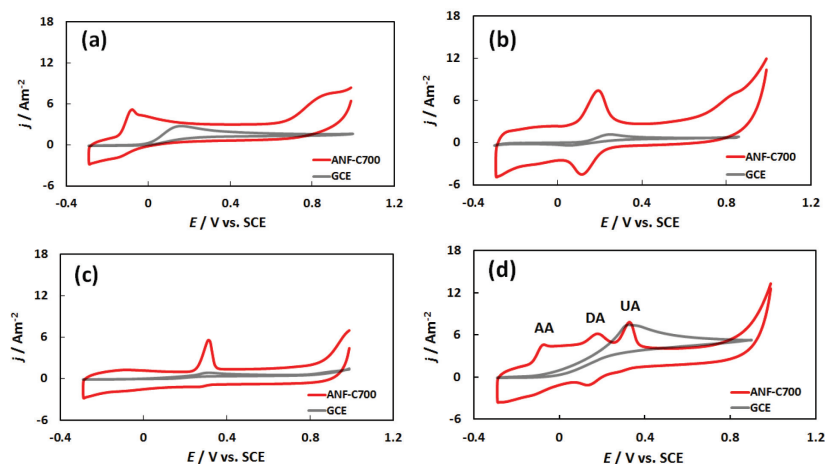


**Figure 14.** CV responses of (a) AA (5 mM), (b) DA (1 mM), (c) UA (1 mM), and (d) mixture of 5 mM AA, 1 mM DA, and 1 mM UA in 0.1 M phosphate buffer (pH 7.0) on ANF-C700 at  $10 \text{ mV s}^{-1}$ , respectively.

As an additional work, ANF-C700 was challenged to determine other three compounds that can be found in our body i.e. EP, AP and Trp. Oxidation peaks of these three were very wide and sensor was not able to detect them analytically (Fig. 15). Therefore, ANF-C400 with updated synthesis protocol was used as substrate. As explained in materials and methods, fabricated material was further functionalized and were studied for determination of EP, AP and Trp. Very well-defined oxidation peaks were observed at 0.244 V, 0.444 V and 0.709 V attributed to EP, AP and Trp, respectively. Peak currents shifted towards more positive potential values on the ANF-C400/Cu as compared to the ANF-C700. The main reason can be due to the more electro active sites on the ANF-C400/Cu and an enhanced catalytic activity in an electrode/analyte interface.

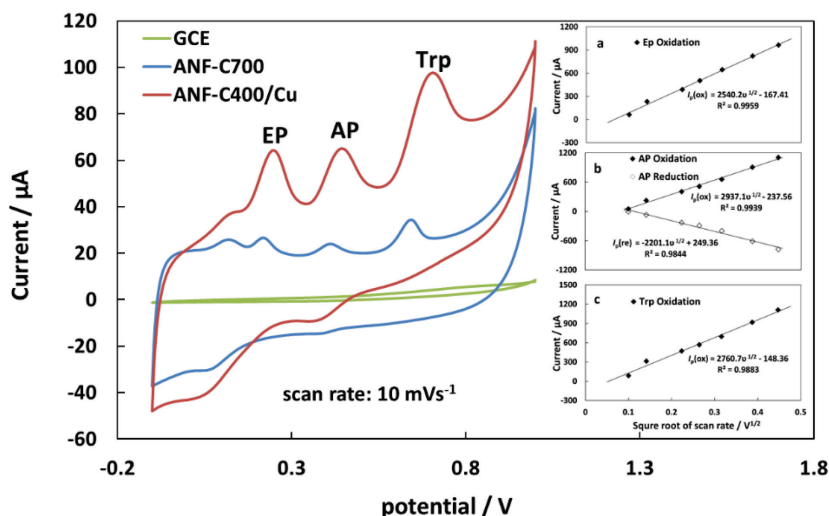


**Figure 15.** CVs of bare GCE (green), ANF-C700 (blue) and ANF-C400/Cu (red) in 0.1M phosphate buffer (pH 6.0) containing 200 $\mu$ M EP, 100  $\mu$ M AP, and 100  $\mu$ M Trp at 10 mV s<sup>-1</sup>. Insets show linear relationships between current and square root of scan rate for ANF-C400/Cu for different analytes.

### 3.3.3 Electrochemical determination of bio analytes

Sensitivity and practical applications of the ANF-C modified electrodes were investigated using differential pulse voltammetry due to its higher current sensitivity and better resolution as compared to CV. Comparing ANF-C300 and ANF-C700 electrodes showed that increase in the concentration of AA containing analyte results in an increase in anodic peak currents corresponding to irreversible oxidation of hydroxyl groups to carbonyl groups of the furan ring at higher concentrations of AA. Additionally, results suggested that ANF-C700 electrode had superior electrocatalytic activity in terms of sensitivity compared to ANF-C300 owing to its structural characteristics and enhanced electrical conductivity of the graphitic foliates of ANF-C700. Then, ANF-C700 electrode were challenged with the mixture analyte containing AA, DA and UA (Fig. 16a). Data collected from ANF-C700 electrode showed superior response. Three well-defined oxidation peaks at -30 mV, 170 mV and 300 mV were detected for AA, DA and UA, respectively. The peak currents linearly depended on corresponding analyte concentrations and described by the following calibration curves (Fig. 16b):

$$j_{AA} (\mu\text{A cm}^{-2}) = 1.99 C_{AA} + 68.10 \quad (R^2 = 0.9908)$$

$$j_{DA} (\mu\text{A cm}^{-2}) = 1.26 C_{DA} + 151.66 \quad (R^2 = 0.9922)$$

$$j_{UA} (\mu\text{A cm}^{-2}) = 2.1644 C_{UA} + 154.4 \quad (R^2 = 0.9921)$$

Linear ranges were of 0.5 – 60  $\mu$ M, 1–80  $\mu$ M and 1–60  $\mu$ M for AA, DA and UA, respectively. Sensitivity for AA was 5.33  $\mu\text{A}\cdot\mu\text{M}^{-1}\cdot\text{cm}^{-2}$ , for DA was determined 6.58  $\mu\text{A}\cdot\mu\text{M}^{-1}\cdot\text{cm}^{-2}$  and UA calculated as 11.27  $\mu\text{A}\cdot\mu\text{M}^{-1}\cdot\text{cm}^{-2}$ , respectively; demonstrating that very large specific surface area for the extraordinary electro catalytic activities has been engaged in analyte/electrode interactions. Experimental detection limit was calculated as 0.59, 0.47 and 0.28  $\mu$ M (S/N = 3) for AA, DA and UA, respectively.

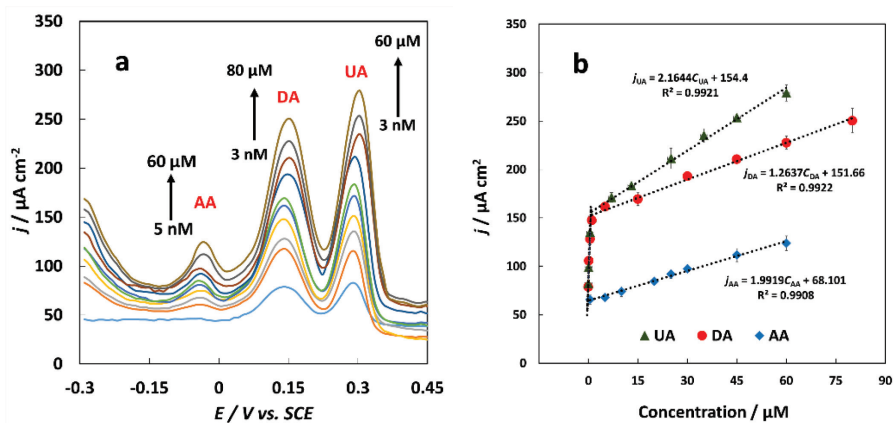


**Figure 16. a)** DPV profiles measured at ANF-C700 in ternary mixture of AA, DA and UA, and **b)** Variation of the DPV oxidation peak currents of AA, DA and UA against their concentration.

DPV data was collected for the ANF-C700 and ANF-C400/Cu electrodes in determining EP, AP and Trp in ternary mixture by varying the concentration of one analyte while the concentrations of the other two remained constant. Three distinct oxidation peaks observed at the potentials of 0.244 V, 0.404 V and 0.678 V for EP, AP and Trp, respectively. In all three cases, peak currents increased with increasing concentration of the compound. Epinephrine peak currents vs concentration was linear in the range of 1 to 1200  $\mu\text{M}$  in presence of 30  $\mu\text{M}$  AP and 50  $\mu\text{M}$  Trp, while the response of acetaminophen and tryptophan remained almost unchanged (Fig. 17a). Corresponding linear function was described as  $I_p (\mu\text{A}) = 0.084C_{EP} (\mu\text{M}) + 8.14$  ( $R^2 = 0.9948$ ).

Similar approach was performed for the acetaminophen in presence of 100  $\mu\text{M}$  EP and 50  $\mu\text{M}$  Trp (Fig. 17b). Increase in AP concentration from 1 to 700  $\mu\text{M}$  resulted to higher oxidation currents which was described as a calibration curve of  $I_p (\mu\text{A}) = 0.19 C_{AP} (\mu\text{M}) + 12.35$  ( $R^2 = 0.9954$ ).

Study was continued with Trp by addition of 100  $\mu\text{M}$  EP and 30  $\mu\text{M}$  AP. By increase in concentration of Trp from 1 to 1000  $\mu\text{M}$ , peak currents increased linearly (Fig. 17c). Overall, results were plotted as a function of current vs concentration  $I_p (\mu\text{A}) = 0.25 C_{Trp} (\mu\text{M}) + 12.99$  ( $R^2 = 0.9917$ ).

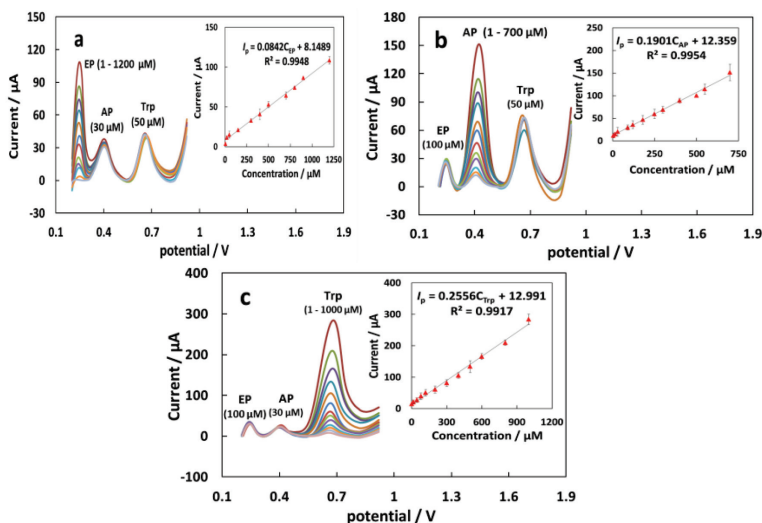


**Figure 17.** DPV profiles measured at ANF-C400/Cu in ternary mixture of EP, AP and Trp, individual determination: **a)** -EP, **b)** -AP and **c)** -Trp in phosphate buffer (pH = 6.0) at a scan rate of  $10 \text{ mV s}^{-1}$ .

Above results demonstrated highly selective properties of the modified samples in which limit of detection were decreased as  $0.027$ ,  $0.012$  and  $0.009 \mu\text{M}$  for EP, AP and Trp, respectively ( $S/N = 3$ ). Peak potential separation was also large enough to achieve the simultaneous determination of three compounds in a solution.

### 3.3.4 Interface properties of sensors

Interface properties of the GCE, ANF-C700 and ANF-C400/Cu samples were investigated using electrochemical impedance spectroscopy. Data obtained in lower and higher frequency region and in a solution of  $5 \text{ mM } [\text{Fe}(\text{CN})_6]^{4-/3-}$  containing  $0.1 \text{ M KCl}$ . Data were fitted by modified Randle equivalent circuit as described in section 2.6.2 (Electrochemical impedance spectroscopy).

Results for ANF-C700 showed smaller semicircle at high frequency region combined with linear behaviour at low frequency region indicating that the process is diffusion limited on ANF-C700 electrode (Fig. 18). Therefore, ANF-C700 with a faster kinetic of charge-transfer and low  $R_{ct}$  value of  $10 \Omega$ , demonstrated excellent conductivity compared to bare GCE ( $R_{ct} = 1350 \Omega$ ).

Electrochemical impedance data of the ANF-C700, and ANF-C400/Cu showed that  $R_{ct}$  value is low in synthesized samples as  $45 \Omega$  and  $10 \Omega$  for the ANF-C700 and ANF-C400/Cu, respectively which is in a good agreement with the CV data justifying the higher peak current ( $I_{pa}$ ) values for the copper modified electrode as compared to the ANF-C700 and GCE electrode.

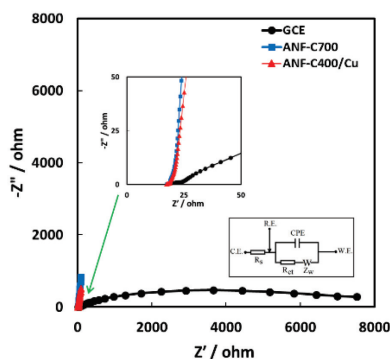


**Figure 18.** Nyquist plot of EIS for ANF-C700, ANF-C400/Cu and GCE electrodes.

### 3.4 Performance characteristic of sensors

#### 3.4.1 Stability and reproducibility of developed sensors

Stability and reproducibility of the sensors were validated by collecting known concentrations of the AA and EP compounds and comparing with the collected data from the measurements. Five successive measurements were performed in 10 days and CV data were recorded for 7 mM AA and 500  $\mu$ M EP in a 0.1 M of phosphate buffer solution. After experiments, electrodes were washed with distilled water and stored in dry room temperature as described in reference papers. Repeatable results were obtained and the relative standard deviations (RSD) were less than 4 % for all the challenged analytes indicating excellent stability and reproducibility of the graphene-decorated alumina nanofibers in electrochemical applications.

#### 3.4.2 Interference and reproducibility study

Anti-interference ability of the developed sensors was studied using chronoamperometry technique. In each set of measurements, common interfering ions and physiological compounds such as ammonium chloride,  $\text{FeCl}_3$ ,  $\text{MgCl}_2$ , KCl, citric acid,  $\text{Na}_2\text{SO}_4$ , NaCl, and  $\text{H}_2\text{O}_2$  were added to the analyte in a way that the tolerance limit causes approximately  $\pm 5$  % relative standard error in the determination (Fig. 19). As discussed in published articles, signal changes in added compounds were negligible and did not affect the results. In case of ANF-C400/Cu sensor, dopamine and uric acid demonstrated some overlapping due to their similar structure with the examined compounds and the close oxidation potentials. Thus, simultaneous determination of DA, UA, EP, AP and Trp was not possible by using ANF-C400 deposited Cu electrode.

The repeatability of the sensors was investigated by collecting responses from 5 successive experiments towards the oxidations of target analytes in ANF-C700 and ANF-C400/Cu sensors. Obtained data showed that fabricated sensor can successfully detect target compounds with relative standard deviation of less than 3.2 %. The storage stability and reusability of the ANF-C700 was verified by storing and reusing the sensor for 10 consecutive days in room temperature (STD = 2.01 %). In case of ANF-C400/Cu, a relative standard deviation of 2.9 % confirmed the excellent stability and reproducibility

of the Cu decorated ANF-C400 electrode, which can be effectively used for analytical investigations and determination of bio-analytes in aqueous solutions.

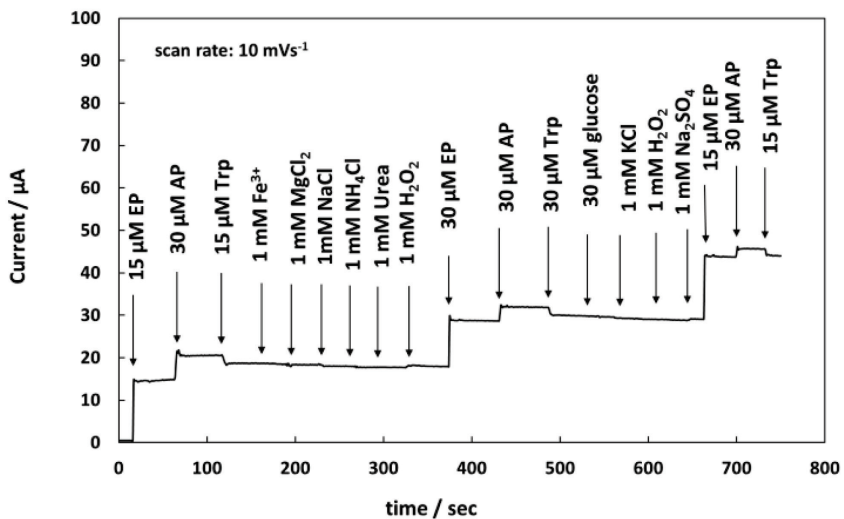


**Figure 19.** Amperometry responses of ANF-C400/Cu upon successive addition of 20  $\mu\text{M}$  EP, AP and Trp, and other chemicals to 0.1 M phosphate buffer (pH = 6.0).

## 4 CONCLUSIONS

Present work was concentrated on development of electrochemical sensors using alumina – graphene hybrid material as the sensing material. Achieving the main goal of the study, following conclusions can be drawn regarding the activities:

- Synthesized hybrid sensor materials were thoroughly characterized by physical (TEM, SEM and Raman spectroscopy) and electrochemical techniques (CV, DPV, CA, EIS). They were additionally compared for their catalytic activities and electrochemical responses;
- For the first time, optimized hybrid sensor material was used for simultaneous determination of ascorbic acid, dopamine and uric acid in human urine. Concentration of each compound was successfully determined and was calibrated in ternary mixture;
- Powder preparation methods were optimized and effect of strong acids on sensor was studied. Obtained results showed that acid treatment enhances sensor parameters such as limit of detection;
- Further sensing enhancement was successfully obtained by electrodeposition of Cu nanoparticles on hybrid material functionalized sensor;
- For the first time, alumina – graphene hybrid material deposited Cu nanoparticles were used for simultaneous determination of epinephrine, acetaminophen and tryptophan in human urine. Linear calibration curves were described in ternary mixture of compounds and very satisfactory limit of detection achieved;
- Above results were further enhanced by optimizing the sensor working conditions such as pH values and adjustment of sweep rate.

To conclude the study, ANF-C material with varied structural properties is an appropriate candidate for analytical chemistry investigations and pharmaceutical applications. Both ANF-C700 and ANF-C400/Cu sensor materials present a very good stability and repeatability that makes them promising materials for simultaneous determination of the biological molecules in different samples.

## List of Figures

**Figure 1.** Three-electrode electrochemical cell and a scheme of a redox reaction [20].

**Figure 2.** Scheme of electrode fabrication (ANF-C400 is called GAIN in reference Paper I)

**Figure 3.** Scheme of a three-electrode compartment electrochemical cell including working, reference and counter electrodes.

**Figure 4.** Scheme of cyclic voltammetry input waveform **(a)**, and a sample of reversible cyclic voltammogram response **(b)**.

**Figure 5.** Differential Pulse Voltammetry

**Figure 6.** sample scheme of a Randles equivalent circuit **(a)** and Nyquist plot arising from the Randles circuit **(b)**.

**Figure 7. a)** Current wave form for amperometry experiments **b)** A typical amperometry plot in stirred solution.

**Figure 8.** HRTEM images of the foliated hybrid nanostructures

**Figure 9.** HRSEM image of the **a)** ANF covered graphene **b)** ANF-C400/Cu after milling

**Figure 10.** Raman spectra of the precursor ANF-C700

**Figure 11.** Effect of pH on **a)** the peak current and **b)** the peak potential for the oxidation of 200  $\mu\text{M}$  EP, 150  $\mu\text{M}$  AP and 100  $\mu\text{M}$  Trp in 0.1 M phosphate buffer (scan rate = 50  $\text{mVs}^{-1}$ ).

**Figure 12.** Effects scan rate at ANF-C700 modified electrode in 0.1 M phosphate buffer (pH 7.0) containing 5 mM AA, 1mM DA, and 1mM of UA at different scan rates (10, 20, 40, 70,100,150, 200  $\text{mV s}^{-1}$ ). Insets: plots of peak current versus square root of the scan rate for individual AA, DA and UA as noted in graph.

**Figure 13. (a)** CVs of ANF-C300, ANF-C700 and GCE electrodes recorded in 5 mM  $\text{Fe}(\text{CN})_6^{3-/4-}$  + 0.1 KCl solution at a scan rate of 10  $\text{mVs}^{-1}$ ; **(b)** anodic and cathodic peak currents of the electrodes vs. the square root of potential scan rates in the range of 10 to 200  $\text{mV s}^{-1}$ .

**Figure 14.** CV responses of **(a)** AA (5 mM), **(b)** DA (1 mM), **(c)** UA (1 mM), and **(d)** mixture of 5 mM AA, 1 mM DA, and 1 mM UA in 0.1 M phosphate buffer (pH 7.0) on ANF-C700 at 10  $\text{mV s}^{-1}$ , respectively.

**Figure 15.** CVs of bare GCE (green), ANF-C700 (blue) and ANF-C400/Cu (red) in 0.1M phosphate buffer (pH 6.0) containing 200 $\mu\text{M}$  EP, 100  $\mu\text{M}$  AP, and 100  $\mu\text{M}$  Trp at 10  $\text{mVs}^{-1}$ . Insets show linear relationships between current and square root of scan rate for ANF-C400/Cu for different analytes.

**Figure 16. a)** DPV profiles measured at ANF-C700 in ternary mixture of AA, DA and UA, and **b)** Variation of the DPV oxidation peak currents of AA, DA and UA against their concentration.

**Figure 17.** DPV profiles measured at ANF-C400/Cu in ternary mixture of EP, AP and Trp, individual determination: **a)** -EP, **b)** -AP and **c)** -Trp in phosphate buffer (pH = 6.0) at a scan rate of 10  $\text{mV s}^{-1}$ .

**Figure 18.** Nyquist plot of EIS for ANF-C700, ANF-C400/Cu and GCE electrodes

**Figure 19.** Amperometry responses of ANF-C400/Cu upon successive addition of 20  $\mu\text{M}$  EP, AP and Trp, and other chemicals to 0.1 M phosphate buffer (pH = 6.0).

## List of Tables

**Table 1.** Optimization of experiments by varying powder preparations techniques.

## References

- [1] K. Honeychurch, M. Piano, *Electrochemical (Bio) sensors for environmental and food analyses*, *Biosensors*, 2018, 8 (3), 57-59.
- [2] C.I. Justino, A.R. Gomes, A.C. Freitas, A.C. Duarte, T.A. Rocha-Santos, *Graphene based sensors and biosensors*, *TrAC Trends in Analytical Chemistry*, 2017, 91, 53-66.
- [3] <https://www.himss.org/what-role-biosensors-next-generation-health-care-0>, (last viewed on: 29.10.2018)
- [4] S. Wu, Q. He, C. Tan, Y. Wang, H. Zhang, *Graphene-based electrochemical sensors*, *Small*, 2013, 9 (8), 1160-1172.
- [5] S. Glavanović, M. Glavanović, V. Tomišić, *Simultaneous quantitative determination of paracetamol and tramadol in tablet formulation using UV spectrophotometry and chemometric methods*, *Spectrochimica Acta Part A: Molecular and Biomolecular Spectroscopy*, 2016, 157, 258-264.
- [6] S. Azodi-Deilami, A.H. Najafabadi, E. Asadi, M. Abdouss, D. Kordestani, *Magnetic molecularly imprinted polymer nanoparticles for the solid-phase extraction of paracetamol from plasma samples, followed its determination by HPLC*, *Microchimica Acta*, 2014, 181 (15), 1823-1832.
- [7] Y. Su, D. Deng, L. Zhang, H. Song, Y. Lv, *Strategies in liquid-phase chemiluminescence and their applications in bioassay*, *TrAC Trends in Analytical Chemistry*, 2016, 82, 394-411.
- [8] Y. Guo, J. Yang, X. Wu, A. Du, *A sensitive fluorimetric method for the determination of epinephrine*, *Journal of Fluorescence*, 2005, 15 (2), 131-136.
- [9] N.R. Stradiotto, H. Yamanaka, M.V.B. Zanoni, *Electrochemical sensors: a powerful tool in analytical chemistry*, *Journal of the Brazilian Chemical Society*, 2003, 14, 159-173.
- [10] M. Pumera, A. Ambrosi, A. Bonanni, E.L.K. Chng, H.L. Poh, *Graphene for electrochemical sensing and biosensing*, *TrAC Trends in Analytical Chemistry*, 2010, 29 (9), 954-965.
- [11] R. Ivanov, I. Hussainova, M. Aghayan, M. Drozdova, D. Pérez-Coll, M.A. Rodríguez, F. Rubio-Marcos, *Graphene-encapsulated aluminium oxide nanofibers as a novel type of nanofillers for electroconductive ceramics*, *J Eur Ceram Soc*, 2015, 35 (14), 4017-4021.
- [12] K. Zhang, Q. Yue, G. Chen, Y. Zhai, L. Wang, H. Wang, J. Zhao, J. Liu, J. Jia, H. Li, *Effects of acid treatment of Pt– Ni alloy nanoparticles@ graphene on the kinetics of the oxygen reduction reaction in acidic and alkaline solutions*, *The Journal of Physical Chemistry C*, 2010, 115 (2), 379-389.
- [13] Y. Li, H.J. Schluesener, S. Xu, *Gold nanoparticle-based biosensors*, *Gold Bulletin*, 2010, 43 (1), 29-41.
- [14] L. Zhu, X. Guo, Y. Liu, Z. Chen, W. Zhang, K. Yin, L. Li, Y. Zhang, Z. Wang, L. Sun, *High-performance Cu nanoparticles/three-dimensional graphene/Ni foam hybrid for catalytic and sensing applications*, *Nanotechnology*, 2018, 29 (14), p.145703.
- [15] W.S. Hughes, *The potential difference between glass and electrolytes in contact with the glass*, *Journal of the American Chemical Society*, 1922, 44 (12), 2860-2867.
- [16] S. Arora, *Detecting food borne pathogens using electrochemical biosensors: An overview*, *IJCS*, 2018, 6 (1), 1031-1039.
- [17] G.G. Guilbault, J.G. Montalvo Jr, *Urea-specific enzyme electrode*, *Journal of the American Chemical Society*, 1969, 91 (8), 2164-2165.
- [18] T.A. Silva, F.C. Moraes, B.C. Janegitz, O. Fatibello-Filho, *Electrochemical biosensors based on nanostructured carbon black: A review*, *Journal of Nanomaterials*, 2017, 2017 1-15.

- [19] M.M. Rana, D.S. Ibrahim, M. Mohd Asyraf, S. Jarin, A. Tomal, A review on recent advances of CNTs as gas sensors, *Sensor Review*, 2017, 37 (2), 127-136.
- [20] A.J. Bard, L.R. Faulkner, J. Leddy, C.G. Zoski, *Electrochemical methods: fundamentals and applications*, Wiley New York, 1980, 1-736.
- [21] W. Siangproh, W. Dungchai, P. Rattanarat, O. Chailapakul, Nanoparticle-based electrochemical detection in conventional and miniaturized systems and their bioanalytical applications: A review, *Analytica chimica acta*, 2011, 690 (1), 10-25.
- [22] J. Wang, Nanoparticle-based electrochemical DNA detection, *Perspectives in Bioanalysis*, Elsevier, 2005, 369-384.
- [23] H. Li, S. Liu, Z. Dai, J. Bao, X. Yang, Applications of nanomaterials in electrochemical enzyme biosensors, *Sensors*, 2009, 9 (11), 8547-8561.
- [24] S. Phadtare, A. Kumar, V. Vinod, C. Dash, D.V. Palaskar, M. Rao, P.G. Shukla, S. Sivaram, M. Sastry, Direct assembly of gold nanoparticle "shells" on polyurethane microsphere "cores" and their application as enzyme immobilization templates, *Chemistry of materials*, 2003, 15 (10), 1944-1949.
- [25] A. Trovarelli, M. Boaro, E. Rocchini, C. de Leitenburg, G. Dolcetti, Some recent developments in the characterization of ceria-based catalysts, *Journal of Alloys and Compounds*, 2001, 323, 584-591.
- [26] W. Song, N. Zhang, Z. Luan, X. Zhang, P. He, Application of a cation-exchange reaction of CuS nanoparticles and fluorescent copper nanoparticles in a DNA biosensor, *RSC Advances*, 2018, 8 (27), 15248-15252.
- [27] X. Zhao, J. Tang, F. Yu, N. Ye, Preparation of graphene nanoplatelets reinforcing copper matrix composites by electrochemical deposition, *Journal of Alloys and Compounds*, 2018, 766, 266-273.
- [28] K.S. Novoselov, A.K. Geim, S.V. Morozov, D. Jiang, Y. Zhang, S.V. Dubonos, I.V. Grigorieva, A.A. Firsov, Electric field effect in atomically thin carbon films, *science*, 2004, 306 (5696), 666-669.
- [29] A.K. Geim, Novoselov K.S., The rise of graphene, *Nat. Mater.*, 2007, 6, 183-191.
- [30] C. Lee, X. Wei, J.W. Kysar, J. Hone, Measurement of the elastic properties and intrinsic strength of monolayer graphene, *science*, 2008, 321 (5887), 385-388.
- [31] A.A. Balandin, S. Ghosh, W. Bao, I. Calizo, D. Teweldebrhan, F. Miao, C.N. Lau, Superior thermal conductivity of single-layer graphene, *Nano letters*, 2008, 8 (3), 902-907.
- [32] K. Bolotin, K. Sikes, J. Hone, H. Stormer, P. Kim, Temperature-dependent transport in suspended graphene, *Physical review letters*, 2008, 101 (9), p.096802.
- [33] R.R. Nair, P. Blake, A.N. Grigorenko, K.S. Novoselov, T.J. Booth, T. Stauber, N.M. Peres, A.K. Geim, Fine structure constant defines visual transparency of graphene, *Science*, 2008, 320 (5881), 1308-1308.
- [34] K.I. Bolotin, K. Sikes, Z. Jiang, M. Klima, G. Fudenberg, J. Hone, P. Kim, H. Stormer, Ultrahigh electron mobility in suspended graphene, *Solid State Communications*, 2008, 146 (9-10), 351-355.
- [35] P. Bollella, G. Fusco, C. Tortolini, G. Sanzò, G. Favero, L. Gorton, R. Antiochia, Beyond graphene: electrochemical sensors and biosensors for biomarkers detection, *Biosensors and Bioelectronics*, 2017, 89, 152-166.
- [36] D.A. Brownson, D.K. Kampouris, C.E. Banks, Graphene electrochemistry: fundamental concepts through to prominent applications, *Chemical Society Reviews*, 2012, 41 (21), 6944-6976.

- [37] D.K. Polyushkin, J. Milton, S. Santandrea, S. Russo, M.F. Craciun, S.J. Green, L. Mahe, C.P. Winolve, W.L. Barnes, Graphene as a substrate for plasmonic nanoparticles, *Journal of Optics*, 2013, 15 (11), p.114001.
- [38] A.K. Geim, P. Kim, Carbon wonderland, *Scientific American*, 2008, 298 (4), 90-97.
- [39] Y. Zhang, L. Zhang, C. Zhou, Review of chemical vapor deposition of graphene and related applications, *Accounts of chemical research*, 2013, 46 (10), 2329-2339.
- [40] I. Hussainova, R. Ivanov, S.N. Stamatini, I.V. Anoshkin, E.M. Skou, A.G. Nasibulin, A few-layered graphene on alumina nanofibers for electrochemical energy conversion, *Carbon*, 2015, 88, 157-164.
- [41] R. Ivanov, V. Mikli, J. Kübarsepp, I. Hussainova, Direct CVD growth of multi-layered graphene closed shells around alumina nanofibers, *Key Eng Mater*, 2016, 674, 77-80.
- [42] T. Kuila, S. Bose, P. Khanra, A.K. Mishra, N.H. Kim, J.H. Lee, Recent advances in graphene-based biosensors, *Biosensors and Bioelectronics*, 2011, 26 (12), 4637-4648.
- [43] J. Xu, Y. Wang, S. Hu, Nanocomposites of graphene and graphene oxides: synthesis, molecular functionalization and application in electrochemical sensors and biosensors. A review, *Microchimica Acta*, 2017, 184 (1), 1-44.
- [44] P. Yáñez-Sedeño, S. Campuzano, J.M. Pingarrón, Carbon nanostructures for tagging in electrochemical biosensing: A review—C, 2017, 3 (1), 3-30.
- [45] E.M. Akinoglu, E. Kätelhön, J. Pampel, Z. Ban, M. Antonietti, R.G. Compton, M. Giersig, Nanoscopic carbon electrodes: Struc, electrical properties and application for electrochemistry, *Carbon*, 2018, 130, 768-774.
- [46] I. Álvarez-Martos, E.E. Ferapontova, Electrocatalytic discrimination between dopamine and norepinephrine at graphite and basal plane HOPG electrodes, *Electroanalysis*, 2018, 30 (6), 1082-1090.
- [47] C. Karuwan, A. Wisitsoraat, D. Phokharatkul, C. Sriprachuabwong, T. Lomas, D. Nacapricha, A. Tuantranont, A disposable screen printed graphene-carbon paste electrode and its application in electrochemical sensing, *RSC Advances*, 2013, 3 (48), 25792-25799.
- [48] A. Ambrosi, M. Pumera, Electrochemically exfoliated graphene and graphene oxide for energy storage and electrochemistry applications, *Chemistry—A European Journal*, 2016, 22 (1), 153-159.
- [49] D.A. Brownson, C.E. Banks, CVD graphene electrochemistry: the role of graphitic islands, *Physical Chemistry Chemical Physics*, 2011, 13 (35), 15825-15828.
- [50] C. Brett, A.M. Oliveira Brett, *Electrochemistry: principles, methods, and applications*, Oxford, Oxford University Press, 1993, 50-173.
- [51] G. Davis, Electrochemical techniques for the development of amperometric biosensors, *Biosensors*, 1985, 1 (2), 161-178.
- [52] S.-M. Park, J.-S. Yoo, Electrochemical impedance spectroscopy for better electrochemical measurements, 2003, 455-461.
- [53] M. Taei, F. Hasanpour, M. Dinari, N. Sohrabi, M.S. Jamshidi, Synthesis of 5-[(2-hydroxynaphthalen-1-yl) diazenyl] isophthalic acid and its application to electrocatalytic oxidation and determination of adrenaline, paracetamol, and tryptophan, *Chin Chem Lett*, 2017, 28 (2), 240-247.
- [54] N.G. Shang, P. Papakonstantinou, M. McMullan, M. Chu, A. Stamboulis, A. Potenza, S.S. Dhesi, H. Marchetto, Catalyst-free efficient growth, orientation and biosensing properties of multilayer graphene nanoflake films with sharp edge planes, *Advanced functional materials*, 2008, 18 (21), 3506-3514.

## Acknowledgements

First of all, I would like to express my special appreciation and thanks to my supervisor Professor Irina Hussainova for the continuous support of my PhD study and related research; for her patience, motivation, and immense knowledge. Her guidance helped me all the time of research and writing of this thesis. I would like to thank her for encouraging my research and for allowing me to grow as a research scientist. I could not have imagined having a better advisor and mentor for my PhD study.

My sincere thanks also go to Dr. Sergei Bereznev, Dr. Sayed Habib Kazemi and Professor Renate Hiesgen, who provided me an opportunity to join their teams, and have access to their laboratory and research facilities to foster my abilities and perform experiments. Without their precious support, it would not be possible to conduct this research.

My Special thanks goes to Roman Ivanov who supported my research activities by providing useful advice, synthesizing materials with varied specifications and giving philosophical speech while I was board. Thanks him to be there all the time and being a good friend of mine during four years reaching this point. I am also grateful of my other colleagues Maria Drozdova, Janis Baroninš, Ramin Rahmaniahranjani, Marina Aghayan, Yaroslav Holovenko, Nikhil Kumar Kamboj, Tatevik Minasyan, Le Liu, and Ali Saffarshamshirgar and thanks for providing inspiring, helpful and pleasant working environment. I also would like to thank Valdek Mikli for nice SEM images.

I am also grateful for all my Iranian friends in Estonia who never let me feel alone. Thanks to Zahra Jafari, Mohsen Tavahhodi, Naghme Nikbakhsh, Nima Sajedi, Hadi Osli, Ali Samiei, Morteza Fakorrad, Negar Yousefi, Payam Shams, Fereshte Azimi and Mojtaba Rostami who provided a happy atmosphere when were together.

I owe a lot to my parents and beloved brothers Amir and Ahad, who encouraged and helped me at every stage of my personal and academic life, and longed to see this achievement come true.

I would like to give my heartfelt thanks to my wife, Zahra Omrani who put her steps in my life and changed every second to a happy moment. She has been extremely supportive throughout this entire process and has made countless sacrifices to help me get to this point.

A very special gratitude goes out to all down at Research Fund and Dora program for helping and providing the funding for the research work and participating conferences and be a professional researcher.

Finally, thanks to Estonia as my second home that opened new doors toward me while I was confused about the way to go. I will never forget this huge amount of kindness and support.

This research was supported by the Estonian Research Council under the personal grant PUT1063 (I. Hussainova). The author also acknowledges Estonian Ministry of Higher Education and Research under Projects IUT19-29 (J. Kübarsepp) and IUT19-28, the European Union through the European Regional Development Fund, Project TK141 and ERA.NET RUS PLUS Project Flexapp (ETAG15028).

## Abstract

# Alumina-graphene Hybrid materials for Electrochemical Sensing of Bio-analytes

Since the successful exfoliation of graphene in 2004, two-dimensional materials have been receiving great attention among research community due to extraordinary physical and chemical properties related to specific effects at nano-scale such as, among others, strong electro-catalytic activity, high electroactive area and low surface fouling. Nowadays, graphene-based nanomaterials and graphenated structures are widely used for electrochemical sensors, including biosensors, mainly due to their obvious advantages over electrodes based on other materials.

On the other hand, in such a network, transition metals such as Cu can improve charge and mass transfer resulting at better sensitivity due to its multiple oxidations and increasing surface area. Copper-based nanomaterials have been successfully applied in electrochemistry and used for determination of biomolecules such as H<sub>2</sub>O<sub>2</sub> and glucose. Thus, the hybrid alumina/graphene nanofibers modified by copper nanoparticles can be interesting matrix for electrochemical applications for example chemo-sensors.

In the present study, novel and ultrasensitive electrode materials were prepared from alumina nanofibers (ANF) by applying one-step chemical vapor deposition method. Prepared material was carbonized and marked as ANF-C300 and ANF-C700 in this study. Synthesized ANF-C300 and ANF-C700 materials were utilized to detect compounds of great biomedical interest such as ascorbic acid (AA), dopamine (DA) and uric acid (UA).

Electron-transfer kinetics at the electrode | electrolyte interface was studied by standard redox reaction of 5 mM ferri-ferrocyanide redox couple in 0.1 M KCl for ANF-C300, ANF-C700 and glassy carbon electrode (GCE) as reference. Difference between oxidation and reduction peak potentials for modified sample was 70 mV. Calculated surface area of the ANF-C700 revealed that modified sample possesses much higher electrochemical active surface than geometric surface area of GCE (0.106 cm<sup>2</sup>) demonstrating the higher electrochemical activity of graphene modified electrode compared to GCE.

Various electrochemical techniques such as cyclic voltammetry and differential pulse voltammetry were performed to detect DA, UA in presence of AA. Obtained data exhibited sharp and intense peak followed by well-separated oxidation peaks towards the electro-oxidation of DA, UA, and AA. Linear relationship was observed between current densities and concentrations of all three compounds, and the limits of detection were down to 290, 250 and 1490 nM for DA, UA and AA, respectively. ANF-C700 electrode displayed a good reproducibility and stability and was successfully tested for detection of DA, UA and AA in human urine samples.

Thereafter adjusted 3D structure of alumina nanofibers covered by multi-layered graphene additionally was decorated by Cu nanoparticles. Obtained composite material was successfully used for simultaneous determination of Epinephrine (EP), Acetaminophen (AP) and Tryptophan (Trp) in phosphate buffer (pH = 6.0).

Analytical performance of the sensor was studied using electrochemical techniques such as cyclic voltammetry, differential pulse voltammetry, chronoamperometry and electrochemical impedance spectroscopy. Obtained sensor was further evaluated in human urine sample and it was found that after the measurements the recovery of the

sensitivity was very good. Collected data showed that calibration curves were linear and detection limits were down to 0.027, 0.012 and 0.009  $\mu\text{M}$  for EP, AP and Trp, respectively. This study demonstrated the practical analytical utility of chemo-sensor based on material ANF-C400/Cu for determination of EP, AP and Trp in real sample analysis, without significant interferences.

## Kokkuvõte

### Alumiiniumoksiid-grafeenhübriidmaterjalid biovedelike elektrokeemiliseks tuvastamiseks

Kahedimensionaalsed materjalid on pälvinud teadlaste kogukonnas suurt tähelepanu pärast grafeeni edukat sünteesi 2004. aastal. Seda eelkõige materjalide nanomõõtmega seotud erakordsete füüsikaliste ja keemiliste omaduste tõttu, nagu kõrge elektrokeemiline aktiivsus, väga suur elektrokeemiliselt aktiivne pindala, pinna madal tundlikkus saasteainete suhtes ja muud taolist. Tänapäeval kasutatakse grafeenil põhinevaid naomaterjale ja grafeeniga kaetud struktuure laialdaselt elektrokeemilistes andurites, sealhulgas bioandurites, peamiselt ilmselgete eeliste tõttu võrreldes teiste elektroodmaterjalidega.

Teisest küljest võivad sellistes struktuurides üleminekugrupi-metallid, nagu vask, oluliselt kiirendada laengu- ja massiülekannet, mille tulemusel paraneb elektroodmaterjali tundlikkus, sest võimalik on mitmeetapiline oksüdeerumine ja kasvab elektrokeemiliselt aktiivne pindala. Vasega legeeritud nanomaterjale on edukalt kasutatud mitmetes elektrokeemilistes rakendustes, selliste biomolekulide nagu vesinikperoksiid ja glükoos määramiseks biovedelikes. Seetõttu võib oletada, et vase nanoosakestega modifitseeritud alumiiniumoksiid-grafeen nanokomposiidid on väga huvitavad struktuurid, mis võivad leida kasutust elektrokeemilistes rakendustes, näiteks elektrokeemilistes andurites.

Doktoritöö raames valmistati uused ja äärmiselt tundlikud alumiiniumoksiidnanokiududel (ANF) baseeruvad elektroodmaterjalid kasutades üheetapilist keemilist aursadestamise meetodit. Valmistatud materjalid kaeti nanosüsiniikuga – grafeeniga (ANF-C300 ja ANF-C700). Sünteesitud materjale kasutati biomeditsiini seisukohast suurt huvi pakkuvate ühendite: askorbiinhape (AA), dopamiin (DA) ja kusiuhape (UA) määramiseks.

Alumiiniumoksiid-grafeenhübriid materjalidest valmistatud elektroodidel ning võrdluseks klaassüsiniikelektroodil kasutati laenguülekande elektrood-elektrolüüt piirpinnal kineetika uurimiseks tavapäraselt 5 mM punase veresoola-kollase veresoola redokspaari 0.1 M KCl lahuses. Modifitseeritud materjalide korral oli oksüdeerimise ja redutseerimise piikide potentsiaalide erinevus 70 mV. Grafeeniga ANF C700 modifitseeritud materjali arvutuslik elektrokeemiliselt aktiivne pindala oli oluliselt suurem, kui klaassüsiniikelektroodi geomeetriline pindala. See näitab, et grafeeniga modifitseeritud elektroodmaterjalil oli oluliselt suurem elektrokeemiline aktiivsus võrreldes klaassüsiniikelektroodiga.

Dopamiini ja kusiuhape määramiseks askorbiinhappe juuresolekul kasutati mitmesuguseid elektrokeemilisi meetodeid, näiteks tsüklilist voltammeetriat, diferentsiaal-impulssvoltammeetriat, kronoamperomeetriat ja elektrokeemilist impedantspektroskoopiat. Voltammogrammidel täheldati järsked ja suure intensiivsusega elektrooksidatsiooni piike, mis on hästi eristatavad. Uuritud kolme ühendi puhul sõltus mõõdetud voolutihedus lineaarselt kontsentratsioonist. Dopamiini, kusi- ja askorbiinhape tuvastustundlikkus olid vastavalt 290, 250 ja 1490 nM. Grafeeniga ANF C700 modifitseeritud materjalist valmistatud elektrood näitas head reprodutseeritavust ja stabiilsust ning seda elektroodi kasutati edukalt uuritavate ühendite määramiseks inimese uriini proovidest.

Grafeeniga ANF C700 hübriidmaterjali sünteesimisel valmistati järgnevalt mitmekihilise grafeeniga kaetud kolmemõõtmeline alumiiniumoksiidnanokiudstruktuur, millesse viidi lisaks ka vase nanoosakesed. Saadud nanokomposiitmaterjali kasutati edukalt epinefriini, atsetaminofeeni ja trüptofaani samaaegseks määramiseks fosfaatpuhvrts (pH = 6,0).

Hinnati anduri käitumist inimese uriini proovides ja leiti, et anduri mõõtmisjärgse tundlikkuse taastumine on väga hea ning ühendite vastavad piigid lahutuvad biovedelikes väga hästi. Mõõtetulemused näitasid, et andurite kalibreerimiskõverad on lineaarsed ning epinefriini, atsetaminofeeni ja trüptofaani tuvastuspiirid olid vastavalt 0,027; 0,012 ja 0,009  $\mu\text{M}$ . Doktoritöös näidati, et alumiiniumoksiidgrafeenil ANF-C700/Cu baseeruv kemoandur on praktikas kasutatav erinevate ühendite analüütiliseks määramiseks biovedelike tegelikes proovides.



## Appendix

### Publication I

**Masoud Taleb**, Roman Ivanov, Sergei Bereznev, Sayed Habib Kazemi, Irina Hussainova, Alumina/graphene/Cu hybrids as highly selective sensor for simultaneous determination of epinephrine, acetaminophen and tryptophan in human urine, (2018), Journal of Electroanalytical Chemistry, 823, 184–192.





Contents lists available at ScienceDirect

## Journal of Electroanalytical Chemistry

journal homepage: [www.elsevier.com/locate/jelechem](http://www.elsevier.com/locate/jelechem)

# Alumina/graphene/Cu hybrids as highly selective sensor for simultaneous determination of epinephrine, acetaminophen and tryptophan in human urine

Masoud Taleb<sup>a</sup>, Roman Ivanov<sup>a</sup>, Sergei Bereznev<sup>b</sup>, Sayed Habib Kazemi<sup>c</sup>, Irina Hussainova<sup>a,d,\*</sup><sup>a</sup> Tallinn University of Technology, Department of Materials Engineering, Ehitajate 5, Tallinn, Estonia<sup>b</sup> Tallinn University of Technology, Department of Materials and Environmental Technology, Ehitajate 5, Tallinn, Estonia<sup>c</sup> Institute for Advanced Studies in Basic Sciences (IASBS), Department of Chemistry, Zanjan, Iran<sup>d</sup> ITMO University, Kronverksky 49, St. Petersburg, Russia

## ARTICLE INFO

## Keywords:

Electrochemical sensor  
Graphene  
Differential pulse voltammetry  
Acetaminophen  
Epinephrine  
Tryptophan

## ABSTRACT

A highly selective electrochemical sensor representing alumina/graphene/Cu hybrid structure was fabricated by electrodeposition of copper nanoparticles on graphene encapsulated alumina nanofibers and was employed for the simultaneous determination of epinephrine (EP), acetaminophen (AP) and L-tryptophan (Trp) with low instrumental detection limits (LOD) and wide linear ranges. Cyclic voltammetry, electrochemical impedance spectroscopy, differential pulse voltammetry and chronoamperometry methods were used to study electrochemical properties of the developed electrode. Well-separated oxidation peaks and enhanced peak currents of EP, AP, and Trp were observed owing to the superior conductivity of highly foliated multi-layered graphene and the excellent catalytic activity of Cu nanoparticles. Specifically, the separation of anodic peak potentials for EP-AP, AP-Trp and EP-Trp were 160, 274 and 434 mV vs. SCE, respectively. The peak currents linearly depended on EP, AP and Trp concentrations in the range of 1–1200, 1–700 and 1–1000  $\mu\text{M}$  with LOD of 0.027, 0.012 and 0.009  $\mu\text{M}$ , respectively ( $S_{\text{bk}}/m = 3$ ). The chemically modified electrode was successfully challenged with some interfering compounds and was evaluated in human urine sample for determination of EP, AP and Trp demonstrating outstanding stability and repeatability. Fabricated sensor is an appropriate candidate for the pharmaceutical applications and clinical investigations.

## 1. Introduction

Since the successful exfoliation of graphene in 2004, two-dimensional materials have been receiving great attention among research community due to extraordinary physical and chemical properties related to specific effects at nano-scale such as, among others, strong electro-catalytic activity, high electroactive area and low surface fouling [1]. Nowadays, graphene based nanomaterials and graphenated structures are widely used for electrochemical sensors, including biosensors, mainly due to their obvious advantages over electrodes based on other materials [2, 3]. For example, graphene-based electrodes have shown superior performance in terms of electro catalytic activity [4] and microscopic scale conductivity [5] than carbon nanotubes based electrodes. Graphene exhibits a wide electrochemical potential window of ca. 2.5 V in 0.1 M phosphate buffer (pH 6.0), which is comparable to that of graphite, glassy carbon (GC), and even boron-doped diamond electrodes. Moreover, charge-transfer resistance on graphene as

determined from AC impedance spectra is much lower than that of graphite and GC electrodes [6]. Recently, three-dimensional interconnected edge-exposed graphene nanostructures deposited onto gamma-alumina nanofibers were used for the preparation of ultrasensitive electrode for simultaneous detection of bio-compounds such as ascorbic acid, uric acid and dopamine [7, 8]. The sensor was successfully applied to the simultaneous determination of DA and UA in the presence of AA in a spiked urine sample demonstrating promising results owing to highly corrugated structure and electrochemical active area of the material.

On the other hand, transition metals such as Cu nano-particles (NP) can further improve charge and mass transfer of the network of alumina/graphene hybrid nanofibers resulting at better sensitivity due to its multiple oxidation states and increasing surface area [9]. A large number of reports have demonstrated that graphene-NP structures can act synergistically to offer unique physicochemical properties that are desirable and advantageous for sensing applications through enhancing

\* Corresponding author at: Tallinn University of Technology, Department of Materials Engineering, Ehitajate 5, Tallinn, Estonia.  
E-mail address: [irina.hussainova@ttu.ee](mailto:irina.hussainova@ttu.ee) (I. Hussainova).

<https://doi.org/10.1016/j.jelechem.2018.06.013>

Received 23 March 2018; Received in revised form 21 May 2018; Accepted 7 June 2018  
Available online 15 June 2018

1572-6657/ © 2018 Elsevier B.V. All rights reserved.

an achievable sensitivity and selectivity. Copper as a low-cost earth abundant transition metal has generated a great deal of interests due to capability to undergo reactions through both one and two-electron pathways, which makes them ideal candidates for electrodes used in supercapacitors, lithium-ion batteries and gas sensors [10]. Moreover, copper-based nanomaterials have been successfully applied in electrochemistry and used for determination of biomolecules,  $H_2O_2$  and glucose [11].

In common, the efficient electro catalyst should possess several key characteristics such as low over-potential, high electro catalytic activity, suitable stability, robustness, and cost-effective production route. One of the ways for preparation of advanced Cu-based nanomaterials is anchoring Cu NPs on a support of carbon-based network. The interactions between the NPs and carbon may have profound effect on the resulting physical and chemical properties of the system. For example, Cu NPs on activated carbon efficiently catalyzed a range of reactions without any pre-treatment [12]. Graphene-supported Cu NPs have been synthesized using various methods. For instance, a modified glass carbon electrode was produced out of graphene sheets adorned with Cu NPs, which were synthesized by electrodepositing the nanoparticles on the graphene [13].

Synthesis of nanostructured catalysts on a conducting substrate can potentially improve the performance of the resultant material because of large catalytic surface area and the synergistic effect between the catalyst and the substrate. In this regard, three-dimensional highly porous network of  $\gamma$ -alumina nanofibers [14], encapsulated by foliated graphene multi-layers [15, 16], can be advantageously utilized as electrode substrates offering a large active surface area and a highly conductive continuous porous 3D network. In this perspective, the development and application of alumina/graphene/copper hybrid sensor and its future prospects are discussed in the present study. In particular, the focus is made on the simultaneous detection of epinephrine, acetaminophen and tryptophan.

Epinephrine (EP), also known as adrenalin, is an important hormone and neurotransmitter in the central nervous system, which is responsible for functioning of cardiovascular system and regulation of blood pressure [17]. Therefore, medically EP has been considered as a common healthcare medicine for emergency treatments. Elevated levels of EP in nervous tissues and body fluids can lead to several diseases such as pheochromocytoma, hypoglycemia and Parkinson's disease [18].

Acetaminophen (*N*-acetyl-*p*-aminophenol, AP), commonly known as paracetamol, is widely used to relieve chronic pain and fever. AP has revealed an effective therapeutic potential in neuro-degenerative syndromes such as Alzheimer's and Parkinson's disease [19]. The large scale therapeutic use of AP has evidenced connection with the formation of some liver and nephrotoxic metabolites, which generated the need for the development of fast, simple and accurate methodologies for the detection of AP [20].

L-Tryptophan (Trp) is one of the essential amino acids for the human body which is a precursor for niacin, serotonin (neurotransmitters) and melatonin (neurohormones) [21]. This amino-acid cannot be synthesized in the human body directly and, therefore, must be taken from food and pharmaceutical formulas due to the scarce presence in vegetables. Recent studies indicate that inappropriate level of Trp in blood can lead to schizophrenia and autism [22].

In this context, development of a simple, sensitive and selective method to quantify EP, AP and Trp individually and simultaneously is needed for the analytical application and diagnostic research. To date, various techniques including spectrophotometry [23], high performance liquid chromatography [24], chemiluminescence [25], fluorometry [26] and electrochemical approaches have been developed for determination of EP, AP and Trp compounds in bio-fluids. Among them, the electrochemical techniques are attractive due to their ease of monitoring, cost efficiency, accuracy and sensitivity [27]. To the best of our knowledge, there are very few reports on simultaneous

determination of EP, AP and Trp compounds using electrochemical approaches. The major reason is their close oxidation potentials, which overlap in conventional electrodes, causing fouling effect and weak repeatability [15, 16].

In the present study and for the first time, an adjusted highly porous 3D nanostructure of foliated graphene augmented inorganic nanofibers (GAIN) decorated by Cu nanoparticles and representing alumina/graphene/copper hybrids was successfully used for simultaneous detection of EP, AP and Trp in phosphate buffer (pH = 6.0). The analytical performance of the sensor was further evaluated in a human urine sample.

## 2. Experimental

### 2.1. Chemicals and apparatus

All chemicals and reagents employed in this work were of analytical grade from Sigma-Aldrich Chemie GmbH, Germany, unless otherwise stated. The  $CuSO_4 \cdot 5H_2O$  was received from Fluka (Buchs, Switzerland), and used as received. Stock solutions of EP, AP and Trp were prepared daily by dissolving a suitable amount of reagents in a millipore water ( $18.2 M\Omega \cdot cm$ , Millipore water Ltd., USA). Phosphate buffer solution as a water-based non-toxic solution was chosen for simulating physiological condition and was prepared by mixing stock solutions of  $Na_2HPO_4$ ,  $NaH_2PO_4$  in a supporting electrolyte of 0.1 M KCl. Prior to the electrochemical measurements, all solutions were deoxygenated with purging  $N_2$  gas through the test cell for about 1 min.

The electrochemical measurements, including cyclic voltammetry (CV), differential pulse voltammetry (DPV), electrochemical impedance spectroscopy (EIS), and chronoamperometry (CA), were carried out with an Autolab potentiostat/galvanostat PGSTAT30 in a conventional three-electrode electrochemical system at a room temperature. A saturated calomel electrode (SCE) and a Pt wire were employed as a reference and a counter electrode, respectively. The working electrode was a glassy carbon electrode coated with alumina/graphene nanofibers decorated by Cu nanoparticles (NPs).

A digital pH meter (Precisa pH 900) was used for pH measurements of the electrolyte. The morphological features of the synthesized material were examined by scanning electron microscopy (SEM) using a Zeiss HR FESEM Ultra 55 at operating voltage of 4 kV and transmission electron microscopy TEM JEOL JEM-200FS.

### 2.2. Synthesis of the hybrids

The graphene augmented inorganic nanofibers with an average single fiber diameter of  $7 \pm 2$  nm were synthesized with the help of a direct catalyst-free chemical vapor deposition (CVD) of carbon onto the dielectric surface of alumina nanofibers in a mixture of methane-hydrogen gases as detailed in [28–31]. The CVD process was performed during 5 h at 1000 °C under methane ( $CH_4$ ) and hydrogen ( $H_2$ ) flow of  $200 \text{ cm}^3 \text{ min}^{-1}$  and  $100 \text{ cm}^3 \text{ min}^{-1}$ , respectively, followed by rapid cooling down to the room temperature under the nitrogen ( $N_2$ ) gas flow of  $2000 \text{ cm}^3 \text{ min}^{-1}$ . Process of carbonization resulted in the carbon weight gain of 400%. Thereafter, the graphene-augmented network (GAIN) was immersed into 80 mL of the oxidizing mixture of  $H_2SO_4/HNO_3$  (3:1, v/v) at 70 °C for 48 h for purification of  $-COOH$  functionalized material. The network was washed with distilled water and was dried at 80 °C in a vacuum for 8 h. The  $-COOH$  modified material was powdered using  $KM^{-1}$  ball milling machine during 3 h and then treated by Hielscher UP200Ht ultrasonic homogenizer for 20 min in 50 ml of water.

Prior to modification, a bare GCE electrode of 5 mm in diameter was thoroughly polished using 0.05  $\mu m$  alumina slurry (Buehler) to a mirror finish. Then, electrode was sonicated in ethanol and double distilled water for 5 min and dried under  $N_2$  gas flow.

A dispersion ink was prepared by suspending GAIN powder in double distilled water/isopropanol (1:7, v/v) as described in author's

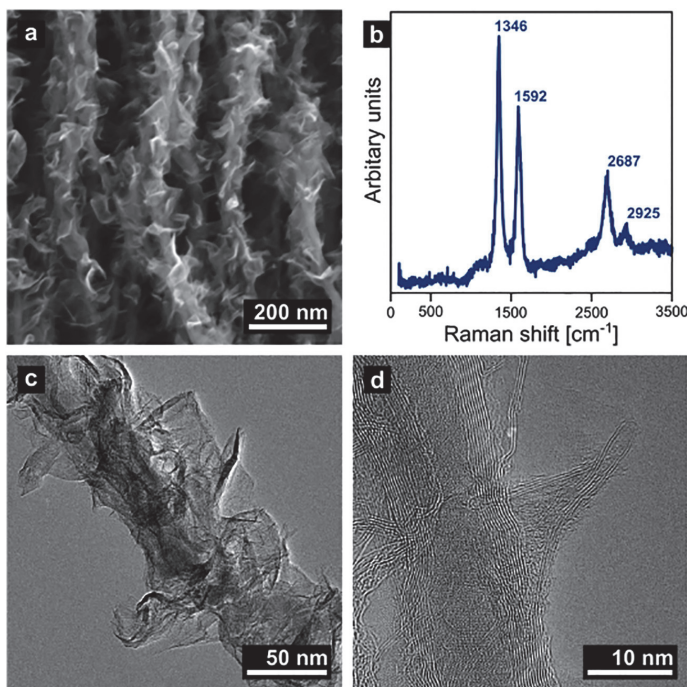


Fig. 1. (a) SEM image of the precursor GAINs; (b) – Raman spectrum of GAINs; and (c, d) HR-TEM images of the foliated hybrid nanostructures.

previous work [32]. The suspension was agitated in an ultrasonic bath for 15 min for thorough wetting and dispersion. Then, Nafion® dispersion solution was added to the mixture and was sonicated for 30 min. Thereafter, 10  $\mu\text{L}$  of the ink was deposited onto the GCE surface and left to dry at the room temperature.

The Cu NPs were electrochemically deposited onto the GCE modified GAIN surface by cycling the potential in the range between  $-0.1$  to  $0.4$  V vs. SCE in an electrolyte consisting of  $0.1$  M  $\text{H}_2\text{SO}_4$  and  $0.01$  M Copper (II) sulfate pentahydrate salt ( $\text{CuSO}_4 \cdot 5\text{H}_2\text{O}$ ) at a scan rate of  $10$   $\text{mV s}^{-1}$  for 10 cycles. The schematic representation of the hybrid electrode preparation is shown in Fig. S1. The alumina/graphene/copper hybrid modified electrode is denoted as GAIN/Cu in this work.

### 3. Results and discussion

#### 3.1. Characterization of the hybrid electrodes

Fig. 1 demonstrates the SEM and TEM images of GAIN network, which is composed of oxide ceramic nanofibers encapsulated by highly foliated graphene with controllable density of the open edges. The diameter of a single fiber after CVD processing and mechanical milling is  $45 \pm 5$  nm and the length is  $2 \pm 1$   $\mu\text{m}$ ; therefore, the aspect ratio of the hybrid fibers may be considered as high enough and equal to around  $10^3$ . The Raman spectrum of alumina/graphene hybrid is shown in Fig. 1b. The spectrum includes a *D*-peak at approximately  $1356$   $\text{cm}^{-1}$ , *G*-band at around  $1592$   $\text{cm}^{-1}$ , and *2D* band at approximately  $2687$   $\text{cm}^{-1}$ . The *D*-band is a characteristic feature indicating defectiveness of the structure. It can be caused by excitation of the edges of graphene sheets and their random orientation [33]. The *G*-band reflects  $sp^2$  vibrations in the graphitic plane, which confirms the presence of graphene sheets. Intense, well-defined *2D* bands with relatively narrow width of full width at half maximum are peculiar for few-layered graphene.

Fig. 1a, c–d indicates the morphology of the graphenated fibers with perpendicular grown foliates of various sizes and density of  $40$ – $60$  per micron length. In general, it can be expected that graphene-based electrochemical sensors will have superior performance over other carbon-related materials due to the presence of more  $sp^2$ -like planes and edge defects presented at the foliated graphene. Taking into account the interlayer spacing, Fig. 1d, which was roughly estimated to be  $0.34$ – $0.37$  nm, and a reported graphene monolayer thickness of  $0.335$ – $0.345$  nm, an average number of the graphene layers on the core ceramic is  $10$ – $15$ .

Fig. 2 shows morphology of GAIN decorated by Cu nanoparticles. Copper NPs with an average diameter of  $50 \pm 5$  nm (estimation from 100 nanoparticles) are dispersed on the external and inner walls of graphene flakes, which provide an effective surface for electro catalytic oxidation of EP, AP, and Trp. The energy-dispersive X-ray spectroscopy (EDX) pattern displays the presence of C, Al, O and Cu elements on the prepared electrode indicating the successful immobilization of Cu particles on the surface of GAIN.

Fig. 3 displays the CV responses of the GAIN and GAIN/Cu electrodes in  $5$  mM  $\text{Fe}(\text{CN})_6^{3-/4-}$  +  $0.1$  M KCl solution. As shown in Fig. 3a, b and S2, fabricated GAIN electrode exhibits well-defined voltammetry waves, in which redox peak currents are linearly dependent on the square root of the potential scan rate. Modification with Cu NPs enhances the catalytic activity of the sensor confirmed by the pronounced oxidation peak at  $0.256$  V and the reduction peak at  $0.209$  V suggesting that the GAIN/Cu owns faster electron transfer rate as compared to both the GAIN and the bare GCE. This may contribute to the superior electrical conductivity and enhanced electron transfer kinetics of the sensor. Additionally, it refers to a huge amount of the electrochemically active sites on the surface of GAIN/Cu electrode. The active surface area of the modified electrodes were estimated according to the Randles–Sevcik equation and a slope of the  $I_p$  vs.  $v^{1/2}$  plot for a known concentration of  $\text{Fe}(\text{CN})_6^{3-/4-}$  as discussed elsewhere [7]. The

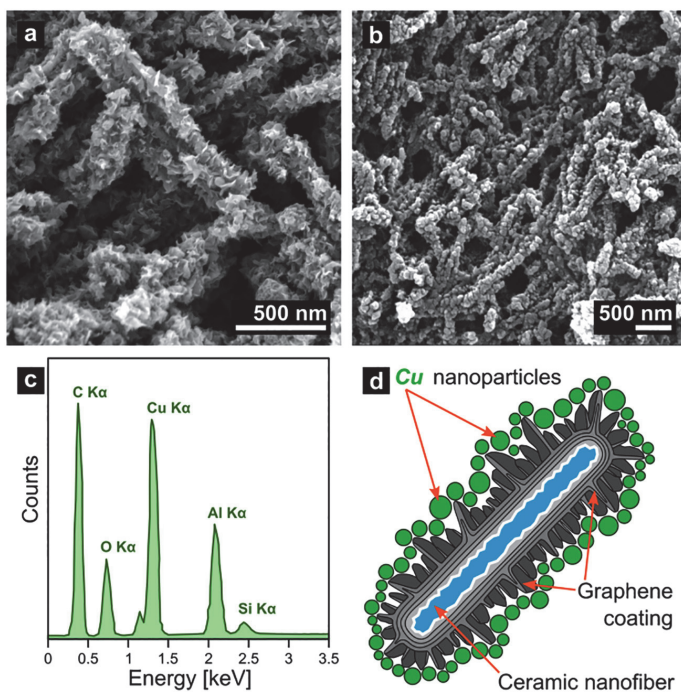


Fig. 2. Scanning electron microscopy image of (a) GAIN modified glassy carbon electrode, (b) GAIN/Cu modified glassy carbon electrode, (c) EDX spectrum taken from GAIN/Cu, and (d) schematic representation of the single graphenated fiber decorated by copper nanoparticles.

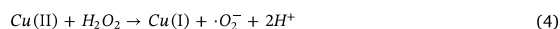
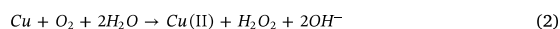
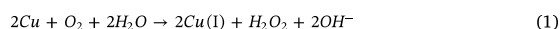
values obtained with the help of these procedures are 0.106, 0.330 and 0.553 cm<sup>2</sup> for the bare GCE, the GAIN and the GAIN/Cu, respectively. These results express a promotional five-fold increase in the electroactive area of the GAIN/Cu electrode as compared to the bare GCE.

The electrochemical impedance spectroscopy was employed to study the electron transfer capability and interface features of the GCE, GAIN, and GAIN/Cu electrode surface in 5 mM L<sup>-1</sup> [Fe(CN)<sub>6</sub>]<sup>3-/4-</sup> (as the redox probe, Fig. 3c). The Nyquist plots were fitted with an equivalent circuit R<sub>s</sub>(CPE [R<sub>ct</sub> Z<sub>w</sub>]), where R<sub>s</sub> referred to the electrolyte resistance, R<sub>ct</sub> is the charge transfer resistance, CPE is the constant phase element, and Z<sub>w</sub> is Warburg impedance coupled to R<sub>ct</sub> in Nernstian diffusion (inset in Fig. 3c). The bare GCE with a very large semicircle presents the biggest R<sub>ct</sub> value of 1350 Ω; however, this value is decreased to 45 Ω and 10 Ω for the GAIN and GAIN/Cu, respectively; implying that the modified electrodes can considerably facilitate electron transfer. The value of R<sub>ct</sub> for the GAIN/Cu is the lowest among the electrodes attributed to the large surface area and a synergistic effect between Cu NPs and graphene flakes. These results are in a good agreement with the CV data justifying the higher peak current (*I*<sub>pa</sub>) values for the copper modified electrode as compared to the GAIN and GCE.

An influence of pH on the anodic peak current and potentials of EP, AP and Trp oxidation and reduction were investigated in phosphate buffer solution by using cyclic voltammetry at various pH values ranging between 4.0 and 9.0 at a scan rate of 50 mV s<sup>-1</sup> (Fig. S3).

The results show that oxidation and reduction potentials were pH dependent: an increase in analyte pH values shifted both anodic and cathodic peaks to more negative values. This can be attributed to a deprotonating step involved into all oxidation processes which is facilitated at the higher pH values [34]. Conditioned by the maximum current obtained for all species, the pH value of 6.0 was chosen for the further experiments. At this pH, EP, AP and Trp are positively charged;

therefore, an electrostatic attraction facilitates their movement towards the GAIN/Cu electrode surface. Immobilized Cu nano particles (Cu) on the GAIN electrode surface are oxidized to Cu<sup>+</sup> and cupric copper (Cu<sup>2+</sup>) with the concomitant generation of hydrogen peroxide (H<sub>2</sub>O<sub>2</sub>), which is the precursor of hydroxyl radicals (·OH) and superoxide anions (·O<sub>2</sub><sup>-</sup>) [35]:



It was shown that ·OH and ·O<sub>2</sub><sup>-</sup> radicals facilitate the oxidative process of EP, AP and Trp in acidic media [35, 36]; therefore, presence of Cu is in favor of the reactions and catalyze the reaction.

### 3.2. Electrocatalytic oxidation of EP, AP and Trp

The electrochemical behavior of EP, AP and Trp was studied using the cyclic voltammetry method at the bare GCE, GAIN and GAIN/Cu modified electrodes at the potential range between -0.1 to 1.0 V vs. SCE with a scan rate of 10 mV s<sup>-1</sup> in 0.1 M phosphate buffer (pH = 6). As shown in Supplementary data (Fig. S4), the voltammetry responses of individual EP (200 μM), AP (100 μM) and Trp (100 μM) represent the broad oxidation waves on the bare GCE electrode demonstrating a weak and sluggish electron transfer rate. However, under the identical conditions, a substantial improvement appeared in the redox peak currents for oxidation of three species due to the possibility of π-π interaction between the aromatic ring of EP, AP, Trp and the GAIN electrodes.

A higher anodic peak current combined with a lower overpotential for the oxidation of EP, AP and Trp species on the GAIN/Cu electrode

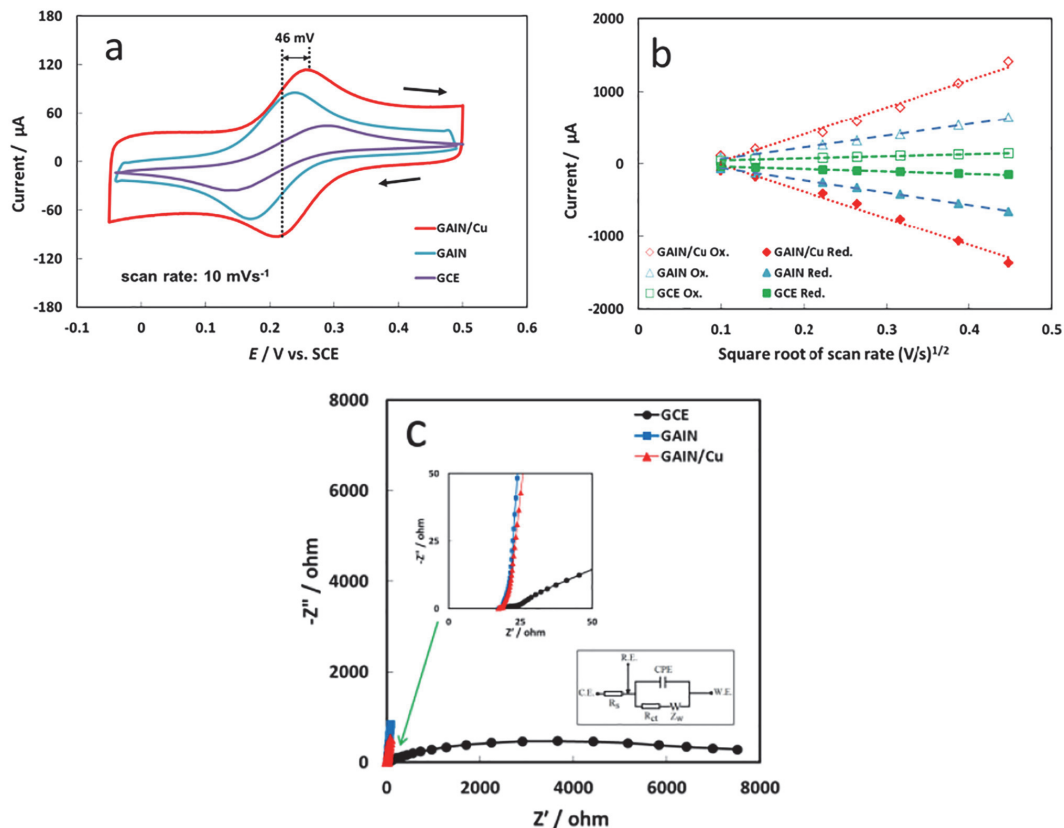


Fig. 3. (a) CVs of GAIN, GAIN/Cu and GCE electrodes recorded in 5 mM  $\text{Fe}(\text{CN})_6^{3-/4-}$  + 0.1 M KCl solution at a scan rate of  $10 \text{ mV s}^{-1}$ ; (b) anodic and cathodic peak currents of the electrodes vs. the square root of potential scan rates in the range of 10 to  $200 \text{ mV s}^{-1}$ ; (c) Nyquist plot of EIS for GAIN, GAIN/Cu and GCE electrodes.

indicates that the rate of an electron transfer can be accelerated by deposition of the Cu NPs on the GAIN structure leading to an excellent electrocatalytic activity and an improved performance of the electrode. Noticeable enhancement in an individual determination of EP, AP and Trp on the GAIN/Cu electrode can be attributed to the large electroactive surface area and the improved electron transfer process in the presence of Cu NPs. The interaction of EP ( $200 \mu\text{M}$ ) and Trp ( $100 \mu\text{M}$ ) on the surface of the GAIN/Cu electrode resulted in well-defined oxidation peaks at 0.26 V and 0.66 V, respectively (Fig. S4a, c). In case of AP ( $100 \mu\text{M}$ ), a redox pair is observed at 0.43 V and 0.36 V ascribed as the oxidation and reduction of AP, respectively (Fig. S4b). Additionally, two deserted peaks are observed at 0.12 and 0.04 V attributed to the oxidation and reduction reaction of Cu NPs, which can be traced in all recorded CVs. This observation indirectly confirms the presence of copper on the electrode.

The mechanism of electrochemical oxidation of EP, AP and Trp was discussed in number of studies, but it was not clearly established [37, 38]. Despite the number of questions regarding the pathways, two different processes can be proposed for EP oxidation: the ECC mechanism (electron transfer–chemical reaction–chemical reaction) and the ECE mechanism (electron transfer–chemical reaction–electron transfer). Our results suggest that ECE mechanism is more likely to happen for EP on GAIN/Cu electrode. Meanwhile, the electro-catalytic mechanism for the oxidation of AP and Trp on the GAIN/Cu electrode can be elucidated as illustrated in Fig. 4 [34].

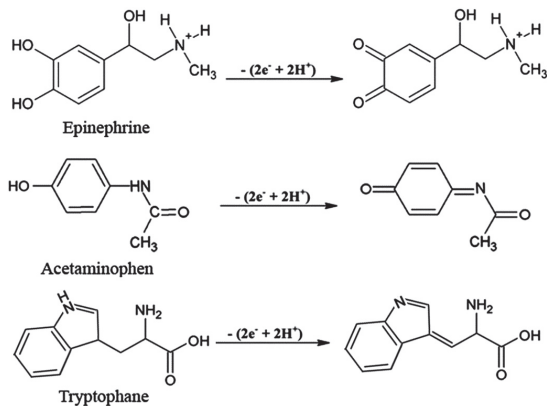
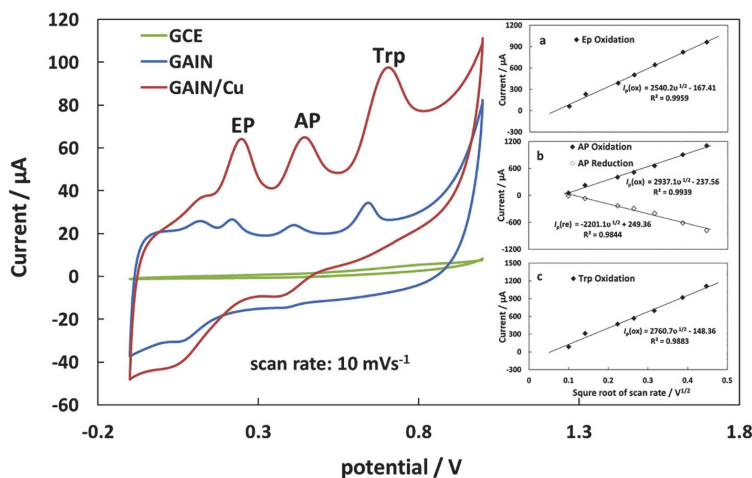


Fig. 4. Electrochemical oxidation of EP, AP, and Trp at GAIN/Cu.

The CV curves of ternary mixture of EP, AP and Trp at the different electrodes in phosphate buffer are demonstrated in Fig. 5. The voltammetric response of EP, AP and Trp is not detectable on the bare GCE; however, for both the GAIN and GAIN/Cu the distinct peaks at



**Fig. 5.** CVs of bare GCE (green), GAIN (blue) and GAIN/Cu (red) in 0.1 M phosphate buffer (pH 6.0) containing 200  $\mu\text{M}$  EP, 100  $\mu\text{M}$  AP, and 100  $\mu\text{M}$  Trp at 10  $\text{mV s}^{-1}$ . Insets show linear relationships between current and square root of scan rate for GAIN/Cu for different analytes. (For interpretation of the references to color in this figure legend, the reader is referred to the web version of this article.)

0.244 V, 0.444 V and 0.709 V attributed to oxidation of EP, AP and Trp, respectively, are clearly recognized. The peak currents obtained for the oxidation of reactant species are substantially enhanced and shifted towards more positive potential values on the GAIN/Cu as compared to the GAIN. This can be explained by a high electro activity of Cu sites and an enhanced catalytic activity in an electrode/analyte interface. The defected redox shoulders of Cu nanoparticles are observed at 0.48 V (reduction) and 0.126 V (oxidation).

The effect of scan rate was studied in a phosphate buffer (pH = 6.0) containing 200  $\mu\text{M}$  EP, 100  $\mu\text{M}$  of AP and 100  $\mu\text{M}$  Trp on the GAIN/Cu electrode surface. Cyclic voltammetry data revealed that the oxidation peak potentials of EP, AP and Trp shifted to more positive values with increase in the potential scan rate confirming the kinetic limitation of the electrochemical reaction. Plots of the electro catalytic peak currents ( $I_p$ ) against the square root of potential scan rates ( $v^{1/2}$ ) are found to be linear (insets in Fig. 5) indicating that at sufficient overpotential, the process of electro catalytic oxidations is rather controlled by diffusion than adsorption of the electroactive species. The linear regression equations for EP, AP, and Trp were expressed as EP:  $I_p(\text{ox}) = 2540.2 v^{1/2} - 167.41$  ( $R^2 = 0.9959$ ), AP:  $I_p(\text{ox}) = 2937.1 v^{1/2} - 237.56$  ( $R^2 = 0.9939$ ), Trp:  $I_p(\text{ox}) = 2760.7 v^{1/2} - 148.36$  ( $R^2 = 0.9883$ ), respectively. The alliegance between currents and  $v^{1/2}$  implies the electrochemical activity of the immobilized copper on the surface of the modified GCE.

### 3.3. Selective determination of EP, AP and Trp on the GAIN/Cu

Differential pulse voltammetry (DPV) technique was employed for characterization of the GAIN/Cu electrode in EP, AP and Trp due to its higher current sensitivity and better resolution as compared to CV. In ternary mixture of EP, AP and Trp, the electro-oxidation processes were examined by varying the concentration of one analyte while the concentrations of the other two remained constant (Fig. 6). Three distinct peaks appeared at 0.244 V, 0.404 V and 0.678 V for EP, AP and Trp, respectively. In case of epinephrine, the peak current increased with increasing concentration from 1 to 1200  $\mu\text{M}$  in the presence of 30  $\mu\text{M}$  AP and 50  $\mu\text{M}$  Trp, while the response of acetaminophen and tryptophan remained almost unchanged (Fig. 6a). The corresponding linear function can be approximated by  $I_p(\mu\text{A}) = 0.084C_{\text{EP}}(\mu\text{M}) + 8.14$  with a coefficient of correlation  $R^2 = 0.9948$  (inset in Fig. 6a).

Similarly, various concentrations of acetaminophen containing 100  $\mu\text{M}$  EP and 50  $\mu\text{M}$  Trp were tested by DPV and no obvious change was observed in the signal of EP and Trp. An increase in AP

concentration from 1 to 700  $\mu\text{M}$  resulted in a linear enhancement in the peak currents, which can be described as  $I_p(\mu\text{A}) = 0.19 C_{\text{AP}}(\mu\text{M}) + 12.35$  with a coefficient of correlation  $R^2 = 0.9954$  (inset of Fig. 6b). Additionally, the effect of EP and AP was examined in various concentrations of Trp involving 100  $\mu\text{M}$  EP and 30  $\mu\text{M}$  AP, Fig. 6c. The peak current of Trp increased with an increase in concentration of Trp in the range from 1 to 1000  $\mu\text{M}$  and the linear regression equation was expressed as  $I_p(\mu\text{A}) = 0.25 C_{\text{Trp}}(\mu\text{M}) + 12.99$  with a coefficient of correlation  $R^2 = 0.9917$  (inset in Fig. 6c).

The results indicated that the peak current at GAIN/Cu is highly selective at the physiological concentrations of EP, AP and Trp. The lowest instrumental detection limits are deduced as 0.027, 0.012 and 0.009  $\mu\text{M}$  for EP, AP and Trp, respectively, based on  $3S_{\text{bk}}/m$ , where  $S_{\text{bk}}$  is the standard deviation of the blank signal and  $m$  is the analytical sensitivity represented by the slope of the calibration curve. Peak separation is large enough to achieve the simultaneous determination of three compounds in a solution.

The analytical characteristics of the developed GAIN/Cu electrode are compared with those of other reported different chemically modified electrodes in Table 1. There are only a few reports on exploitation of the electrochemical approaches for simultaneous determination of acetaminophen, epinephrine, and tryptophan. However, the GAIN/Cu electrode demonstrates either improved or comparable analytical performance as compared to other sensors [34, 37, 39]. The proposed GAIN/Cu electrode produced with the help of the time- and cost-effective method can effectively separate the peak potentials of the EP, AP, and Trp in the ternary mixture in contrast to the electrodes, which require complicated approaches for synthesis [38, 40, 41]. Therefore, the GAIN/Cu material with a very low LOD and wide linear response ranges can be considered as a promising sensor for medical and pharmaceutical applications.

### 3.4. Interference, repeatability and stability

In order to evaluate the anti-interference ability of the developed GAIN/Cu sensor, several compounds and ions from common co-existing substances in the physiological samples were selected and were probed by CA method at a potential of 0.2 V. The tolerance limit was considered as the maximum concentration of each interference, when causes approximately  $\pm 5\%$  relative error in the determination. As validated in Fig. 7, EP, AP and Trp demonstrate clear signals; however, no significant interference was observed for the ions and physiological interferences such as ammonium chloride,  $\text{FeCl}_3$ ,  $\text{MgCl}_2$ , KCl,  $\text{Na}_2\text{SO}_4$ ,

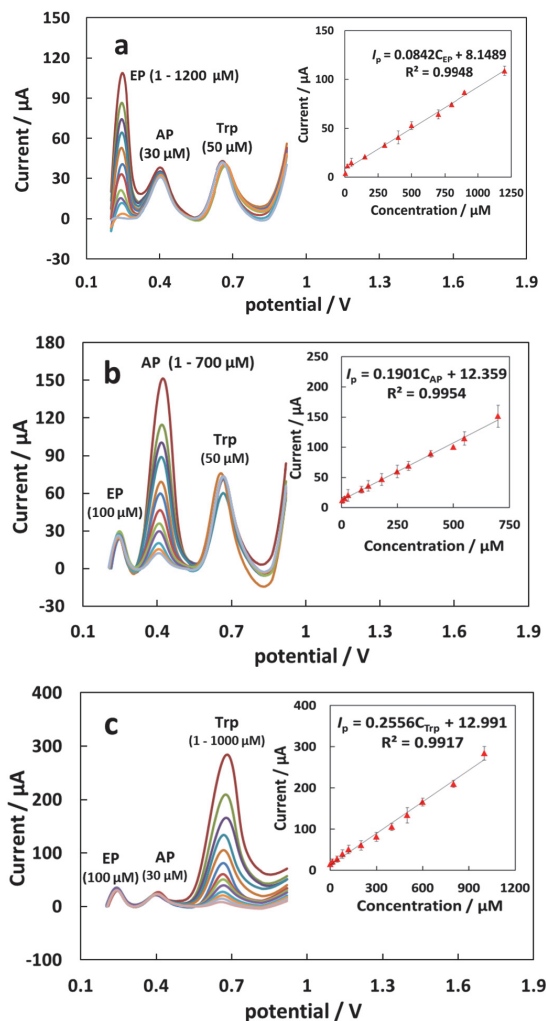


Fig. 6. DPV profiles measured at GAIN/Cu in ternary mixture of EP, AP and Trp, individual determination of (a) EP, (b) AP and (c) Trp in phosphate buffer (pH = 6.0) at a scan rate of  $10 \text{ mV s}^{-1}$ .

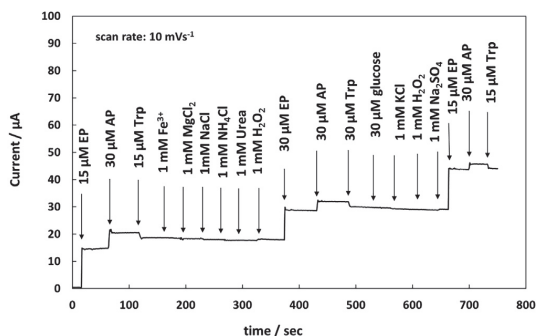


Fig. 7. Amperometric responses of GAIN/Cu upon successive addition of  $20 \mu\text{M}$  EP, AP and Trp, and other chemicals to  $0.1 \text{ M}$  phosphate buffer (pH = 6.0).

NaCl, Urea, Glucose and  $\text{H}_2\text{O}_2$ . In this experiment, dopamine and uric acid exhibit some overlapping due to their similar structure with the examined compounds and the close oxidation potentials. The repeatability of the sensor was evaluated by collecting responses from 5 successive experiments towards the oxidations of  $1 \mu\text{M}$  EP, AP, and Trp. The results showed a good repeatability with a relative standard deviation of 2.5%, 3.2% and 2.5% for EP, AP and Trp, respectively. RSD values at the center of each linear range deviated  $\pm 8\%$  from the above values. Between sensor standard deviation was calculated from the DPV data of the ternary mixture of Ep ( $100 \mu\text{M}$ ), Ap ( $30 \mu\text{M}$ ) and Trp ( $25 \mu\text{M}$ ) as 2.9%, 2.2%, and 2.6%, respectively. The storage stability and reusability of the fabricated sensor was verified by keeping it unused at the room temperature for 10 days and then tested with  $500 \mu\text{M}$  EP in the phosphate buffer. A relative standard deviation of 2.9% of the peak current response was detected at the GAIN/Cu electrode.

### 3.5. Real samples analysis

Analytical applicability and accuracy of the GAIN/Cu modified electrode were validated by determining different concentrations of EP, AP, and Trp in a human urine sample using the standard addition method. Urine samples were collected from healthy people in lab and were analyzed for possible traces of Ep, Ap and Trp. Thereafter, samples were diluted 50 folds with the phosphate buffer to prevent the matrix effect of authentic samples. Thus, different concentrations of EP, AP, and Trp were spiked to the solution and analyzed using the DPV technique. Table 2 summarizes the results demonstrating recoveries in the range of 97–102% (RSD % = 0.84–2.85) and a considerable accuracy the GAIN/Cu electrode. Therefore, the developed sensor can be effectively used for the simultaneous determination of EP, AP, and Trp in the real samples.

Table 1

Comparison of different chemically modified electrodes for the simultaneous detection of EP, AP and Trp.

Electrode	Peak separations (mV)			Linear range ( $\mu\text{M}$ )			Detection limit (LOD) ( $\mu\text{M}$ )			Refs.
	$\Delta E_1^a$	$\Delta E_2^a$	$\Delta E_3^a$	EP	AP	Trp	EP	AP	Trp	
$\text{Fe}_2\text{O}_3(0.5)/\text{SnO}_2(0.5)$ -GCE	160	280	440	0.6–270.0	4.5–876.0	0.6–70.0	0.07	0.2	0.1	[34]
IMWCNT-GCE	192	324	516	1.3–833.3	136.4–500.0	227.3–833.3	0.38	–	–	[37]
OMC/GCE	200	–	–	4.0–100	0.2–15.0	–	0.94	0.07	–	[38]
Ni-LFORCPE	364	313	677	7–560	5–580	4–560	0.45	0.27	0.38	[39]
DHPB-MWCNTPE	–	250	–	–	0.6–452	0.7–270.0	–	0.3	0.4	[40]
Au-NPs/poly(NDI)/GCE	210	190	400	0.01–680	0.05–498	3–632	0.009	0.005	0.09	[41]
GAIN/Cu	160	274	434	1–1200	1–700	1–1000	0.027	0.012	0.009	(This work)

<sup>a</sup>  $E_1$ ,  $E_2$ ,  $E_3$  are peak potential separations of EP-AP, AP-Trp, EP-Trp.

**Table 2**  
Determination results of EP, AP and Trp in real urine samples.

Sample	Compound	Added ( $\mu\text{M}$ )	Found ( $\mu\text{M}$ )	Recovery (%)	RSD (%)
Urine 1	EP	1	0.96	96	4.96
Urine 2	EP	25	24.75	99	1.00
Urine 3	EP	60	61.39	102	1.71
Urine 4	EP	100	99.96	100	0.97
Urine 5	EP	1200	1245.05	104	3.68
Urine 1	AP	1	0.95	95	4.06
Urine 2	AP	25	24.30	97	2.85
Urine 3	AP	60	60.99	102	0.84
Urine 4	AP	100	99.22	99	1.13
Urine 5	AP	700	669.02	96	3.92
Urine 1	Trp	1	1.04	104	3.81
Urine 2	Trp	25	25.35	101	1.89
Urine 3	Trp	60	60.25	100	1.86
Urine 4	Trp	100	97.58	98	0.96
Urine 5	Trp	1000	1051.12	105	3.80

#### 4. Conclusions

The developed material representing the graphene augmented nanofibers and decorated by copper nanoparticles (GAIN/Cu) displayed excellent electrochemical sensing capabilities without any post-transfer procedures or any further surface treatment. The direct one-stage catalyst-free growth of graphene nano-foliates forming a network of highly fuzzy graphenated nanofibers is exploited for preparation of the sensor for the simultaneous and highly sensitive determination of EP, AP and Trp. The CV and DPV examinations demonstrated synergistic effects of graphene–Cu nanoparticle hybrid structures on overall performance of the electrode by means of an improvement in electron transfer efficiency, enhancement of the selectivity and an increase in electro catalytic activity towards EP, AP and Trp in their individual and simultaneous determination. The collected data demonstrated the linear calibration curves and the outstanding instrumental detection limits of 0.027, 0.012 and 0.009  $\mu\text{M}$  for EP, AP and Trp, respectively. This study validated the practical analytical utility of the GAIN/Cu chemo-sensor for determination of EP, AP and Trp in a real samples analysis, without any significant interference with other species. In our perception, the GAIN/Cu electrochemical sensor with a good stability and repeatability can be an appropriate candidate for the pharmaceutical applications and clinical investigations.

#### Acknowledgments

This research was supported by the Estonian Research Council under the personal grant PUT1063 (I. Hussainova). The authors also acknowledge Estonian Ministry of Higher Education and Research under Projects IUT19-29 and IUT19-28, the European Union through the European Regional Development Fund, Project TK141 and TTÜ base finance project B54.

#### Appendix A. Supplementary data

Supplementary data to this article can be found online at <https://doi.org/10.1016/j.jelechem.2018.06.013>.

#### References

- J. Xu, Y. Wang, S. Hu, Nanocomposites of graphene and graphene oxides: synthesis, molecular functionalization and application in electrochemical sensors and biosensors. A review, *Microchim. Acta* 184 (1) (2017) 1–44, <http://dx.doi.org/10.1007/s00604-016-2007-0>.
- X. Yang, B. Feng, X. He, F. Li, Y. Ding, J. Fei, Carbon nanomaterial based electrochemical sensors for biogenic amines, *Microchim. Acta* 180 (11) (2013) 935–956, <http://dx.doi.org/10.1007/s00604-013-1015-6>.
- S. Sabury, S.H. Kazemi, F. Sharif, Graphene-gold nanoparticle composite: application as a good scaffold for construction of glucose oxidase biosensor, *Mater. Sci. Eng. C* 49 (2015) 297–304, <http://dx.doi.org/10.1016/j.msec.2015.01.018>.
- J. Lai, A. Nsabimana, R. Luque, G. Xu, 3D porous carbonaceous electrodes for electrocatalytic applications, *Joule* 2 (1) (2018) 76–93, <http://dx.doi.org/10.1016/j.joule.2017.10.005>.
- E. Wierzbicka, G.D. Sulka, Nanoporous spongelike Au–Ag films for electrochemical epinephrine sensing, *J. Electroanal. Chem.* 762 (2016) 43–50, <http://dx.doi.org/10.1016/j.jelechem.2015.12.013>.
- M. Zhou, Y. Zhai, S. Dong, Electrochemical sensing and biosensing platform based on chemically reduced graphene oxide, *Anal. Chem.* 81 (14) (2009) 5603–5613, <http://dx.doi.org/10.1021/ac900136z>.
- M. Taleb, R. Ivanov, S. Bereznev, S.H. Kazemi, I. Hussainova, Graphene-ceramic hybrid nanofibers for ultrasensitive electrochemical determination of ascorbic acid, *Microchim. Acta* 184 (3) (2017) 897–905, <http://dx.doi.org/10.1007/s00604-017-2085-7>.
- M. Taleb, R. Ivanov, S. Bereznev, S.H. Kazemi, I. Hussainova, Ultra-sensitive voltammetric simultaneous determination of dopamine, uric acid and ascorbic acid based on a graphene-coated alumina electrode, *Microchim. Acta* 184 (12) (2017) 4603–4610, <http://dx.doi.org/10.1007/s00604-017-2510-y>.
- P. Arul, S. Abraham John, Electrodeposition of CuO from Cu-MOF on glassy carbon electrode: a non-enzymatic sensor for glucose, *J. Electroanal. Chem.* 799 (2017) 61–69, <http://dx.doi.org/10.1016/j.jelechem.2017.05.041>.
- M.B. Gawande, A. Goswami, F.-X. Felpin, T. Asefa, X. Huang, R. Silva, X. Zou, R. Zboril, R.S. Varma, Cu and Cu-based nanoparticles: synthesis and applications in catalysis, *Chem. Rev.* 116 (6) (2016) 3722–3811, <http://dx.doi.org/10.1021/acs.chemrev.5b00482>.
- P. Gao, D. Liu, Facile synthesis of copper oxide nanostructures and their application in non-enzymatic hydrogen peroxide sensing, *Sensors Actuators B Chem.* 208 (2015) 346–354, <http://dx.doi.org/10.1016/j.snb.2014.11.051>.
- F. Alonso, Y. Moglie, G. Radivoy, M. Yus, Multipoint click synthesis of potentially biologically active triazoles catalysed by copper nanoparticles on activated carbon in water, *Heterocycles* 84 (2) (2012) 1033–1044, [http://dx.doi.org/10.3987/COM-11-S\(P\)81](http://dx.doi.org/10.3987/COM-11-S(P)81).
- S. Song, C.M. Ortega, Z. Liu, J. Du, X. Wu, Z. Cai, L. Sun, In situ study of copper electrodeposition on a single carbon fiber, *J. Electroanal. Chem.* 690 (2013) 53–59, <http://dx.doi.org/10.1016/j.jelechem.2012.12.005>.
- M. Aghayan, M. Gasik, I. Hussainova, F. Rubio-Marcos, L. Kollo, J. Kübarsepp, Thermal and microstructural analysis of doped alumina nanofibers, *Thermochim. Acta* 602 (2015) 43–48, <http://dx.doi.org/10.1016/j.tca.2015.01.009>.
- H. Karimi-Maleh, M. Moazampour, H. Ahmar, H. Beitollahi, A.A. Ensafi, A sensitive nanocomposite-based electrochemical sensor for voltammetric simultaneous determination of isoproterenol, acetaminophen and tryptophan, *Measurement* 51 (2014) 91–99, <http://dx.doi.org/10.1016/j.measurement.2014.01.028>.
- B. Liu, X. Ouyang, Y. Ding, L. Luo, D. Xu, Y. Ning, Electrochemical preparation of nickel and copper oxides-decorated graphene composite for simultaneous determination of dopamine, acetaminophen and tryptophan, *Talanta* 146 (2016) 114–121, <http://dx.doi.org/10.1016/j.talanta.2015.08.034>.
- E. Wierzbicka, G.D. Sulka, Fabrication of highly ordered nanoporous thin Au films and their application for electrochemical determination of epinephrine, *Sensors Actuators B Chem.* 222 (2016) 270–279, <http://dx.doi.org/10.1016/j.snb.2015.08.066>.
- M.D. Tezerjani, A. Benvidi, A. Dehghani Firoozabadi, M. Mazloum-Ardakani, A. Akbari, Epinephrine electrochemical sensor based on a carbon paste electrode modified with hydroquinone derivative and graphene oxide nano-sheets: simultaneous determination of epinephrine, acetaminophen and dopamine, *Measurement* 101 (Supplement C) (2017) 183–189, <http://dx.doi.org/10.1016/j.measurement.2017.01.029>.
- B.-R. Adhikari, M. Govindhan, H. Schraft, A. Chen, Simultaneous and sensitive detection of acetaminophen and valacyclovir based on two dimensional graphene nanosheets, *J. Electroanal. Chem.* 780 (2016) 241–248, <http://dx.doi.org/10.1016/j.jelechem.2016.09.023>.
- C. Bunchorntavakul, K.R. Reddy, Acetaminophen (APAP or N-acetyl-p-aminophenol) and acute liver failure, *Clin. Liver Dis.* (2018), <http://dx.doi.org/10.1016/j.cld.2018.01.007>.
- O. Mardones, E. Devia, B.S. Labbé, R. Oyarzún, L. Vargas-Chacoff, J.L.P. Muñoz, Effect of *l*-tryptophan and melatonin supplementation on the serotonin gastrointestinal content and digestive enzymatic activity for *Salmo salar* and *Oncorhynchus kisutch*, *J. Aquac. Res. Dev.* 482 (Supplement C) (2018) 203–210, <http://dx.doi.org/10.1016/j.aquaculture.2017.10.003>.
- B. Kanchanatawan, S. Sirivichayakul, A.F. Carvalho, G. Anderson, P. Galecki, M. Maes, Depressive, anxiety and hypomanic symptoms in schizophrenia may be driven by tryptophan catabolite (TRYCAT) patterning of IgA and IgM responses directed to TRYCATs, *Prog. Neuropsychopharmacol. Biol. Psychiatry* 80 (2018) 205–216, <http://dx.doi.org/10.1016/j.pnpbp.2017.06.033>.
- S. Glavanović, M. Glavanović, V. Tomišić, Simultaneous quantitative determination of paracetamol and tramadol in tablet formulation using UV spectrophotometry and chemometric methods, *Spectrochim. Acta A* 157 (2016) 258–264, <http://dx.doi.org/10.1016/j.saa.2015.12.020>.
- S. Azodi-Deilami, A.H. Najafabadi, E. Asadi, M. Abdouss, D. Kordestani, Magnetic molecularly imprinted polymer nanoparticles for the solid-phase extraction of paracetamol from plasma samples, followed its determination by HPLC, *Microchim. Acta* 181 (15) (2014) 1823–1832, <http://dx.doi.org/10.1007/s00604-014-1230-9>.
- Y. Su, D. Deng, L. Zhang, H. Song, Y. Lv, Strategies in liquid-phase chemiluminescence and their applications in bioassay, *TrAC Trends Anal. Chem.* 82 (2016) 394–411, <http://dx.doi.org/10.1016/j.trac.2016.07.002>.
- Y. Guo, J. Yang, X. Wu, A. Du, A sensitive fluorimetric method for the determination of epinephrine, *J. Fluoresc.* 15 (2) (2005) 131–136, <http://dx.doi.org/10.1007/s10895-005-2520-8>.

- [27] G.A. Rivas, M.C. Rodríguez, M.D. Rubianes, F.A. Gutierrez, M. Eguilaz, P.R. Dalmasso, E.N. Primo, C. Tettamanti, M.L. Ramírez, A. Montemero, P. Gallay, C. Parrado, Carbon nanotubes-based electrochemical (bio)sensors for biomarkers, *Appl. Mater. Today* 9 (2017) 566–588, <http://dx.doi.org/10.1016/j.apmt.2017.10.005>.
- [28] I. Hussainova, R. Ivanov, S.N. Stamatina, I.V. Anoshkin, E.M. Skou, A.G. Nasibulin, A few-layered graphene on alumina nanofibers for electrochemical energy conversion, *Carbon* 88 (2015) 157–164, <http://dx.doi.org/10.1016/j.carbon.2015.03.004>.
- [29] R. Ivanov, I. Hussainova, M. Aghayan, M. Drozdova, D. Pérez-Coll, M.A. Rodríguez, F. Rubio-Marcos, Graphene-encapsulated aluminium oxide nanofibers as a novel type of nanofillers for electroconductive ceramics, *J. Eur. Ceram. Soc.* 35 (14) (2015) 4017–4021, <http://dx.doi.org/10.1016/j.jeurceramsoc.2015.06.011>.
- [30] R. Ivanov, V. Mikli, J. Kübarsepp, I. Hussainova, Direct CVD growth of multi-layered graphene closed shells around alumina nanofibers, *Key Eng. Mater.* 674 (2016) 77–80 (10.4028).
- [31] S.N. Stamatina, I. Hussainova, R. Ivanov, P.E. Colavita, Quantifying graphitic edge exposure in graphene-based materials and its role in oxygen reduction reactions, *ACS Catal.* 6 (8) (2016) 5215–5221, <http://dx.doi.org/10.1021/acscatal.6b00945>.
- [32] M. Taleb, J. Nerut, T. Tooming, T. Thomborg, E. Lust, Oxygen electroreduction on platinum nanoparticles activated electrodes deposited onto  $\alpha$ -glucose derived carbon support in 0.1 M KOH, *J. Electrochem. Soc.* 163 (10) (2016) F1251–F1257, <http://dx.doi.org/10.1149/2.1051610jes>.
- [33] C. Neumann, S. Reichardt, P. Venezuela, M. Drögeler, L. Banzerus, M. Schmitz, K. Watanabe, T. Taniguchi, F. Mauri, B. Beschoten, Raman spectroscopy as probe of nanometre-scale strain variations in graphene, *Nat. Commun.* 6 (2015) 8429, <http://dx.doi.org/10.1038/ncomms9429>.
- [34] M. Taei, M. Shavakhi, H. Hadadzadeh, M. Movahedi, M. Rahimi, S. Habibollahi, Simultaneous determination of epinephrine, acetaminophen, and tryptophan using  $\text{Fe}_2\text{O}_3$  (0.5)/ $\text{SnO}_2$  (0.5) nanocomposite sensor, *J. Appl. Electrochem.* 45 (2) (2015) 185–195, <http://dx.doi.org/10.1007/s10800-014-0756-1>.
- [35] Q.C. Do, D.-G. Kim, S.-O. Ko, Catalytic activity enhancement of a  $\text{Fe}_3\text{O}_4/\text{SiO}_2$  yolk-shell structure for oxidative degradation of acetaminophen by decoration with copper, *J. Clean. Prod.* 172 (2018) 1243–1253, <http://dx.doi.org/10.1016/j.jclepro.2017.10.246>.
- [36] Y. Zhang, J. Fan, B. Yang, W. Huang, L. Ma, Copper-catalyzed activation of molecular oxygen for oxidative destruction of acetaminophen: the mechanism and superoxide-mediated cycling of copper species, *Chemosphere* 166 (2017) 89–95, <http://dx.doi.org/10.1016/j.chemosphere.2016.09.066>.
- [37] N. Nasirizadeh, Z. Shekari, H.R. Zare, M.R. Shishehbore, A.R. Fakhari, H. Ahmar, Electrosynthesis of an imidazole derivative and its application as a bifunctional electrocatalyst for simultaneous determination of ascorbic acid, adrenaline, acetaminophen, and tryptophan at a multi-wall carbon nanotubes modified electrode surface, *Biosens. Bioelectron.* 41 (2013) 608–614, <http://dx.doi.org/10.1016/j.bios.2012.09.028>.
- [38] J.B. Raoof, F. Chekin, R. Ojani, S. Barari, M. Anbia, S. Mandegarzad, Synthesis and characterization of ordered mesoporous carbon as electrocatalyst for simultaneous determination of epinephrine and acetaminophen, *J. Solid State Electrochem.* 16 (12) (2012) 3753–3760, <http://dx.doi.org/10.1007/s10008-012-1807-3>.
- [39] S. Bahmanzadeh, M. Noroozifar, Fabrication of modified carbon paste electrodes with Ni-doped Lewatit FO36 nano ion exchange resin for simultaneous determination of epinephrine, paracetamol and tryptophan, *J. Electroanal. Chem.* (2017), <http://dx.doi.org/10.1016/j.jelechem.2017.11.073>.
- [40] A.A. Ensafi, H. Karimi-Maleh, S. Mallakpour, Simultaneous determination of ascorbic acid, acetaminophen, and tryptophan by square wave voltammetry using *N*-(3,4-dihydroxyphenethyl)-3,5-dinitrobenzamide-modified carbon nanotubes paste electrode, *Electroanalysis* 24 (3) (2012) 666–675, <http://dx.doi.org/10.1002/elan.201100465>.
- [41] M. Taei, F. Hasanpour, M. Dinari, N. Sohrabi, M.S. Jamshidi, Synthesis of 5-[(2-hydroxynaphthalen-1-yl) diazenyl] isophthalic acid and its application to electrocatalytic oxidation and determination of adrenaline, paracetamol, and tryptophan, *Chin. Chem. Lett.* 28 (2) (2017) 240–247, <http://dx.doi.org/10.1016/j.ccllet.2016.07.025>.



## **Publication II**

**Masoud Taleb**, Roman Ivanov, Sergei Bereznev, Sayed Habib Kazemi, Irina Hussainova, Ultra-sensitive voltammetric simultaneous determination of dopamine, uric acid and ascorbic acid based on a graphene-coated alumina electrode, (2017), *Microchimica Acta*, 184 (12) 4603–4610.



# Ultra-sensitive voltammetric simultaneous determination of dopamine, uric acid and ascorbic acid based on a graphene-coated alumina electrode

Masoud Taleb<sup>1</sup> · Roman Ivanov<sup>1</sup> · Sergei Bereznev<sup>2</sup> · Sayed Habib Kazemi<sup>3</sup> · Irina Hussainova<sup>1,4,5</sup> 

Received: 17 July 2017 / Accepted: 8 September 2017 / Published online: 15 September 2017  
© Springer-Verlag GmbH Austria 2017

**Abstract** The authors describe the fabrication of an interconnected edge-exposed graphene nanostructure via chemical vapor deposition (CVD) of foliated graphene onto a network of alumina nanofibers. The fibers such obtained are shown to enable ultra-sensitive voltammetric determination of dopamine (DA), uric acid (UA) and ascorbic acid (AA). The electrode displays powerful and persistent electro oxidative behavior and excellent electron transport properties. Cyclic voltammetry and differential pulse voltammetry demonstrate excellent selectivity and sensitivity for AA, DA and UA, with typical peaks at  $-0.08$  V,  $+0.19$  V, and  $+0.34$  V (vs. SCE), respectively. Under optimum conditions, the calibration plots are linear in the  $1-80$   $\mu$ M range for DA, in the  $1-60$   $\mu$ M range for UA, and in the  $0.5-60$   $\mu$ M range for AA, with detection limits of  $0.47$   $\mu$ M,  $0.28$   $\mu$ M and  $0.59$   $\mu$ M, respectively. The sensor was successfully applied to the simultaneous determination of DA and UA in the presence of AA in spiked urine sample.

**Electronic supplementary material** The online version of this article (<https://doi.org/10.1007/s00604-017-2510-y>) contains supplementary material, which is available to authorized users.

✉ Irina Hussainova  
irina.hussainova@ttu.ee

<sup>1</sup> Department of Mechanical and Industrial Engineering, Tallinn University of Technology, Ehitajate 5, 19086 Tallinn, Estonia

<sup>2</sup> Department of Materials and Environmental Technologies, Tallinn University of Technology, Ehitajate 5, 19086 Tallinn, Estonia

<sup>3</sup> Department of Chemistry, Institute for Advanced Studies in Basic Sciences (IASBS), Zanjan 4513766731, Iran

<sup>4</sup> ITMO University, Kronverksky 49, St. Petersburg, Russian Federation 197107

<sup>5</sup> Department of Mechanical Science and Engineering, University of Illinois at Urbana-Champaign, Urbana, IL 61801, USA

**Keywords** Differential pulse voltammetry · Nano-sensor · Alumina nanofibers · Glassy carbon electrode

## Introduction

Dopamine (DA), uric acid (UA) and ascorbic acid (AA) are compounds of a great biomedical interest, which play a fundamental role in human metabolism. DA is recognized as one of the best-known neurotransmitters with wide variety of proved functions controlling central nervous, cardiovascular, renal and hormonal systems. Abnormal concentration level of DA may cause several diseases including schizophrenia and Parkinson's disease [1]. Uric acid (UA) is a physiologically important hydrophilic antioxidant and the primary end-product of purine metabolism that can be found in different concentrations in urine and human blood plasma. The abnormal concentration level of UA may indicate spreading cancer, hyperuricemia, gout, Lesch-Nyhan syndrome, rhabdomyolysis and Fanconi syndrome [2]. Ascorbic acid (AA) is another important water-soluble component that is present in many biological fluids and pharmaceuticals. AA plays a crucial role for the clinical applications for prevention and treatment of common cold, mental illness, infertility, cancer and AIDS [3]. As significant molecules for physiological processes in living systems, AA, DA and UA usually coexist in biological fluids such as human body. Therefore, selective and sensitive determination of these molecules are in great deal of attention.

A wide variety of instrumental techniques has been employed for selective determination of these compounds. Among them, there are high-performance chromatography [4], spectrophotometry [5], liquid chromatography [6], gas chromatography [7] and solid phase micro-extraction coupled

to LC-UV diode array [8]. However, most of the reported methods suffer from several drawbacks including but not limited by high price and requirement for pretreatment of samples. Moreover, just a few of them can efficiently be used for simultaneous determination of DA, UA and AA [9]. Therefore, the development of simple, cost-effective, fast, stable, and sensitive sensors for simultaneous analysis of these three analytes is still a great challenge.

In the past few decades, the electrochemical methods have been recognized as rapid, simple and selective approaches for detection of small biological molecules [10, 11]. However, selectivity and sensitivity of dopamine in the presence of other electroactive interfering species such as uric and ascorbic acids is still an issue. These small biomolecules usually oxidized at nearly the same potential with poor sensitivity at conventional electrodes. To overcome this problem, a wide variety of electrode materials, such as platinum, gold, and silver electrodes, metal alloys and metal-nanoparticles based electrodes, conducting polymers, and organic redox mediators modified electrodes were extensively studied [12]. In last decade, carbon-based nanomaterials, such as carbon nanofiber, multi-walled carbon nanotube, and graphene sheets have been considered as attractive materials in the design of novel sensors owing to their wide potential window, high electro catalytic activity, large electrochemically active surface area, and superior conductivity [13]. There are several reviews available that consider applications of graphene and graphene oxide in electroanalytical chemistry [14]. Metal oxide nanoparticles deposited onto graphene oxide sheets have received extensive attention in analytics due to their advantages of good biocompatibility, easy manufacturability, high adsorption and catalytic activity. However, despite the considerable advances in the field, much effort remains to be devoted to facilitating the practical applications of functional graphene nanocomposite and broadening the scope of their electrochemical and bio-sensing [14].

In the present study, for the first time a network of nano-scaled oxide ceramic fibers of 10 nm in diameter and several centimeters in length decorated by a few layers of highly foliated graphene, which was grown on the fibers by means of chemical vapor deposition technique (CVD) [15–17], was used for simultaneous determination of DA, UA, and AA. A novel strategy for synthesis of hybrid metal oxide – graphene nanocomposite of finely controlled architectures was developed by the authors [15–17]. Herein, the electrochemical response of the material representing graphene with a high edge density on the sidewalls of multi-layered graphene wraps around alumina nanofibers was studied towards simultaneous and sensitive analysis of three bio-analytes using cyclic voltammetry and differential pulse voltammetry methods. Furthermore, analytical performance of the sensor was successfully evaluated in human urine samples and very satisfactory result obtained for the detection of DA in the presence of UA and AA.

## Experimental

### Reagents and apparatus

All reagents and chemicals were of analytical grade and used as received without any further purification. DA, UA and AA were purchased from Sigma-Aldrich Chemie GmbH (<http://www.sigmaaldrich.com>), and all corresponding solutions were freshly prepared prior to use. The electrochemistry measurements were performed using a standard phosphate buffer of pH 7.0 which was prepared immediately prior to experiments by mixing stock solutions of  $\text{Na}_2\text{HPO}_4$ ,  $\text{NaH}_2\text{PO}_4$  and 0.1 M KCl (<http://www.sigmaaldrich.com>) as the supporting electrolyte. Millipore water (18.2  $\text{M}\Omega\cdot\text{cm}$ , Millipore water Ltd., USA, [www.millipore.com](http://www.millipore.com)) was used for preparation of aqueous solutions and throughout the whole experiments.

All the electrochemical and sensing measurements were carried out with a potentiostat/ galvanostat (Autolab PGSTAT30, <http://www.ecochemie.nl>) at a room temperature. Electrochemical cyclic voltammetry (CV), differential pulse voltammetry (DPV) and electrochemical impedance spectroscopy (EIS) were performed using a conventional three-electrode electrochemical cell, which contained a modified electrode as the working electrode with a diameter of 5 mm, a platinum counter electrode and a saturated calomel reference electrode (SCE). The cyclic voltammograms were recorded by immersing of the working electrode in phosphate buffer with volume of 30 mL. All solutions were deoxygenated by purging with high purity nitrogen gas (99.999%) for 1 min. The CVs were recorded in the potential range from  $-0.3$  to  $1.0$  V (vs. SCE). All the potentials given in this work were reported with respect to the saturated calomel reference electrode (SCE).

The morphology of the hybrid nanocomposite fibers used for electrode preparation were examined using a transmission electron microscope (HRTEM JEOL 2200-S, Japan) and a scanning electron microscope (Zeiss Ultra with an Oxford instruments EDX detector ([www.zeiss.com](http://www.zeiss.com)) equipped with an energy dispersive X-ray spectrometer.

### Preparation of graphene covered ceramic nanofibers

The graphene layers were grown on a surface of highly-aligned alumina ( $\gamma\text{-Al}_2\text{O}_3$ ) nanofibers [18] along the longitudinal axis by means of a single step catalyst-free CVD technique in a tube furnace at the temperature of  $1000$  °C. Prior the processing, a bundle of alumina nanofibers was annealed in an air atmosphere for 3 min. Thereafter, a gas flow replaced with nitrogen ( $\text{N}_2$ ) for 5 min and further the process continued in methane ( $\text{CH}_4$ ) under the flow rate of  $200\text{ cm}^3\text{ min}^{-1}$  at atmospheric pressure. Based on screening experiments and key factors such as deposition time and the total gas flow rate,

carbonization process continued for 2 h to reach the carbon weight gain of 700% [17, 19]. After the complete reaction time, the prepared specimens, further denoted as ANF-C700, were cooled down to the room temperature in a nitrogen gas flow. The ANF-C700 represents alumina nanofibers of 10 nm in diameter encapsulated by highly damaged multi-layers of foliated graphene. Thereafter, fibers modified by several carbon layers were additionally treated using a Hielscher UP400S ultrasonic processor with a power of 200 watts for 15 min before being employed as working electrodes.

### Fabrication of the sensor

Glassy carbon was chosen for a substrate because of its wide potential window with low background currents and chemical stability. Prior modification, a glassy carbon electrode (GCE) pressed into a Teflon holder of 5 mm in diameter was polished to a mirror finish using 0.05  $\mu\text{m}$  alumina slurry (Buehler) followed by thoroughly rinsing with Millipore water and treated with ultrasound for 3 min to remove adsorbed substances from the surface. Subsequently, the GCE electrode dried in a stream of nitrogen gas. An electrode modifier ink was prepared (as described in author's previous work [20]) by mixing 5 mg ANF-C700, 25  $\mu\text{L}$  isopropanol, 178  $\mu\text{L}$  Millipore water, and 5  $\mu\text{L}$  Nafion® dispersion solution (5 wt.%) under sonication for 30 min. The working electrode prepared by spin-casting of modifier ink onto the GCE and dried in room temperature (Fig. S1).

## Results and discussion

### Characterization of graphenated nanofibers

The SEM and TEM techniques were applied to study the morphology of ANF-C700 hybrid nanofibers (Fig. 1). The images clearly show the presence of foliates homogeneously distributed along the fibers, which is favorable for electron transfer processes. A single fiber diameter in an array of self-oriented alumina nanofibers (ANF) was  $10 \pm 2$  nm and a fraction of open well-aligned porosity was over 90% with an average channel size of 20 nm (Fig. S2). The Raman spectra data collected for ANF-C700 material presented a strong G and D band peak at around 1346, 1593  $\text{cm}^{-1}$  indicating formation of nanocrystalline structure of the carbon deposited onto the fibers. Additional peaks at 2685 and 2929  $\text{cm}^{-1}$  interpreted as 2D, D + D', respectively, are characteristic for multi-layered graphene (Fig. S3). X-ray photoelectron spectrum data showed 99% of carbon and 1 % of oxygen as residual mark of substrate. The C 1 s spectra interpretations indicated 69% of trigonally bonded carbon, 14% of tetrahedrally bonded carbon, 12% of C – O/C = O, and C = OOH groups and  $\pi - \pi^*$  shake-up peaks as 5% in sum. ANF-C700 XPS

analysis and comparison with lower carbon amount samples can be found in [15]. The detailed characterization of physical properties and surface morphology of the ANF-C700 material is given in the authors previous works and can be found elsewhere [15–17, 19].

### Electrochemical behavior

In authors' previous work [21], electrochemical properties and kinetics of electrons transfer of the constructed electrode was studied through the redox reaction of 5 mM  $\text{Fe}(\text{CN})_6^{3-/4-}$  in 0.1 M KCl. The results for the ANF-C700 electrode demonstrated the well-defined voltammetry waves, in which oxidation and reduction peak currents showed linear dependence on the square root of a potential scan rate indicating a semi-infinite diffusion-controlled reaction at the electrode/solution interface [22]. The electroactive surface area of the ANF-C700 sample estimated through voltammetry experiments to be 0.426  $\text{cm}^2$  that almost four fold higher than the bare GCE (0.106  $\text{cm}^2$ ) providing more electroactive sites for the analyte/electrode interaction.

To study the interface properties of the ANF-C700 and bare GCE, electrochemical impedance spectroscopy data were collected in a solution of 5 mM  $[\text{Fe}(\text{CN})_6]^{4-/3-}$  containing 0.1 M KCl (Fig. 1f). By fitting the data using the modified Randle equivalent circuit (inset of Fig. 1f), the electron transfers resistance values ( $R_{ct}$ ) obtained as 10 for ANF-C700 and 1350  $\Omega$  for bare GCE. The considerably smaller semicircle at high frequency region and linear behavior at low frequency region for ANF-C700 electrode indicated a diffusion limited process with a faster kinetic of charge-transfer compared to bare GCE. Results demonstrated that graphene flakes connected to ceramic core on ANF-C700 material, possess excellent conductivity and can accelerate electron transfers.

### Cyclic voltammetric behaviour of DA, UA and AA on the modified electrode

The CV responses of 1 mM DA, 1 mM UA, 5 mM AA and ternary mixture of the DA, UA and AA solutions are shown in Fig. 2. Dominantly, the pronounced oxidation peaks appeared at the peak potentials of  $-70$  mV, 210 mV and 320 mV for AA, DA and UA, respectively. The oxidation potential of AA is negatively shifted about 240 mV as compared to the peak potential at bare GCE due to the formation of hydrogen bonds between lactone bonds of AA and remaining carboxyl of ANF-C700. This phenomenon activates the hydroxyl in the furan nucleus of AA [23]. Such a large negative shift indicates that AA easily oxidizes at ANF-C700 also enabling determination of three (AA, DA and UA) species simultaneously, which have the close oxidation potentials (Fig. 2a). For dopamine, the redox peaks with enhanced currents were observed at the peak potentials of 130 mV and 210 mV, corresponding to the two

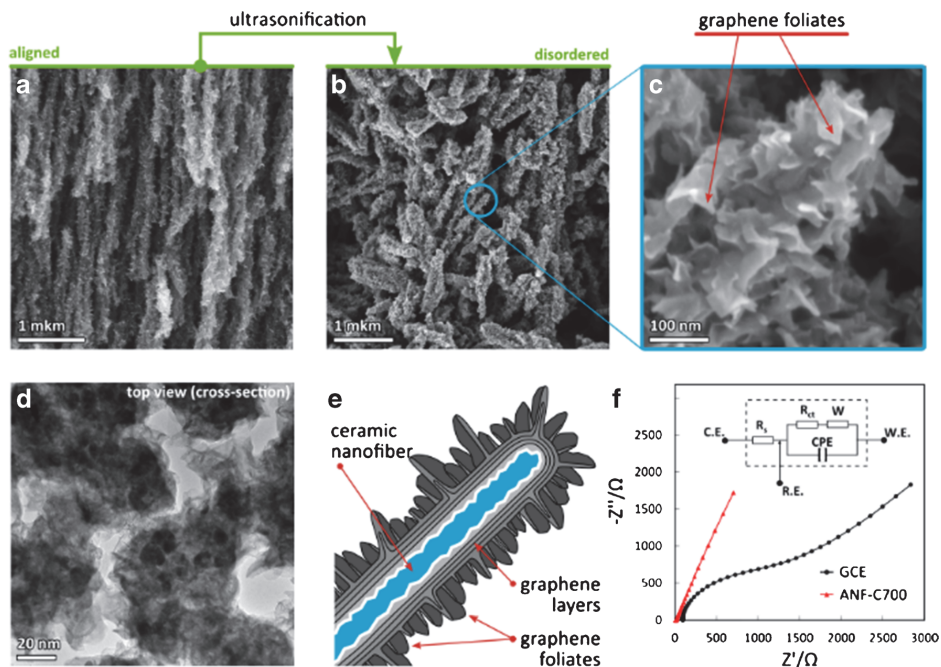


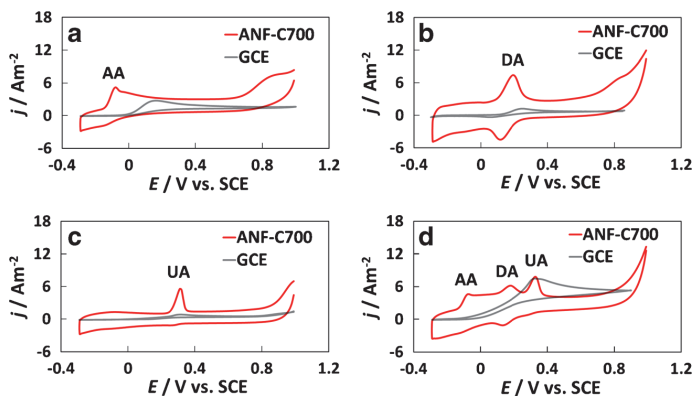
**Fig. 1** SEM images of alumina nanofibers covered by carbon ANF-C700 (a) as grown, (b) dispersed by ultrasound, (c) magnified specimens, (d) top view cross sectional TEM image, (e) scheme of a fiber, graphene

layers and foliates, (f) electrochemical impedance spectra (frequency range:  $10^5$  to 1 Hz; potential: 0.09 V. The inset represents the Randles equivalent circuit applied to fit the data)

electrons oxidation of DA to o-dopaminequinone and subsequent reduction of o-dopaminequinone to DA, respectively [24]. Separation between the oxidation and reduction peaks for dopamine is about 80 mV and the peak current is six fold higher as compared to bare GCE ( $0.12 \text{ mA cm}^{-2}$ ), suggesting an excellent electrocatalytic behavior of ANF-C700 modified electrode towards dopamine (Fig. 2b). For uric acid, the well-defined oxidation peak is found at 320 mV; however, a very weak reduction peak is observed at 280 mV. The oxidation

peak current is 6.8 times higher than the corresponding peak at bare GCE surface indicating considerable electro catalytic activity of ANF-C700 toward UA (Fig. 2c). The CV response recorded for the ternary mixture solution of AA, DA and UA is presented in Fig. 2d. Three clearly separated oxidation peaks appear at  $-80 \text{ mV}$ ,  $190 \text{ mV}$  and  $340 \text{ mV}$  for AA, DA and UA, respectively. Positions of the peaks keep unchanged with reference to the peaks recorded for individually examined analytes by voltammetry indicating the selectivity and viability of the

**Fig. 2** CV responses of (a) AA (5 mM), (b) DA (1 mM), (c) UA (1 mM), and (d) mixture of 5 mM AA, 1 mM DA, and 1 mM UA in 0.1 M phosphate buffer (pH 7.0) on ANF-C700 at  $10 \text{ mV s}^{-1}$ , respectively



modified electrode to the simultaneous detection of three components under consideration. The larger oxidation potential separations combined with the enhanced peak currents at ANF-C700 modified electrode as compared to the oxidation peaks of AA, DA and UA at the GCE surface is evidenced in Table 1. Moreover, the results of cyclic voltammetry demonstrate excellent electro catalytic activities of ANF-C700 toward the oxidation of DA in the presence of UA and AA, which originates from the unique structural features as well as electrochemical properties of ANF-C700.

### Optimization of method

In order to achieve the optimum results, the following parameters were optimized in experiments: (a) pH value of analyte; and (b) effect of the scan rate. The respective data and figures are presented in the electronic supporting material (Fig. S4). The following experimental conditions were found to provide the best results: (a) in the pH range of 5.0–9.0; use of a phosphate buffer; pH of 7.0; (b) a scan rate of  $10 \text{ mVs}^{-1}$  (the peak currents are linearly dependent on the square root of the scan rate).

### Determination of DA, UA and AA on the ANF-C700 by differential pulse voltammetry

Individual as well as simultaneous detection of AA, DA and UA on the ANF-C700 modified electrode was carried out with

the help of differential pulse voltammetry (DPV) technique in order to obtain a better peak resolution and a higher sensitivity. As discussed in section 3.3, the bare GCE shows the oxidation peaks with very low currents that originated from sluggish electron transfer kinetic of the reactions. However, DPV data on the ANF-C700 modified electrode represents a considerable catalytic activity reflected by the sharp and well-defined oxidation peaks towards both individual biomolecules and mixture of AA, DA and UA indicating that ANF-C700 surface can effectively facilitate the electron transfers involved in an oxidation processes. The oxidation peak currents linearly increases with increase in analyte concentration providing the ability to determine the individual concentrations of AA, DA, and UA, Fig. 3. In case of AA, enhancement in the peak currents originates from the oxidation of hydroxyl groups of the furan ring to carbonyl groups, Fig. 3a; in case of DA, explained by oxidation of catechol to o-quinone, Fig. 3b; and in case of UA the peak currents improved due to oxidation of bridging double bond to hydroxyl groups [25], Fig. 3c. Peak potentials of the individual species are almost constant at  $-30 \text{ mV}$ ,  $173 \text{ mV}$  and  $305 \text{ mV}$  for AA, DA and UA, respectively.

To verify feasibility of the simultaneous detection of AA, DA and UA at ANF-C700 electrode, the DPV data were collected from concurrent variables on concentrations of their ternary mixture. Three well-defined oxidation peaks at  $-30 \text{ mV}$ ,  $170 \text{ mV}$  and  $300 \text{ mV}$  are easily recognizable for AA, DA and UA, respectively. The peak currents linearly

**Table 1** Comparative analytical performance of ANF-C700 with other reported materials for simultaneous determination of AA, DA and UA

Electrode	Peak separations (mV)			Linear range ( $\mu\text{M}$ )			Detection limit ( $\mu\text{M}$ )			Refs.
	$\Delta E_1^a$	$\Delta E_2^a$	$\Delta E_3^a$	AA	DA	UA	AA	DA	UA	
GO/MWNT <sup>b</sup>	240	70	310	5-300	5-500	3-60	1	1.5	1	[2]
ERGO/GCE <sup>c</sup>	240	130	370	300-2000	0.5-60	0.5-60	300	0.5	0.5	[27]
MoS <sub>2</sub> /PEDOT/GC <sup>d</sup>	180	140	320	20-140	1-80	2-25	5.83	0.52	0.95	[28]
Pd <sub>3</sub> Pt <sub>1</sub> /PDDA-RGO/GCE <sup>e</sup>	184	116	300	40-1200	4-200	4-400	0.61	0.04	0.1	[29]
PAH-HCNTs/GCE <sup>f</sup>	245	102	347	7.5-180	2.5-105	6.7-65	0.92	0.8	1.5	[30]
[Ni(phen) <sub>2</sub> ] <sup>2+</sup> /SWCNTs/GCE <sup>g</sup>	204	152	356	30-1546	1-780	1-1407	12	1	0.76	[31]
PImox-Go <sup>h</sup>	140	60	200	75-2275	12-278	3.6-249.6	18	0.63	0.59	[32]
Au-Cys-Bt/GC <sup>i</sup>	–	–	220	1-25,000	–	1-200	0.87	–	0.93	[33]
ANF-C700	270	150	420	0.5-60	1-80	1-60	0.59	0.47	0.28	(This work)

<sup>a</sup>  $E_1$ ,  $E_2$ ,  $E_3$  are peak potential separations of AA-DA, DA-UA, AA-UA

<sup>b</sup> Graphene oxide and multi-walled carbon nanotube decorated glassy carbon electrode

<sup>c</sup> Electrochemically reduced graphene oxide

<sup>d</sup> MoS<sub>2</sub> / PEDOT nanocomposite modified GCE

<sup>e</sup> Graphene anchored with Pd-Pt Nanoparticles

<sup>f</sup> Poly allylamine hydrochloride helical carbon nanotube modified glassy carbon electrode

<sup>g</sup> glassy carbon electrode modified nickel(II)-bis(1,10-phenanthroline) complex single-walled carbon nanotubes

<sup>h</sup> Polyimidazole and graphene oxide copolymer modified glassy carbon electrode

<sup>i</sup> glassy carbon electrode modified gold nanoparticles linked bentonite via cysteine groups

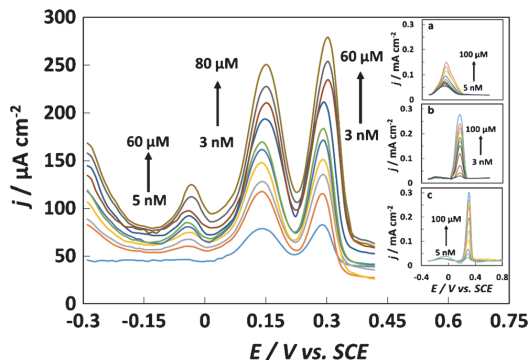


**Fig. 3** DPV profiles measured at ANF-C700 in ternary mixture of AA, DA and UA. **a**) individual determination of AA, **b**) DA and **c**) UA in phosphate buffer (pH 7.0) at a scan rate of  $10 \text{ mV s}^{-1}$  (concentrations noted in figure)

increase with concentrations of the analyte, Fig. 4. For AA, the calibration curve of current density vs analyte concentration is expressed as  $j_{AA} (\mu\text{A cm}^{-2}) = 1.99 C_{AA} + 68.10$  ( $R^2 = 0.9908$ ) in the concentration range of  $0.5\text{--}60 \mu\text{M}$ ; the limit of detection is  $0.59 \mu\text{M}$  ( $S/N = 3$ ) and sensitivity is  $5.33 \mu\text{A} \cdot \mu\text{M}^{-1} \cdot \text{cm}^{-2}$ . For DA and UA, two linear segments are depicted: (i) in the range of  $0.003\text{--}1 \mu\text{M}$  weak reproducibility is obtained for both species; however, (ii) in the dynamic range of  $1\text{--}80 \mu\text{M}$  for DA, and in the range of  $1\text{--}60 \mu\text{M}$  for UA the experimental detection limit is calculated as  $0.47$  and  $0.28 \mu\text{M}$  ( $S/N = 3$ ), respectively. This phenomenon most probably reflects the attachment of DA, UA and AA reaction residuals/products on the electrode surface [26]. Although AA and UA can be easily removed from the surface of the ANF-C700 modified electrode, the residual DA can not be washed out even after 10 cycles in water/fresh buffer resulting in non-zero signal. Corresponding regression curves of DA and UA are described as  $j_{DA} (\mu\text{A cm}^{-2}) = 1.26 C_{DA} + 151.66$  ( $R^2 = 0.9922$ ) and as  $j_{UA} (\mu\text{A cm}^{-2}) = 2.1644 C_{UA} + 154.4$

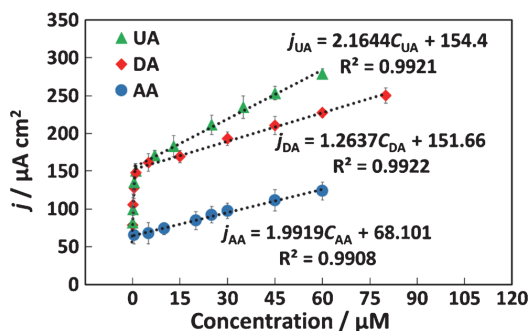


**Fig. 4** Variation of the DPV oxidation peak currents against their concentration in working voltages of  $-0.3 \text{ V}$ ,  $0.17 \text{ V}$  and  $0.3 \text{ V}$  for AA, DA and UA, respectively. Data collected from the measurements performed in a ternary mixture of AA + DA + UA (Fig. 3)

( $R^2 = 0.9921$ ) in the linear ranges of  $1\text{--}80 \mu\text{M}$  and  $1\text{--}60 \mu\text{M}$ , respectively. Sensitivity of DA and UA were calculated as  $6.58 \mu\text{A} \cdot \mu\text{M}^{-1} \cdot \text{cm}^{-2}$  and  $11.27 \mu\text{A} \cdot \mu\text{M}^{-1} \cdot \text{cm}^{-2}$ , respectively; demonstrating that very large specific surface area for the extraordinary electro catalytic activities has been engaged in analyte/electrode interactions.

Table 1 provides a comparison between several previously reported and highly sensitive sensors and the prepared electrode at the present work in terms of analytical merits for simultaneous detection of UA, DA, and AA. The ANF-C700/GCE sensor shows larger peak potential separations as compared to other sensors. Moreover, the ANF-C700 electrode possesses comparable or better limit of detection in a wide concentration range for DA, UA and AA species [2, 27, 28] due to its unique three-dimensional structure providing much larger electroactive surface area. Taking into consideration a cost effective method for fabrication of the sensor, the prepared electrode based on highly foliated graphene grown on the surface of ceramic nanofibers has obvious advantages as compared to the sensors prepared either through complicated procedure [29–31] or cost-consuming fabrication methods [29, 32, 33]. The ANF-C700 can be produced in a single step eliminating any post-processing treatment or special chemical functionalization and activation procedures. The ANF-C700 material shows an excellent electrochemical behavior such as peak-to-peak separation and high sensitivity towards AA, DA, and UA and, therefore, can be considered as an ideal candidate for development of cheap sensors to study the minute fluctuations in bio-fluids. In addition, this sensor can be employed for simultaneous determination of DA in the presence of UA and AA in clinical applications.

### Real samples analysis

In order to evaluate the practical performance for analysis of a real sample, the ANF-C700 modified electrode was applied for determination of AA, UA and DA in human urine samples.

**Table 2** Determination results of AA, DA and UA in real urine samples ( $n = 3$ )

Sample	Added ( $\mu\text{M l}^{-1}$ )	Found ( $\mu\text{M l}^{-1}$ )	RSD (%)	Recovery (%)
Urine 1	AA 30	29.3	3.61	98
	DA 20	20.9	4.51	105
	UA 10	50.7	2.65	95
Urine 2	AA 30	30.9	2.52	103
	DA 20	21.5	1.73	108
	UA 10	43.6	6.66	99
Urine 3	AA 30	31.0	1.00	104
	DA 20	19.1	4.04	96
	UA 10	60.2	6.03	102

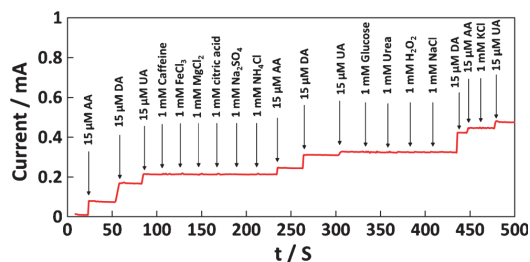


**Fig. 5** Hydrodynamic amperometric responses of ANF-C700/GCE sensor upon successive addition of 15  $\mu\text{M}$  of AA, DA, UA, and other interfering chemicals to phosphate buffer (pH 7.0) at applied potential of 0.4 V vs SCE

A fresh urine sample was prepared by the standard addition method by 50-fold dilution of urine with phosphate buffer to reduce the matrix effect of the real sample. DPV measurement was performed in an electrochemical cell containing 400  $\mu\text{L}$  of urine sample and 20 mL of phosphate buffer. Different amount of DA, UA and AA was added into the sample to evaluate the recoveries. Table 2 summarizes the collected data in which the recovery of the spiked samples ranged within 95% to 108%; indicating that the ANF-C700 modified electrode can be used effectively for the simultaneous detection of DA, UA and AA in real biological samples with satisfactory results.

### Selectivity, stability and reproducibility of ANF-C700 electrode

Selectivity of the ANF-C700/GCE sensor was evaluated in several potential interfering species such as ammonium chloride,  $\text{FeCl}_3$ ,  $\text{MgCl}_2$ , KCl, citric acid,  $\text{Na}_2\text{SO}_4$ , NaCl, Urea, Glucose, Caffeine and  $\text{H}_2\text{O}_2$ . Insignificant interferences (signal change <3%) observed in hydrodynamic amperometric ( $i-t$ ) response of AA, DA and UA (Fig. 5), suggested the sensor for potential application in clinical investigations.

To estimate the stability and reusability of the ANF-C700/GCE sensor, the CV responses of 7 mM AA in phosphate buffer (pH 7.0) were collected using the constructed electrode during ten consecutive days, reported in previous work [21]. The relative standard deviation (RSD) of the oxidation peak currents was less than 2.0% indicating the excellent stability and reproducibility of the sensor.

### Conclusions

Ceramic nanofibers encapsulated by highly foliated multi-layered graphene were used for selective and simultaneous detection of AA, DA, and UA. The GCE electrode modified by these hybrid nanostructured fibers not only detects the individual compounds but also well separates oxidation waves

of AA, DA, and UA permitting their simultaneous analysis in a single measurement. The developed sensor exhibits the superior electrocatalytic activities providing excellent selectivity and sensitivity towards ternary mixture of AA, DA, and UA. Moreover, the sensor was successfully probed in human urine samples and further was challenged with some common interfering species. In this study, no effective limitations were observed, which makes the sensor reliable to be employed for different samples. In our perception, the combination of analytical and physical features of the ANF-C700 material presents a distinct opportunity for design and fabrication of a new class of sensors to detect electroactive biomolecules with low detection limits of 0.47  $\mu\text{M}$ , 0.28  $\mu\text{M}$  and 0.59  $\mu\text{M}$  for dopamine, uric and ascorbic acids, respectively, and high sensitivity.

**Acknowledgments** This research was supported by the Estonian Research Council under the personal grant PUT1063 (I. Hussainova). The authors also acknowledge Estonian Ministry of Higher Education and Research under Projects IUT19-28 and IUT19-29, the European Union through the European Regional Development Fund, Project TK141 and ERA.NET RUS PLUS Project Flexapp (ETAG15028).

**Compliance with ethical standards** The author(s) declare that they have no competing interests.

### References

- Ma W, Liu H-T, Long Y-T (2015) Monitoring dopamine quinone-induced dopaminergic neurotoxicity using dopamine functionalized quantum dots. *ACS Appl Mater Interfaces* 7:14352–14358
- Yang YJ, Li W (2014) CTAB functionalized graphene oxide/multiwalled carbon nanotube composite modified electrode for the simultaneous determination of ascorbic acid, dopamine, uric acid and nitrite. *Biosens Bioelectron* 56:300–306
- Atta NF, El-Kady MF, Galal A (2010) Simultaneous determination of catecholamines, uric acid and ascorbic acid at physiological levels using poly (N-methylpyrrole)/Pd-nanoclusters sensor. *Anal Biochem* 400:78–88
- Pengfei J, Lufeng X, Zheng L, Ning C, Ding Z, Xin H (2012) Rapid determination of thiamine, riboflavin, niacinamide, pantothenic acid, pyridoxine, folic acid and ascorbic acid in vitamins with minerals tablets by high-performance liquid chromatography with diode array detector. *J Pharm Biomed Anal* 70:151–157
- Rasheed PA, Lee J-S (2017) Recent advances in optical detection of dopamine using nanomaterials. *Microchim Acta* 184:1239–1266
- Uutela P, Karhu L, Piepponen P, Käenmäki M, Ketola RA, Kostianen R (2009) Discovery of dopamine glucuronide in rat and mouse brain microdialysis samples using liquid chromatography tandem mass spectrometry. *Anal Chem* 81:427–434
- Zhang F, Wang D, Li X, Li Z, Chao J, Qin X (2013) Metabolomic study of the fever model induced by baker's yeast and the antipyretic effects of aspirin in rats using nuclear magnetic resonance and gas chromatography–mass spectrometry. *J Pharm Biomed Anal* 81:168–177
- Aresta A, Zamboni C (2016) Simultaneous determination of salicylic, 3-methyl salicylic, 4-methyl salicylic, acetylsalicylic and benzoic acids in fruit, vegetables and derived beverages by SPME–LC–UV/DAD. *J Pharm Biomed Anal* 121:63–68

9. Bhakta AK, Mascarenhas RJ, D'Souza OJ, Satpati AK, Detriche S, Mekhalif Z, Dalhale J (2015) Iron nanoparticles decorated multi-wall carbon nanotubes modified carbon paste electrode as an electrochemical sensor for the simultaneous determination of uric acid in the presence of ascorbic acid, dopamine and l-tyrosine. *Mater Sci Eng C* 57:328–337
10. Kazemi SH, Mohamadi R (2013) Electrochemical fabrication of a novel conducting metallopolymer nanoparticles and its electrocatalytic application. *Electrochim Acta* 109:823–827
11. Sanghavi BJ, Wolfbeis OS, Hirsch T, Swami NS (2015) Nanomaterial-based electrochemical sensing of neurological drugs and neurotransmitters. *Microchim Acta* 182:1–41
12. Zheng Y, Huang Z, Zhao C, Weng S, Zheng W, Lin X (2013) A gold electrode with a flower-like gold nanostructure for simultaneous determination of dopamine and ascorbic acid. *Microchim Acta* 180:537–544
13. Novoselov KS, Geim AK, Morozov S, Jiang D, Zhang Y, Dubonos Sa, Grigorieva I, Firsov A (2004) Electric field effect in atomically thin carbon films. *Science (New York, NY)* 306:666–669
14. Xu J, Wang Y, Hu S (2017) Nanocomposites of graphene and graphene oxides: synthesis, molecular functionalization and application in electrochemical sensors and biosensors. A review. *Microchim Acta* 184:1–44
15. Stamatina SN, Hussainova I, Ivanov R, Colavita PE (2016) Quantifying graphitic edge exposure in graphene-based materials and its role in oxygen reduction reactions. *ACS Catal* 6:5215–5221
16. Hussainova I, Ivanov R, Stamatina SN, Anoshkin IV, Skou EM, Nasibulin AG (2015) A few-layered graphene on alumina nanofibers for electrochemical energy conversion. *Carbon* 88:157–164
17. Ivanov R, Mikli V, Kübarsepp J, Hussainova I (2016) Direct CVD growth of multi-layered graphene closed shells around alumina nanofibers. *Key Eng Mater* 674:77–80
18. Aghayan M, Hussainova I, Gasik M, Kutuzov M, Friman M (2013) Coupled thermal analysis of novel alumina nanofibers with ultra-high aspect ratio. *Thermochim Acta* 574:140–144
19. Ivanov R, Hussainova I, Aghayan M, Drozdova M, Pérez Coll D, Rodríguez MA, Rubio Marcos F (2015) Graphene-encapsulated aluminium oxide nanofibers as a novel type of nanofillers for electroconductive ceramics. *J Eur Ceram Soc* 35:4017–4021
20. Taleb M, Nerut J, Tooming T, Thomberg T, Lust E (2016) Oxygen electroreduction on platinum nanoparticles activated electrodes deposited onto D-glucose derived carbon support in 0.1 M KOH. *J Electrochem Soc* 163:F1251–F1257
21. Taleb M, Ivanov R, Bereznev S, Kazemi SH, Hussainova I (2017) Graphene-ceramic hybrid nanofibers for ultrasensitive electrochemical determination of ascorbic acid. *Microchim Acta* 184:897–905
22. Shang NG, Papakonstantinou P, McMullan M, Chu M, Stamboulis A, Potenza A, Dhessi SS, Marchetto H (2008) Catalyst-free efficient growth, orientation and biosensing properties of multilayer graphene nanoflake films with sharp edge planes. *Adv Funct Mater* 18:3506–3514
23. Chang JL, Chang KH, Hu CC, Cheng WL, Zen JM (2010) Improved voltammetric peak separation and sensitivity of uric acid and ascorbic acid at nanoplatelets of graphitic oxide. *Electrochem Commun* 12:596–599
24. Łuczak T (2008) Preparation and characterization of the dopamine film electrochemically deposited on a gold template and its applications for dopamine sensing in aqueous solution. *Electrochim Acta* 53:5725–5731
25. Kaur B, Pandiyan T, Satpati B, Srivastava R (2013) Simultaneous and sensitive determination of ascorbic acid, dopamine, uric acid, and tryptophan with silver nanoparticles-decorated reduced graphene oxide modified electrode. *Colloids Surf B* 111:97–106
26. Roy PK, Ganguly A, Yang WH, Wu CT, Hwang JS, Tai Y, Chen KH, Chen LC, Chattopadhyay S (2015) Edge promoted ultrasensitive electrochemical detection of organic bio-molecules on epitaxial graphene nanowalls. *Biosens Bioelectron* 70:137–144
27. Yang L, Liu D, Huang J, You T (2014) Simultaneous determination of dopamine, ascorbic acid and uric acid at electrochemically reduced graphene oxide modified electrode. *Sens Actuators B* 193:166–172
28. Li Y, Lin H, Peng H, Qi R, Luo C (2016) A glassy carbon electrode modified with MoS<sub>2</sub> nanosheets and poly(3,4-ethylenedioxythiophene) for simultaneous electrochemical detection of ascorbic acid, dopamine and uric acid. *Microchim Acta* 183:2517–2523
29. Yan J, Liu S, Zhang Z, He G, Zhou P, Liang H, Tian L, Zhou X, Jiang H (2013) Simultaneous electrochemical detection of ascorbic acid, dopamine and uric acid based on graphene anchored with Pd–Pt nanoparticles. *Colloids Surf B* 111:392–397
30. Cui R, Wang X, Zhang G, Wang C (2012) Simultaneous determination of dopamine, ascorbic acid, and uric acid using helical carbon nanotubes modified electrode. *Sens Actuators B* 161:1139–1143
31. Yan S, Li X, Xiong Y, Wang M, Yang L, Liu X, Li X, Alshahrani LAM, Liu P, Zhang C (2016) Simultaneous determination of ascorbic acid, dopamine and uric acid using a glassy carbon electrode modified with the nickel(II)-bis(1,10-phenanthroline) complex and single-walled carbon nanotubes. *Microchim Acta* 183:1401–1408
32. Liu X, Zhang L, Wei S, Chen S, Ou X, Lu Q (2014) Overoxidized polyimidazole/graphene oxide copolymer modified electrode for the simultaneous determination of ascorbic acid, dopamine, uric acid, guanine and adenine. *Biosens Bioelectron* 57:232–238
33. Yadav DK, Gupta R, Ganesan V, Sonkar PK (2017) Individual and simultaneous voltammetric determination of ascorbic acid, uric acid and folic acid by using a glassy carbon electrode modified with gold nanoparticles linked to bentonite via cysteine groups. *Microchim Acta* 184:1951–1957

### **Publication III**

**Masoud Taleb**, Irina Hussainova, Roman Ivanov, Iwona Jasiuk, Graphenated ceramic nanofibers for highly sensitive simultaneous detection of dopamine, uric acid and ascorbic acid, (2017), *Advanced Materials Letters*, 8 (12) 1178–1183.



# Graphenated ceramic nanofibers for highly sensitive simultaneous detection of dopamine, uric acid and ascorbic acid

Masoud Taleb<sup>1</sup>, Irina Hussainova<sup>1, 2, 3\*</sup>, Roman Ivanov<sup>1</sup>, Iwona Jasiuk<sup>3</sup>

<sup>1</sup>Tallinn University of Technology, Department of Materials Engineering, Ehitajate 5, Tallinn, Estonia

<sup>2</sup>ITMO University, Kronverksky 49, St. Petersburg, Russian Federation

<sup>3</sup>University of Illinois at Urbana-Champaign, Department of Mechanical Science and Engineering, Urbana, IL 61801, USA

\*Corresponding author: Tel: (+372) 6203371; E-mail: irina.hussainova@ttu.ee

Received: 18 December 2016, Revised: 05 February 2017 and Accepted: 07 April 2017

DOI: 10.5185/amlett.2017.1557  
www.vbripress.com/aml

## Abstract

The present study reports the simultaneous determination of ascorbic acid (AA), dopamine (DA) and uric acid (UA) in 0.1 M phosphate buffer solution (pH = 7.0) using a novel electrode material prepared from oxide ceramic nanofibers by applying a single step chemical vapor deposition method. Electron-transfer kinetics at the electrode/solution interface was studied by standard redox reaction of 5 mM Fe(CN)<sub>6</sub><sup>3-/4-</sup> in 1 M KCl. Electrochemical and sensing measurements such as cyclic voltammetry and differential pulse voltammetry were performed to detect DA and UA in the presence of AA. The developed electrode was shown to separate the overlapping voltammetric responses of three analytes into the individual voltammetric peaks, totally eliminate the interference from AA, and distinguish DA from UA. Linear relationship was observed between current intensities and concentrations of all three compounds, and the limits of detection (LOD) were reached 0.57 μM, 0.77 μM and 0.84 μM for DA, UA and AA, respectively. The electrode of graphenated nanofibers displayed a very good reproducibility and stability, and was successfully tested for detection of DA, UA and AA in real urine samples. Copyright © 2017 VBRI Press.

**Keywords:** Graphene, ascorbic acid, dopamine, uric acid, voltammetry.

## Introduction

Dopamine (DA), uric acid (UA) and ascorbic acid (AA) are compounds of a great biomedical interest, which play a fundamental role in human metabolism [1]. Dopamine is one of the most important neurotransmitters that controls the function of the central nervous system, renal and the balance of hormones in a human body. Abnormal level of DA can cause several neurological diseases, including Schizophrenia, Parkinson's disease, HIV, and Alzheimer's diseases [2]. UA is another important biomolecule in a human body, which is the primary product of purine metabolism. Its abnormal level of concentration points to several possible diseases such as gout, hyperuricemia, and Lesch-Nyhan syndrome [3]. On the other hand, AA is a vital component known for its antioxidant peculiarity and its role in treatment of the common cold, mental illness, and infertility [4]. Since AA, DA, and UA are electroactive compounds and coexist in physiological fluids, development of a technique for effective, selective and simultaneous detection has recently received considerable interest. Electrochemical techniques have been widely applied due to fast detection, simplicity, reproducibility, and cost-effectiveness. However, the electrochemical oxidation

potentials of AA, DA, and UA are very close and obtained response can easily be affected by the presence of other biomolecules. In order to overcome this problem, a wide variety of materials have been tested in order to improve the electrocatalytic performance of the electrode surface to separate their oxidation potentials [5, 6]. Among studied materials, carbon nanostructures and, especially, graphene have been utilized for surface modification of the electrode due to their unique structures, outstanding charge-transfer properties and good chemical stability [7, 8]. The advanced analytical approaches require high sensitivity and selectivity combined with simplicity of sample manufacturing and its modification added by good stability and signal enhancement as compared to bare electrodes. A linear working concentration range, clear separation between oxidation peak potentials and low limit of detection are essential criteria to be met for development of a novel electrode material. As electrochemical sensors, many advanced electrode interfaces were constructed through modification of electrode surface with graphene or its composites, which can effectively decrease the overpotential and enhance the current response. It is widely documented that any surface modifications can

play a catalytic role and very small changes in surface characteristics can determine the sensitivity of measurement in electroanalytical applications. Therefore, the reliable and precisely monitored procedure for fabrication of modified electrodes is of particular importance for clinical applications.

In this work, by combining the unique electronic properties of graphene with a large surface area of self-aligned ceramic nanofibers, a highly sensitive sensor was developed for simultaneous determination of DA, UA, and AA. The nanofibers covered by highly foliated multi-layer graphene were produced with the help of a simple and well – controllable single-step chemical vapor deposition (CVD) process and electrochemically studied using cyclic voltammetry (CV) and differential pulse voltammetry (DPV) techniques. It is believed that graphitic edge planes/defects are essentially responsible for the fast electron-transfer (ET) kinetics and excellent sensing and biosensing performance [9]. At the present study, the CVD process was adjusted to get a high density of graphenic foliates to ensure fast electron-transfer kinetics and an excellent electrocatalytic activity for simultaneous determination of dopamine (DA), ascorbic acid (AA) and uric acid (UA). Furthermore, the developed electrode was successfully evaluated in human urine samples presenting good sensitivity and selectivity.

## Experimental

### Materials and reagents

All reagents and materials were of analytical grade and used as received. All the solutions were prepared using a Millipore water (18.2 M $\Omega$ .cm, Millipore water Ltd., USA). The 0.1 M phosphate buffer solution with pH 7.0 that is close to a human blood pH value was prepared by mixing 0.1 M K<sub>2</sub>HPO<sub>4</sub> and 0.1 M KH<sub>2</sub>PO<sub>4</sub> with the 0.1 M HCl as the supporting electrolyte. Potassium ferrocyanide, AA, DA and UA were purchased from Organics. The stock solutions of AA, DA and UA were freshly prepared in phosphate buffer solution at room temperature (22 ± 1 °C).

A network of the well-aligned alumina nanofibers was developed by a controlled liquid phase oxidation of aluminium melt as described in [10]. The graphenated Al<sub>2</sub>O<sub>3</sub> fibers (a single fiber diameter was of 7±2 nm) were prepared by deposition of highly foliated graphene layers onto the surface of self-aligned oxide ceramic fibers through a CVD process under methane (CH<sub>4</sub>) gas flow of 200 cm<sup>3</sup> min<sup>-1</sup> and at temperature of 1000 °C as described elsewhere [11-13]. Schematic representation of the fabrication process is shown in Fig. 1. The particularly attractive fact is that the hybrid graphene/alumina nanofibers were produced without the use of catalysts, although their growth mechanism is still not completely understood.

The weight gain after the treatment was 700 %. Thus, the material to be used for preparation of the electrode was named ANF-C700 indicating weight gain of carbon on alumina nanofibers (ANF).

The array of the graphenated fibers was crushed by mortar and additionally powdered using MLW KM1 ball milling machine and Hielscher UP200S ultrasonic processor (power 100 watts) in presence or absence of tungsten carbide (WC, particles size 370±25  $\mu$ m) powder based on optimized conditions shown in Table 1. The WC particles were used in order to elucidate a role of hard particles in a wet-milling and micro-grinding of the specimens as discussed in [14].

**Table 1.** Optimization of experiments by varying powder preparations techniques.

Sample	Mortar	Ball milling	Presence of WC	Ultrasound treatment
Sample 1	√	-	-	10 min in water
Sample 2	√	-	√	10 min in water
Sample 3	√	30 min	√	10 min in water
Sample 4	√	30 min	-	10 min in water
Sample 5	√	180 min	-	30 min in isopropanol

The obtained powders were suspended in an optimum amount of isopropanol and Nafion<sup>®</sup> dispersion solution as described in [15], agitated for 30 min in an ultrasonic bath, drop casted on a polished glassy carbon disk electrode (GCE) and dried in room temperature.

### Characterization

Electrochemical measurements, i.e. cyclic voltammetry and differential pulse voltammetry, were performed in a potentiostat/galvanostat Autolab PGSTAT30 in a standard three - electrode electrochemical cell. A GCE modified with ANF-C700, a Pt wire and a saturated calomel electrode (SCE) were used as the working, counter and reference electrodes, respectively.

The morphology and physical properties of the developed material were studied by scanning electron microscopy (SEM, Zeiss HR FESEM Ultra 55), high resolution transmission microscopy (HR-TEM, JEOL 2100F), and X-ray photoelectron spectroscopy (XPS, Omicron Multiprobe XPS system). Materials characterization performed by X-ray diffraction (XRD, Bruker) and Raman spectroscopy (Horiba's LabRam HR800) is detailed in [16].



**Fig. 1.** Schematic representation of the fabrication of GCE modified with ANF-C700

## Results and discussion

### Characterization of ANF-C700

The Raman spectra [14], SEM and TEM examination confirmed presence of several layers of highly defected graphene with graphene sheet foliates grown on sidewalls of the outer layers of graphene wraps around the longitudinal axis of the nanofiber. Mass gain of 700 % corresponds to 5 – 15 layers of graphene-like layers with lots of admixture of the graphitic flakes developing the hybrid nanostructure of closed shell of graphene multi-layers and nano-foliates with a high density of open edges. The advantages of exploitation of such kind of structure are relatively large surface area, high electrical conductivity, simple and controllable single-step method of preparation, and good stability of the structure. The graphene nano-foliates are randomly entangled and cross-linked on the surface of graphene. Representative images of the graphene-decorated fibers are given in (Fig. 2a, b and c). Fig. 1b reveals that the majority of graphene foliates have a preferentially perpendicular orientation with respect to the fiber surface.

Density of the foliates was calculated to be  $50 \pm 10$  per micron length of the fiber. An average fiber diameter after treatment was  $45 \pm 10$  nm providing a specific surface area of  $120 \text{ m}^2 \text{ g}^{-1}$  (BET).

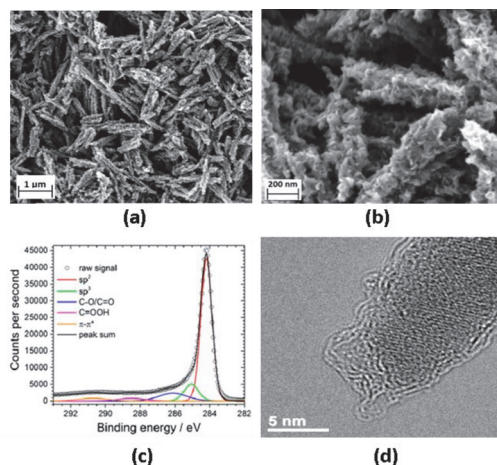


**Fig. 2.** (a), (b) SEM images of ANF-C700 sample 4; (c) XPS spectrum of ANF-C700; (d) TEM micrograph of a single fiber covered by foliated graphene.

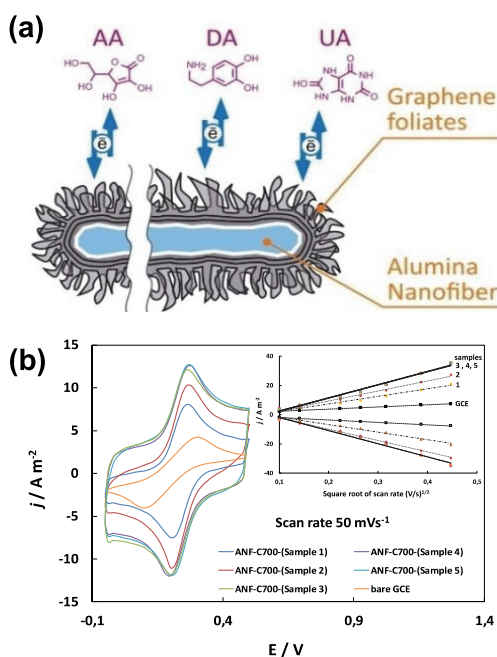
XPS analysis exhibited a low content of oxygen, thus indicating that the growth process leads to the deposition of a film with high carbon purity [16], (Fig. 2d). The  $sp^2$ -associated peak at 284.3 eV attributed to the highest contribution of trigonally bonded carbon. After the subtraction of a Shirley background followed by fit using a mixture function of Lorentzian and Gaussian, the C 1s peak can be mainly deconvoluted into five sub-peaks, which have been assigned to C-C ( $sp^2$ ), so-called “defect peak” with 0.5 eV energy shift, C-O and C=O bonds,

respectively. This demonstrates that the foliated carbon nanostructures consist of metal-free graphitic materials with some oxygen adsorbates due to physical adsorption of oxygen or vapor mainly on the edge defects at room temperature after exposure of the sample to air.

Fig. 3a schematically shows the structure of a single fiber used for the simultaneous detection of AA, DA, and UA.

### Electrochemical behavior of sample

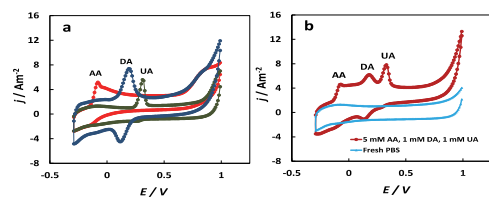
For optimization of the experiments, five distinct samples prepared from the ANF-C700 powders and the bare GC electrode, indicated in Table 1, were studied for their electrocatalytic activity in 1 M KCl + 5 mM  $\text{K}_3\text{Fe}(\text{CN})_6$  system.



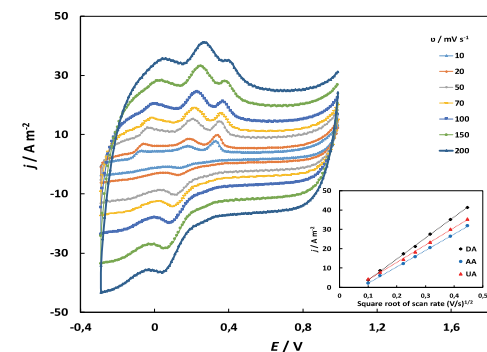
**Fig. 3.** (a) Schematic representation of the structure of the single ANF-C700 fiber; (b) CV responses of comparative voltammograms of ANF-C700 electrodes. Inset - the linear relation of the anodic and cathodic peak currents against the square root of potential scan rates in the range of 10 to 200  $\text{mV s}^{-1}$ .

Fig. 3 displays the voltammograms of differently prepared ANF-C700 modified electrodes at a scan rate of  $50 \text{ mV s}^{-1}$ . The bare GCE exhibits a wide peak with and a peak to peak separation of 210 mV representing a quasi-reversible reaction. In contrast, the ANF-C700 electrodes present significantly higher peak currents with a redox potential difference ( $\Delta E_p$ ) ranging 60–65 mV, indicating that the process under consideration is approximately reversible and reaction is diffusion controlled, similar to that observed, for example, for Ag nanoparticles [17].

According to the obtained results, the sample 4 (see Table 1) prepared by 30 min milling in water without WC, was chosen for further consideration due to its well-pronounced oxidation peak.



**Fig. 4.** CV responses of (a) individual sensing of 5 mM AA, 1 mM DA, and 1 mM UA; (b) ternary mixture of 5 mM AA, 1 mM DA, and 1 mM UA in 0.1 M phosphate buffer solution (pH 7.0) on ANF-C700 at  $10\text{mV s}^{-1}$ .



**Fig. 5.** Effect of scan rate on sensing mixture of 5 mM AA, 1 mM DA, and 1 mM UA in 0.1 M phosphate buffer solution with pH 7.0 (Inset - plots of peak current versus square root of the scan rate at 10, 20, 40, 70, 100, 150, 200  $\text{mV s}^{-1}$ )

#### Cyclic voltammetric detection of DA, UA and AA on the ANF-C700

Cyclic voltammetry technique was used to investigate the electrocatalytic activity of the developed electrode by adding AA, DA and UA ranging from  $-0.3$  to  $1\text{V}$  (vs. SCE) in  $0.1\text{M}$  pH  $7.0$  phosphate buffer solution (Fig. 4a, b). A large peak-potential separation was obtained at pH  $7.0$ . The voltammetric responses of these biomolecules show the well-defined and resolved oxidation peaks at  $-60\text{mV}$ ,  $210\text{mV}$  and  $320\text{mV}$  for AA, DA and UA, respectively. The reduction peak for AA is resolved; however, for DA a clearly separated peak is found at  $120\text{mV}$ . In case of UA, a weak reduction peak is observed at  $280\text{mV}$ . In order to demonstrate the selective and sensitive behavior of the electrode, a mixture of AA, DA and UA was tested in phosphate buffer solution by CV. The cyclic voltammograms of ternary mixture containing  $5\text{mM}$  AA,  $1\text{mM}$  DA, and  $1\text{mM}$  UA, shown in (Fig. 4b), clearly present three well-recognized anodic peaks corresponding to AA, DA and UA at  $-40\text{mV}$ ,  $200\text{mV}$  and  $340\text{mV}$ , respectively. This separation indicates that the interference between AA, DA and UA oxidation potential is eliminated by utilizing ANF-C700. The

anodic peak interval potentials were  $240\text{mV}$ ,  $140\text{mV}$  and  $380\text{mV}$  for AA-DA, DA-UA and AA-UA, respectively. Besides, a strong cathodic peak of DA was observed at  $150\text{mV}$ . The obtained results show that the synthesized ANF-C700 material exhibits an excellent selective electrocatalytic behavior for the simultaneous electro-oxidation of three bio-analytes being under consideration.

Fig. 5 displays the cyclic voltammograms of the developed sensor in presence of  $5\text{mM}$  AA,  $1\text{mM}$  DA, and  $1\text{mM}$  UA. The oxidation peak currents increase consistently with increase in a scan rate from  $10$  up to  $200\text{mV s}^{-1}$ . A linear relationship between the anodic peak current and square root of scan rate was observed for oxidation of AA, DA or UA.

The oxidation peaks current increases with the scan rate, and the oxidation peak potential is shifted positively, while the reduction peak potential shifts negatively.

The CV results show that ANF-C700 is able to determine not only AA, DA, and UA individually, but also separate them in the mixture of these biomolecules, demonstrating the negligible interfering effect from interactions among AA, DA and UA.

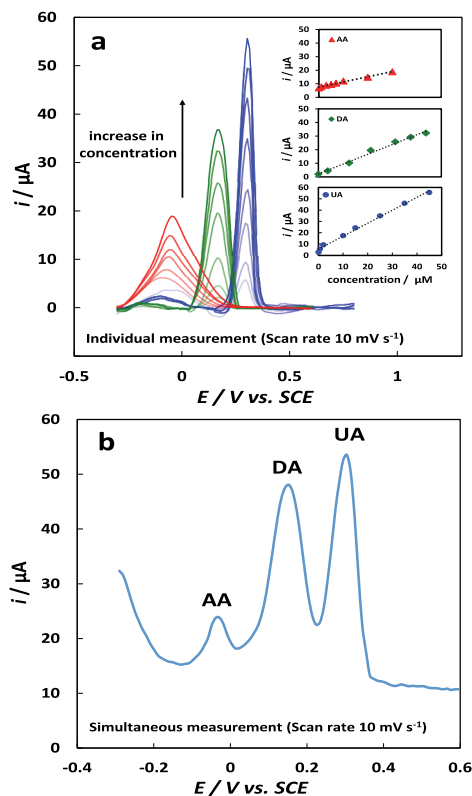


**Fig. 6.** DPV response at ANF-C700 electrode (a) individual sensing of AA, DA, and UA concentrations from  $5\text{nM}$  to  $45\mu\text{M}$ ; and (b) mixture of  $50\mu\text{M}$  AA,  $60\mu\text{M}$  DA,  $50\mu\text{M}$  UA in phosphate buffer solution (pH  $7.0$ ) at a scan rate of  $10\text{mV s}^{-1}$ .

**Table 2.** Performance of different electrodes for simultaneous determination of AA, DA and UA.

Electrode	Linear range ( $\mu\text{M}$ )			LoD ( $\mu\text{M}$ )			Reference s
	AA	DA	UA	AA	DA	UA	
Helical CNTs	7.5–180	2.5–105	6.7–65	0.92	0.8	1.5	[19]
Tryptophan-graphene	0.2–12.9	0.5–110	10–1000	10.09	0.29	1.24	[20]
SWCNH	30–400	0.2–3.8	0.06–10	5	0.06	0.02	[21]
N-doped graphene	5–1300	0.5–170	0.1–20	2.2	0.25	0.045	[22]
ANF-C700	0.005–30	0.005–45	0.005–45	0.84	0.57	0.77	This work

### Determination of DA, UA and AA on the ANF-C700 by differential pulse voltammetry

To study the sensitivity and defining linear ranges, the differential pulse voltammetry (DPV) data of the developed electrode were collected in 0.1 M pH 7.0 phosphate buffer solution in the presence of AA, DA, and UA, as shown in (Fig. 6a, b). The oxidation peaks of AA, DA and UA are clearly separated from each other confirming the results obtained by CV. The oxidation peak currents increase linearly with an increase in concentrations of bio-analytes providing the steady peak potentials at  $-28$  mV,  $183$  mV and  $314$  mV for AA, DA and UA, respectively. The linear ranges of AA, DA and UA are found as  $0.005\text{--}30$   $\mu\text{M}$ ,  $0.005\text{--}45$   $\mu\text{M}$  and  $0.005\text{--}45$   $\mu\text{M}$  and the detection limits ( $S/N = 3$ ) are  $0.84$   $\mu\text{M}$  and  $0.57$   $\mu\text{M}$ , and  $0.77$   $\mu\text{M}$ . Corresponding linear regression equations can be expressed as follows:  $I_p$  AA ( $\mu\text{A}$ ) =  $0.3814x + 7.5176$  ( $\mu\text{M}$ ) ( $R = 0.9905$ );  $I_p$  DA ( $\mu\text{A}$ ) =  $0.8798x + 2.4099$  ( $\mu\text{M}$ ) ( $R = 0.9919$ ); and  $I_p$  UA ( $\mu\text{A}$ ) =  $2.638x + 3.6626$  ( $\mu\text{M}$ ) ( $R=0.9986$ ). The DPV results for the mixture of AA, DA and UA show that the ANF-C700 is able to selectively detect each of the interfering compounds (Fig. 6a, b). Table 2 presents a comparison between current study and some other works indicating that ANF-C700 has comparable or even better analytical performance to be applied in sensor applications.

### Real samples analysis

In order to study the selectivity of the ANF-C700 electrode in the real samples, a human urine was selected as a biological object. Three urine samples were tested for detection of their AA, DA, and UA levels. The test samples were diluted 50-fold before use with pH 7.0 phosphate buffer solution to prevent the matrix effect of the authentic samples. The DPV technique was applied to ascertain the results before and after the samples were spiked with  $30$   $\mu\text{M}$  AA,  $20$   $\mu\text{M}$  DA and  $10$   $\mu\text{M}$  UA. Recovery rates of the samples were found to be between  $95.5\%$  and  $106\%$ , indicating that ANF-C700 material can be effectively utilized for the simultaneous determination of AA, DA, and UA in the real samples analysis. Anti-interference ability of the fabricated sensor, studied in previous work [18], showed very clear amperometric signal of AA, DA and UA; while addition of common interfering compounds such as ammonium chloride,  $\text{FeCl}_3$ ,  $\text{MgCl}_2$ ,  $\text{KCl}$ , citric acid,  $\text{Na}_2\text{SO}_4$ ,  $\text{NaCl}$ , Urea and  $\text{H}_2\text{O}_2$  did not affect the response (signal change  $<3\%$ ).

### Conclusions

In summary, the ceramic nanofibers were coated by highly foliated graphene deposited by a simple single – step CVD process, and employed to develop a sensor for simultaneous selection of several important bio-molecules such as AA, DA, and UA. The electrode of GCE modified with ANF-C700 was tested for its electrochemical and showed not only high sensitivity and selectivity toward individual detection of AA, DA and UA, but also successfully resolved their overlapped oxidation peaks into three well-defined peaks.

High selectivity and good antifouling ability of ANF-C700 electrode was proved by simultaneous determination of AA, DA and UA in a ternary mixture of these bio-analytes.

The excellent analytical performance and successful application of this electrode on human urine sample suggests ANF-C700 as a promising candidate applicable for highly sensitive and selective electrochemical sensors.

### Acknowledgements

This research was supported by the Estonian Research Council under the personal grant PUT1063 (I. Hussainova). The authors also acknowledge Estonian Ministry of Higher Education and Research under the Project IUT19-29 as well as Baltic-American Freedom Foundation under a research grant to I. Hussainova. The TEM examination was carried out in the Frederick Seitz Materials Research Laboratory Central Facilities, University of Illinois at Urbana-Champaign, USA.

### References

- Argüello, J., V.L. Leidsen, H.A. Magosso, R.R. Ramos, et al., *Electrochim. Acta.*, **2008**, *54*, 560.  
DOI: [10.1016/j.electacta.2008.07.021](https://doi.org/10.1016/j.electacta.2008.07.021)
- Mo, J.-W. and B. Ogorevc, *Anal. Chem.*, **2001**, *73*, 1196.  
DOI: [10.1021/ac0010882](https://doi.org/10.1021/ac0010882)
- Zou, H.L., B.L. Li, H.Q. Luo, and N.B. Li, *Anal. Biochem. B: Chemical*, **2015**, *207*, 535.  
DOI: [10.1016/j.snb.2014.10.121](https://doi.org/10.1016/j.snb.2014.10.121)
- Atta, N.F., M.F. El-Kady, and A. Galal, *Anal. Biochem.*, **2010**, *400*, 78.  
DOI: [10.1016/j.ab.2010.01.001](https://doi.org/10.1016/j.ab.2010.01.001)
- Wang, H., P. Jiang, X. Bo, and L. Guo, *Electrochim. Acta.*, **2012**, *65*, 115.  
DOI: [10.1016/j.electacta.2012.01.027](https://doi.org/10.1016/j.electacta.2012.01.027)
- Zhang, W., R. Yuan, Y.-Q. Chai, Y. Zhang, et al., *Sensors and Actuators B: Chemical*, **2012**, *166*, 601.  
DOI: [10.1016/j.snb.2012.03.018](https://doi.org/10.1016/j.snb.2012.03.018)
- McCreery, R.L., *Chemical Reviews*, **2008**, *108*, 2646.  
DOI: [10.1021/cr068076m](https://doi.org/10.1021/cr068076m)

8. Xiao, C., X. Chu, Y. Yang, X. Li, et al., *Biosens. Bioelectron.*, **2011**, *26*, 2934.  
**DOI:**[10.1016/j.bios.2010.11.041](https://doi.org/10.1016/j.bios.2010.11.041)
9. Shang, N.G., P. Papakonstantinou, M. McMullan, M. Chu, et al., *Adv. Funct. Mater.*, **2008**, *18*, 3506.  
**DOI:** [10.1002/adfm.200800951](https://doi.org/10.1002/adfm.200800951)
10. Aghayan, M., I. Hussainova, M. Gasik, M. Kutuzov, et al., *Thermochim. Acta.*, **2013**, *574*, 140.  
**DOI:** [10.1016/j.tca.2013.10.010](https://doi.org/10.1016/j.tca.2013.10.010)
11. Ivanov, R., V. Mikli, J. Kübarsepp, and I. Hussainova, *Key Engineering Materials*, **2016**, *674*, 77.  
**DOI:** [10.4028/www.scientific.net/KEM.674.77](https://doi.org/10.4028/www.scientific.net/KEM.674.77)
12. Ivanov, R., I. Hussainova, M. Aghayan, M. Drozdova, et al., *J. Eur. Ceram. Soc.*, **2015**, *35*, 4017.  
**DOI:**[10.1016/j.jeurceramsoc.2015.06.011](https://doi.org/10.1016/j.jeurceramsoc.2015.06.011)
13. Hussainova, I., R. Ivanov, S.N. Stamatina, I.V. Anoshkin, et al., *Carbon*, **2015**, *88*, 157.  
**DOI:**[10.1016/j.carbon.2015.03.004](https://doi.org/10.1016/j.carbon.2015.03.004)
14. Bang, J.H. and K.S. Suslick, *Adv. Mater.*, **2010**, *22*, 1039.  
**DOI:** [10.1002/adma.200904093](https://doi.org/10.1002/adma.200904093)
15. Taleb, M., J. Nerut, T. Tooming, T. Thomberg, et al., *J. Electrochem. Soc.*, **2016**, *163*, F1251.  
**DOI:** [10.1149/2.1051610jes](https://doi.org/10.1149/2.1051610jes)
16. Stamatina, S.N., I. Hussainova, R. Ivanov, and P.E. Colavita, *ACS Catalysis*, **2016**, *6*, 5215.  
**DOI:** [10.1021/acscatal.6b00945](https://doi.org/10.1021/acscatal.6b00945)
17. Lin, Y., L. Li, L. Hu, K. Liu, et al., *Sensors and Actuators B: Chemical*, **2014**, *202*, 527.  
**DOI:**[10.1016/j.snb.2014.05.113](https://doi.org/10.1016/j.snb.2014.05.113)
18. Taleb, M.; Ivanov, R.; Bereznev, S.; Kazemi, S. H.; Hussainova, I., *Microchimica Acta*, **2017**, *184*, 897.  
**DOI:** [10.1007/s00604-017-2085-7](https://doi.org/10.1007/s00604-017-2085-7)
19. Cui, R., X. Wang, G. Zhang, and C. Wang, *Sensors and Actuators B: Chemical*, **2012**, *161*, 1139.  
**DOI:**[10.1016/j.snb.2011.11.040](https://doi.org/10.1016/j.snb.2011.11.040)
20. Lian, Q., Z. He, Q. He, A. Luo, et al., *Anal. Chim. Acta.*, **2014**, *823*, 32.  
**DOI:**[10.1016/j.aca.2014.03.032](https://doi.org/10.1016/j.aca.2014.03.032)
21. Zhu, S., H. Li, W. Niu, and G. Xu, *Biosens. Bioelectron.*, **2009**, *25*, 940.  
**DOI:**[10.1016/j.bios.2009.08.022](https://doi.org/10.1016/j.bios.2009.08.022)
22. Sheng, Z.-H., X.-Q. Zheng, J.-Y. Xu, W.-J. Bao, et al., *Biosens. Bioelectron.*, **2012**, *34*, 125.  
**DOI:**[10.1016/j.bios.2012.01.030](https://doi.org/10.1016/j.bios.2012.01.030)

#### **Publication IV**

**Masoud Taleb**, Roman Ivanov, Sergei Bereznev, Sayed Habib Kazemi, Irina Hussainova, Graphene-ceramic hybrid nanofibers for ultrasensitive electrochemical determination of ascorbic acid, (2017), *Microchimica Acta*, 184 (3) 897–905.



# Graphene-ceramic hybrid nanofibers for ultrasensitive electrochemical determination of ascorbic acid

Masoud Taleb<sup>1</sup> · Roman Ivanov<sup>1</sup> · Sergei Bereznev<sup>2</sup> · Sayed Habib Kazemi<sup>3</sup> · Irina Hussainova<sup>1,4,5</sup> 

Received: 3 October 2016 / Accepted: 10 January 2017 / Published online: 17 January 2017  
© Springer-Verlag Wien 2017

**Abstract** The authors describe the fabrication of a 3-dimensional interconnected edge-exposed graphene nanostructure. It was fabricated by single-step chemical vapor deposition of highly foliated graphene on a network of  $\gamma$ -alumina nanofibers having a single fiber diameter of around 7 nm. It is shown that a highly sensitive electrochemical sensor can be prepared for simultaneous detection of ascorbic acid, uric acid and dopamine from such graphene-coated nanofibers possessing different but controllable density of foliates. The study concentrates on the determination of ascorbic acid in a concentration range that extends from as low as 5 nM to 1 mM. The electrochemical properties of the materials were studied by cyclic voltammetry, chronoamperometry and differential pulse voltammetry using hexacyanoferrate as a redox probe. Response is linear in the 1  $\mu$ M to 60  $\mu$ M ascorbate concentration range, the sensitivity is 1.06  $\mu$ A $\cdot\mu$ M<sup>-1</sup> $\cdot$ cm<sup>-2</sup>, and the detection limit is 117 nM at foliate density of 50 foliates  $\mu$ m<sup>-1</sup>. The sensor was successfully applied to the determination of ascorbic acid in

spiked urine samples. These results demonstrate a method for controllable growth of graphene possessing tailored morphology. In our perception, the application of such graphene-decorated nanostructures paves the way to the design of ultrasensitive electrochemical sensors of high stability.

**Keywords** Nanosensor · Cyclic voltammetry · Chronoamperometry · Differential pulse voltammetry · Ascorbic acid · Glassy carbon electrode

## Introduction

Recent success in synthesis of graphene nano sheets via various protocols and the integration of graphene with different nanomaterials, including metal oxides, provides abundant opportunities for development of sensors with enhanced performance [1]. Graphene, representing one-atom-thick sp<sup>2</sup> hybridized carbon structure, has received considerable attention in the field of electrochemical sensing, due to its extraordinary structural, electronic and chemical properties such as large specific surface area (2630 m<sup>2</sup> g<sup>-1</sup>) and excellent electrical conductivity (550 S cm<sup>-1</sup>) [1]. Graphene possesses a strong absorbance efficiency and can be relatively easy functionalized [2, 3]. Therefore, several approaches have been reported for fabrication of graphene-based electrochemical sensors including surface modification of bare electrode [1], graphene paste [4], sol-gel derived ceramic composite electrodes [5], metal nanoparticles (such as Au, Pd, and Pt) [6, 7], graphene oxide [8], conductive polymers [9], and three-dimensional (3D) structures based on assembly of graphene sheets [2]. However, most of these composites suffer from serious limitations such as high cost, long preparation time, weak mechanical stability, and low reproducibility.

**Electronic supplementary material** The online version of this article (doi:10.1007/s00604-017-2085-7) contains supplementary material, which is available to authorized users.

✉ Irina Hussainova  
irina.hussainova@ttu.ee

- <sup>1</sup> Department of Materials Engineering, Tallinn University of Technology, Ehitajate 5, Tallinn, Estonia
- <sup>2</sup> Department of Materials Science, Tallinn University of Technology, Ehitajate 5, Tallinn, Estonia
- <sup>3</sup> Department of Chemistry, Institute for Advanced Studies in Basic Sciences (IASBS), Zanjan, Iran
- <sup>4</sup> ITMO University, Kronverksky 49, St. Petersburg, Russian Federation
- <sup>5</sup> Department of Mechanical Science and Engineering, University of Illinois at Urbana-Champaign, Urbana, IL 61801, USA

To overcome above limitations, investigations for developing novel structures such as 3D graphene employed on the surface of metal oxides (i.e. nanofibers) and applicable in ultrasensitive determination of bioanalytes is still desirable [10]. Three-dimensional metal oxide/graphene interface, can not only significantly improve the catalytic activity of the sensor, but also can provide concentrated surface active sites for sensing small bio-molecules such as ascorbic acid (AA), uric acid (UA) and dopamine (DA) [11, 12]. In this study, a network of hybrid electrocatalyst consisting of alumina ( $\text{Al}_2\text{O}_3$ ) nanofibers covered by multi-layered graphene has been prepared through a cost-effective and simple single-step process of chemical vapor deposition (CVD) of carbon onto a surface under consideration.

Although the typical chemical vapor deposition (CVD) procedure involves growth of graphene over the surface of a flat metal foil, the CVD method was shown to be a powerful tool to grow complex 3D graphene structures on different substrates. Recently, a catalyst-free CVD process to deposit graphenated nanostructures of tailored morphology on a dielectric substrate of nanofibers has been developed by I. Hussainova's group [13–15]. Highly foliated graphene was formed through surface catalytic decomposition of hydrocarbon precursors on a surface of oxide ceramic. The fundamental advantage of a fuzzy graphenated fiber-foliate structure is the high surface area framework coupled with the high edge density of the graphene sheets. The current contribution further develops the method for growth of graphene sheets with controlled density and morphology over the surfaces of periodically arranged 3D nanostructures. A control of graphene nanoscopic morphology allows usage graphene-based and hybrid nanomaterials in different applications. Moreover, alumina nanoparticles have shown considerable stability at the metal oxide/graphene interface, which can provide effective electrochemical stability by improving catalytic activity [15]. In this work, a connection between morphology and possibility to use the graphene-ceramic hybrid nanofibers for electrochemical detection of AA is thoroughly studied. Ascorbic acid usually coexists with UA and DA in human blood and/or urine and their electrochemical signals can hardly be separated with the help of a conventional bare electrode because of overlapped oxidation peaks [17]. In this work, high selectivity and sensitivity of the developed electrode material was successfully demonstrated through simultaneous detection of AA, UA and DA, although detailed consideration of electrochemical response of these three components is out of scope of the present paper.

The particular attention is paid to ascorbic acid, or Vitamin C, because AA is a fundamental vitamin compound found in all life forms and one of the most prominent members of compounds known for their anti-oxidant properties. Moreover, AA is a crucially significant compound for human health influencing body treatment such as wounds healing,

bones repairing, teeth maintaining, as well as synthesis of collagen, and immunological response. Dissolved form of ascorbic acid is a positively-charged cation ( $\text{H}^+$ ) and a negatively-charged anion (ascorbate). Ascorbate anions participate in the electron-donating process by involving in adsorption and reduction at the electrode surface. Although several published reports on the use of graphene-modified electrodes for analysis of AA are available, response is subject to electrode fouling by oxidation products, and hence the electrodes require to be rebuilt to obtain reproducible result [16]. Therefore, development of electrode with high sensitivity, selectivity and stability against surface fouling represents a challenging task.

Because electrocatalytic activity of a graphene nano-flake film electrode has been shown mainly to be due to edge plane sites and their ability to serve as nano-connectors, the hybrid materials representing the alumina nanofibers encapsulated into foliated graphene wraps has been recently developed [18]. The fundamental advantage of an integrated nanofiber – graphene structures is the high surface area of a three-dimensional network of free-standing self-aligned fibers coupled with high edge density of graphene foliates.

In this work, the produced hybrid nanostructures of the lightweight ceramic and graphene sheets has been tested for detection of ascorbic acid in a phosphate buffer proving ultra-high sensitivity and impressively low detection limit. The study has also been extended by detection of some interfering compounds (DA and UA). Influence of foliates density on sensing capacity of the electrodes has been studied for the first time. Fabricated material is shown to offer cost-effectiveness and excellent chemical stability. The analytical performance of the electrode material has been successfully evaluated in human urine sample.

## Experimental

### Materials and reagents

Ascorbic acid, uric acid,  $\text{NaH}_2\text{PO}_4$  and Nafion® were acquired from Sigma-Aldrich (<http://www.sigmaldrich.com/>).  $\text{Na}_2\text{HPO}_4$  was purchased from VWR chemicals (<https://ch.vwr.com/store/>) and dopamine was obtained from Alfa Aesar ([www.alfa.com](http://www.alfa.com)). All other chemicals in this study were of analytical reagent grade from commercial sources and were used without further purification. Millipore water ( $18.2 \text{ M}\Omega\cdot\text{cm}$ , [www.millipore.com](http://www.millipore.com)) was used for the solutions. The 0.1 M phosphate buffer with pH 7.0 (close to human blood pH value) was prepared from 0.1 M  $\text{NaH}_2\text{PO}_4$ , 0.1 M  $\text{Na}_2\text{HPO}_4$  and the supporting electrolyte was 0.1 M KCl. Standard AA molar solutions were freshly prepared before each electrochemical test by dissolving the required amount of AA in 0.1 M phosphate buffer at room

temperature ( $22 \pm 1$  °C). Pure nitrogen was bubbled through the prepared solutions to eliminate the oxygen presence and improve stability of dissolved ascorbic acid.

### Preparation of ANF-C300 and ANF-C700

The network of aligned free-standing self-oriented  $\gamma$ -alumina nanofibers (ANF) with a single fiber diameter of  $7 \pm 2$  nm were employed as a highly porous substrate for carbon deposition as detailed in [13, 18]. Graphene foliates were grown along the longitudinal axis of nanofibers using a hot-wall single-step process of catalyst-free chemical vapor deposition (CVD) at a treatment temperature of 1000 °C and in methane ( $\text{CH}_4$ ) gas flowing through a CVD chamber at a rate of  $50 \text{ cm}^3 \text{ min}^{-1}$ . A process of carbonization was performed either for 60 min or 120 min resulting in the carbon weight gain of 300% and 700%, respectively. The temperature was recorded by a thermocouple, which was in contact with the sample holder, which is exposed to the same thermal treatment as the fibrous substrate. Through adjustments in growth conditions, the density of the graphitic features can vary from none to high density [14, 19]. The graphenated alumina nanofibers were subsequently cooled down to room temperature in the nitrogen ( $\text{N}_2$ ) flow of  $1000 \text{ cm}^3 \text{ min}^{-1}$ . In this study, the processed networks of hybrid fibers were designated as ANF-C300 and ANF-C700 reflecting a weight gain of the specimens. The synthesized specimens were carefully crushed in ceramic mortar and treated in water using Hielscher UP200S ultrasonic processor ([www.hielscher.com](http://www.hielscher.com)) with the power of 200 watts for 15 min.

### Apparatus and procedures

Surface morphology and structural characterization of the hybrid network of nanofibers covered by graphene was studied by scanning electron microscopy (SEM) using Zeiss HR FESEM Ultra 55 at operating voltage of 4 kV ([www.zeiss.com](http://www.zeiss.com)) and Raman spectroscopy using Horiba LabRam HR800 spectrometer (<http://www.horiba.com>). Electrochemical and sensing measurements i.e. cyclic voltammetry (CV), chronoamperometry (CA), and differential pulse voltammetry (DPV) were conducted with the help of a potentiostat/galvanostat Autolab PGSTAT30 (<http://www.ecochemie.nl>) in a standard three-electrode electrochemical cell. A Pt wire and a saturated calomel electrode (SCE) were used as the counter and reference electrodes, respectively. To prepare the working electrode, a conventional glassy carbon electrode (GCE) with a diameter of 5 mm pressed into a Teflon holder (geometrical surface area of all working electrodes  $=0.196 \text{ cm}^2$ ) was polished and dried under  $\text{N}_2$  gas flow. The dried and ground ANF-C300 / ANF-C700 specimen was subsequently suspended in a mixed solution of 20 wt% isopropanol (Sigma-Aldrich, > 99%), Millipore water

and Nafion® dispersion (to achieve 5 wt% content of Nafion® ionomer in the final layer [20]) and agitated in an ultrasonic bath for 30 min. Thereafter, 10  $\mu\text{L}$  of the homogeneous suspension was drop casted onto the clean and mirror-polished surface of GCE (Fig. 1). The thickness of the covered layer was estimated to be 30  $\mu\text{m}$ . To achieve a stable response, all working electrodes were cycled for several times from  $-0.3$  to 1 V vs. SCE prior to measurements.

## Results and discussion

### Characterization of the hybrid nanofibers

Representative SEM micrographs of the three-dimensional arrays of graphenated alumina nanofibers with perpendicular oriented foliates as well as HR-TEM image of a single foliate are shown in Fig. 2. Density of foliates per micron of nanofiber length increases from  $30 \pm 5$  to  $50 \pm 10$ , and the core diameter of the graphenated fiber increases from  $20 \pm 5$  nm to  $45 \pm 10$  nm for the ANF-C300 and ANF-C700 materials, respectively, corresponding to increase in CVD treatment time. The carbon formed on the surface of nanofibers is wrapped up around the fiber with lots of admixture of the graphitic flakes developing the nanostructure of closed shell of graphene multi-layers and nano-flakes with controlled density. Schematic representation of the complex structure with divergent graphene foliates is shown in Fig. 2f. The microscopy analysis conducted in [20] has demonstrated that, at the early stage of CVD treatment, the alumina fibers were coated by a few graphene layers rolled around the fiber. An increase in number of the graphene layers and development of protrusions (foliates) was accomplished by an increase in time of deposition. The surface area Brunauer-Emmett-Teller measurements revealed the very close values of  $125 \text{ m}^2 \text{ g}^{-1}$  and  $119 \text{ m}^2 \text{ g}^{-1}$  for ANF-C300 and ANF-C700, respectively [20]. Raman scattering spectra obtained from both ANF-C300 and ANF-C700 showed narrow and well defined G and D band peaks located at  $1350$  and  $1590 \text{ cm}^{-1}$ , suggesting the formation of a graphitized nanocrystalline structure of foliates. Intensity ratios (denoted as  $I_D / I_G$ ) were used to determine the degree of carbon graphitization (S1). XPS analysis, comprehensively discussed in [20], showed that the surface of graphenated fibers was mainly composed of carbon with a presence of oxygen in a very low concentrations in both materials. The results demonstrated a lower concentration of oxidized carbon centers in ANF-C700 as compared to ANF-C300.

### Electrochemical behavior of electrodes

The kinetic of electrons transfer at an electrode/solution interface was studied with the help of a standard redox reaction of

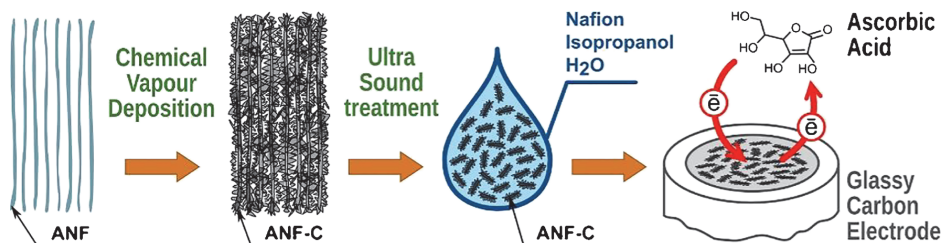
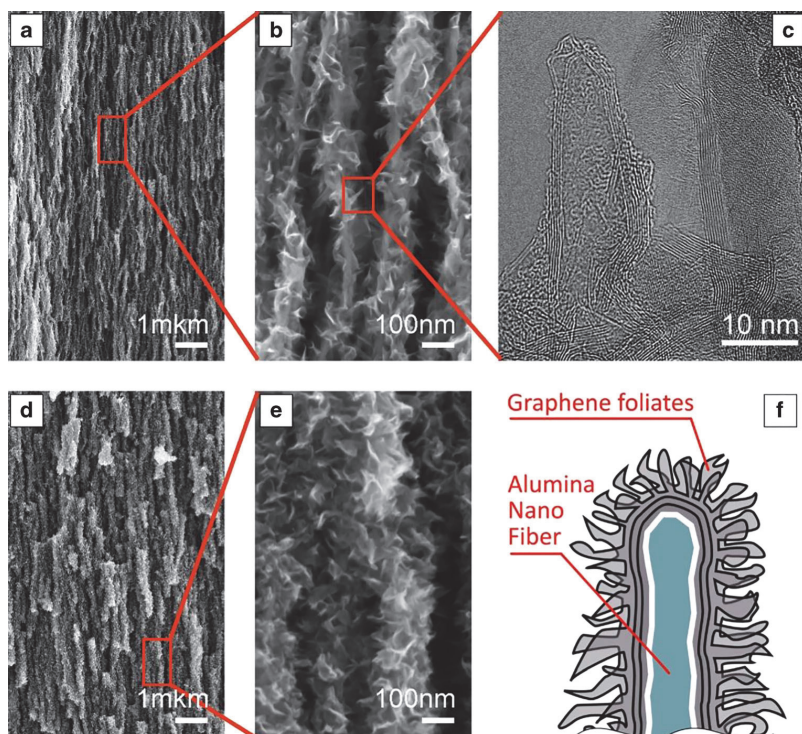


**Fig. 1** The schematic representation of the working electrode preparation

0.5 mM  $\text{Fe}(\text{CN})_6^{3-/4-}$  in 0.1 M KCl. Both ANF-C300 and ANF-C700 electrodes exhibit well-pronounced peak currents ( $I_p$ ), which increases with an increase in the scan rate from 10 to 200  $\text{mV s}^{-1}$  (Fig. S2). The separation between anodic and cathodic peak potentials ( $\Delta E_p$ ) is around 70 mV for both samples at the scan rate of 10  $\text{mV s}^{-1}$  (Fig. 3a). Peak current intensities enhance and peak potentials shift to more positive values with an increase in the scan rate; however, a linear dependency is observed between the peak currents and a square root of the potential scan rate (Fig. 3b). A set of improved reversible reactions are found for the specimens suggesting a semi-infinite diffusion-controlled reaction on the

electrode interface [21]. Redox peaks for GCE and ANF-C300 are relatively weak; but ANF-C700 exhibits redox peaks of higher intensity combined with a narrow potential difference indicating the high electron transfer rate. This observation indicates that the kinetics of electron transfer at the electrode/electrolyte interface is enhanced due to highly porous three-dimensional structure of the electrode material with a relatively high electrochemically accessible surface area. The electroactive surface areas of the ANF-C300 and ANF-C700 electrodes are calculated as 0.333 and 0.426  $\text{cm}^2$  using the Randles–Sevcik eq. (S2), respectively, indicating a higher surface area of the graphenated nanofibers as compared to

**Fig. 2** SEM and HR-TEM images of alumina nanofibers covered by carbon: (a) SEM image of the network of highly aligned fibers covered by foliated graphene, ANF-C300 sample; (b) high magnification SEM micrograph of ANF-C300; (c) HR-TEM of a graphene foliate taken from ANF-C300; (d) SEM images of the ANF-C700 sample; (e) high magnification SEM micrograph of ANF-C700; and (f) a schematic representation of the nanostructures used for electrode material



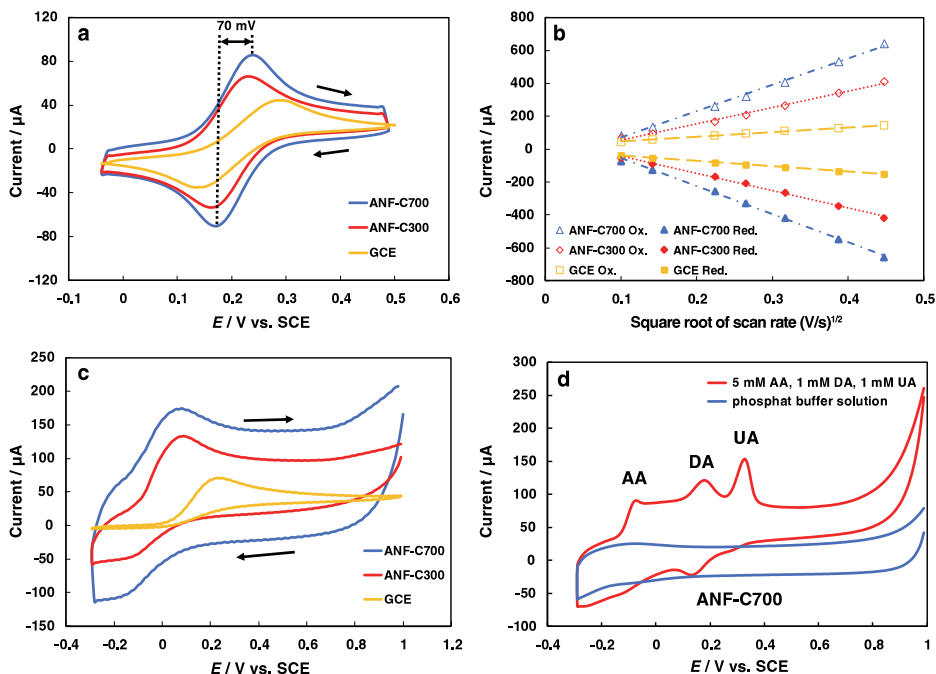


**Fig. 3** CV profiles of (a) comparative voltammograms of ANF-C300, ANF-C700 and GCE electrodes at a scan rate of  $10 \text{ mV s}^{-1}$ ; (b) the linear relation of the anodic and cathodic peak currents against the square root of potential scan rates in the range of 10 to  $200 \text{ mV s}^{-1}$ ; (c) voltammograms

for ANF-C300, ANF-C700 and GCE electrodes in  $0.1 \text{ M}$  phosphate buffer ( $\text{pH} = 7.0$ ) containing  $7 \text{ mM}$  AA at a scan rate of  $50 \text{ mV s}^{-1}$ ; and (d) CV of  $5 \text{ mM}$  AA and interfering species,  $1 \text{ mM}$  DA and  $1 \text{ mM}$  UA in  $0.1 \text{ M}$  phosphate buffer

GCE ( $0.106 \text{ cm}^2$ ). Therefore, the enhanced electrochemical activity of the graphene modified ANF electrode can originate from the active surface area of graphene foliates at the electrode surface suggesting a promising nature of ANF-C electrode for electrocatalytic oxidation of small organic molecules and electrochemical sensing.

Cyclic voltammetry responses shown in Fig. 3c demonstrates the electrocatalytic behavior of ANF-C300, ANF-C700 and GCE electrodes in phosphate buffer ( $\text{pH} = 7.0$ ) in the presence of  $7 \text{ mM}$  AA at the scan rate of  $50 \text{ mV s}^{-1}$ . In case of GCE, the oxidation peak is very broad and appeared at  $+0.24 \text{ V}$ , while the CV oxidation peaks for both ANF-C300 and ANF-C700 are observed at  $+0.07$  and  $+0.05 \text{ V}$ , respectively. Moreover, the peak current detected for GCE is of a low intensity; in contrast, the peaks demonstrated by ANF-C300 and ANF-C700 are of much higher intensities. The peak current intensity on the ANF-C700 electrode ( $174.6 \mu\text{A}$ ) is 2.5 times higher as compared to GCE due to its larger effective electroactive surface area related to a higher density of the graphene foliates. The substantial negative shift was observed for both graphenated alumina nanofibers electrodes and well-revolved current signals approved strong electrocatalytic ability of the ANF-C structures. The

results indicate that AA molecules are adsorbed onto the electroactive sites of the electrode surface and are oxidized to dehydroascorbic acid with the release of two protons and two electrons [22].

Cyclic voltammetry was employed to study the electrocatalytic oxidation of AA, DA and UA at modified electrode surfaces (Fig. 3d). Three well separated peaks at  $-70 \text{ mV}$ ,  $190 \text{ mV}$  and  $330 \text{ mV}$  were detected corresponding to the oxidation of AA, DA and UA, respectively. This finding demonstrates the potential applicability of the materials for simultaneous determination of these analytes with enhanced selectivity and sensitivity.

The kinetics of the electrode reaction were studied by examining the influence of the scan rate on oxidation peak current and potential by variations of the AA oxidation peak potential from  $-0.3$  to  $1.0 \text{ V}$  vs. SCE (Fig. S3). Based on a plot of log peak current versus log scan rate and discussion provided in supplementary data (S3), a linear relation was described for both ANF-C300 and ANF-C700 electrodes with the slopes of the lines  $0.21$  and  $0.43$ , respectively. The slope determined for AA oxidation at ANF-C700 electrode is very close to the theoretical value of  $0.5$  reported for the diffusion-controlled processes [22].

## Chronoamperometry measurements

The chronoamperometry measurements of ANF-C300 and ANF-C700 electrodes were performed to study the catalytic oxidation of AA at a potential step of 0.1 V vs. reference electrode and to estimate the diffusion coefficient of AA in a 0.1 M phosphate buffer (Fig. S4). The experimental plots of  $I$  vs.  $t^{1/2}$  were plotted and the slopes of fitted lines were determined at various AA concentrations. Based on the Cottrell equation, the diffusion coefficient of AA is estimated as  $0.79 \times 10^{-6} \text{ cm}^2 \text{ s}^{-1}$  and  $5.3 \times 10^{-6} \text{ cm}^2 \text{ s}^{-1}$  for ANF-C300 and ANF-C700, respectively.

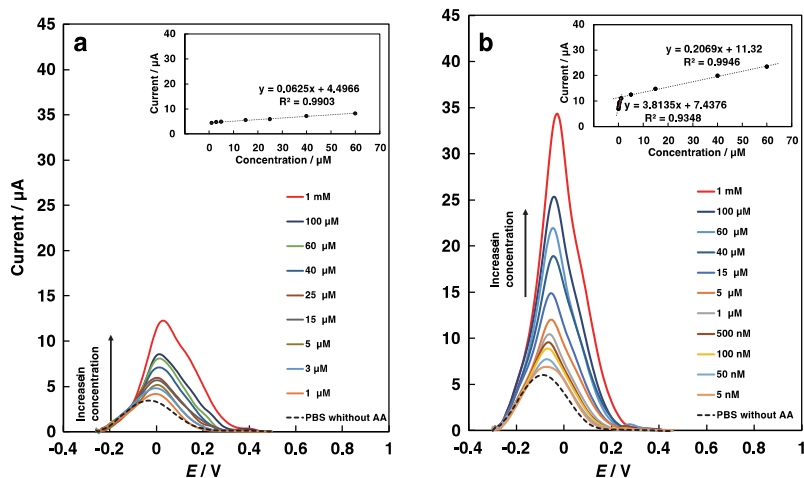
## Determination of AA at the ANF-C electrodes by differential pulse voltammetry

To analyze sensitivity and evaluate possible practical applications of the ANF-C electrodes, differential pulse voltammetry tests were carried out at various concentrations of AA in 20 mL phosphate buffer (pH = 7.0). The potential range applied was between -0.3 and 0.5 V and potential scan rate adjusted to be  $20 \text{ mV s}^{-1}$ , Fig. 4. For both graphene modified electrodes, increase in the concentration of analyte results in an increase in anodic peak current, which corresponds to the irreversible oxidation of hydroxyl groups to carbonyl groups of the furan ring in AA and is revealed by asymmetric peaks at higher concentrations. Moreover, in absence of AA, a considerable background current was found for both samples. As compared to ANF-C300, the electrode ANF-C700 demonstrates superior electrocatalytic activity in terms of sensitivity and the limit of detection (LoD) due to the structural characteristics and enhanced electrical conductivity of the graphitic foliates of ANF-C700 [23], which had no obvious effect on the AA signal detection in provided range. The LoD calculated for

both samples are given in Table 1. The ANF-C300 exhibits a weak sensitivity of  $0.30 \mu\text{A } \mu\text{M}^{-1} \text{ cm}^{-2}$  and limit of detection of 8586 nM in the range of 1–60  $\mu\text{M}$ ; however, at the same experimental condition, ANF-C700 demonstrates an enhanced sensitivity of  $1.06 \mu\text{A } \mu\text{M}^{-1} \text{ cm}^{-2}$  and LoD of 117 nM. The linear relationship between the anodic peak currents ( $I$ ) vs. ascorbic acid concentrations ( $X$ ) is shown by a calibration curve for ANF-C300 that can be approximated as  $I(\mu\text{A}) = 0.06X + 4.49$  ( $R^2 = 0.9903$ ) in the range of 1–60  $\mu\text{M}$ . Two distinct segments are obtained for ANF-C700: in the range of 0.005–1  $\mu\text{M}$ , current signals are very close to each other and deviated from linearity; however, very good linear relationship was maintained in the range of 1–60  $\mu\text{M}$ . For the ANF-C700, equations for anodic peak currents vs. AA concentration are described as  $I(\mu\text{A}) = 3.81X + 7.43$  ( $R^2 = 0.9348$ ) and  $I(\mu\text{A}) = 0.20X + 11.32$  ( $R^2 = 0.9946$ ) in ranges 0.005–1  $\mu\text{M}$  and 1–60  $\mu\text{M}$ , respectively.

Table 1 compares the analytical performance of the GCE modified ANF-C300 and ANF-C700 materials with previously reported works. The ANF-C700 exhibits either improved or comparable analytical performance as compared to similar 3D carbonic structures [10, 24–26]. The linear range of the modified electrode is wider than the range reported in [6, 10, 27]. Moreover, an excellent working stability of the electrode (Fig. S6) makes it attractive for detection of unknown concentration of AA in real biological samples. Cost-effectiveness and simplicity of preparation make the developed ANF-C700 electrode favorably compared to expensive noble metal-based sensors [2, 28, 29] or sensors required a complicated procedure for their fabrication [2, 8, 30]. The electrode of graphenated oxide nanofibers does not require any additional treatment or activation before usage and, therefore, can be considered as a promising nanomaterial to be utilized as a chemosensor.

**Fig. 4** DPV data for (a) ANF-C300; and (b) ANF-C700 measured in different AA concentrations. Respective insets depict the oxidation peak currents as a function of AA concentrations measured at a potential scan rate of  $20 \text{ mV s}^{-1}$  and in 0.1 M phosphate buffer



### Selectivity, stability and reproducibility

In order to evaluate the anti-interference ability of the GCE modified ANF-C700 material, a chronoamperometry study was performed by using interfering compounds such as uric acid, dopamine, ammonium chloride, FeCl<sub>3</sub>, MgCl<sub>2</sub>, KCl, citric acid, Na<sub>2</sub>SO<sub>4</sub>, NaCl, urea and H<sub>2</sub>O<sub>2</sub> in 0.1 M phosphate buffer (pH 7.0) with continuous stirring at the applied potential of 0.1 V. The GCE modified ANF-C700 material demonstrated clear responses towards the addition of AA, UA, and DA, while addition of ammonium chloride, FeCl<sub>3</sub>, MgCl<sub>2</sub>, KCl, citric acid, Na<sub>2</sub>SO<sub>4</sub>, NaCl, urea and H<sub>2</sub>O<sub>2</sub> did not cause any significant changes in the response with respect to various potential interferential species indicating a very good selectivity of the developed electrode (Fig. S5).

Reproducibility and stability of ANF-C700 were evaluated by determination of 7 mM AA in a 0.1 M of phosphate buffer (pH = 7.0). Five successive measurements were conducted with the same electrode during continuous period of time (Fig. S6). After each measurement, the electrode was washed by distilled water and treated with voltammetric cycles in phosphate buffer. The reproducible responses and the relative

**Table 2** Determination results of AA in real urine samples ( $n = 3$ )

Urine samples	Added concentration ( $\mu\text{M L}^{-1}$ )	Found concentration ( $\mu\text{M L}^{-1}$ )	RSD (%)	Recovery (%)
1	30	31.6	3.6	98.2
2	30	32.5	2.5	103
3	30	34.9	1.0	104

standard deviation (RSD) of 2.01% indicate that AA detection ability can be recovered even after 240 h of experiments. This result confirms excellent stability and reproducibility of the graphene-decorated alumina nanofibers, which can be successfully used for analytical determination of bio-analytes in aqueous solutions.

### Real sample analysis

In order to verify the applicability of the modified electrode in the practical use, the ANF-C700 material was further tested for the detection of AA in a three human urine samples using a

**Table 1** Comparison of an analytical performance of different electrodes for determination of ascorbic acid

Electrode	Method	Sensitivity ( $\mu\text{A } \mu\text{M}^{-1} \text{ cm}^2$ ) Linear range in $\mu\text{M}$	Limit of detection (nM)	Application	Reference
3DGH-AuNPs <sup>a</sup>	DPV	– (6–350)	28	Human serum	[2]
Au-Pd/rGO	DPV	– (0.03–9.50)	15.7	Urine sample	[6]
EGNWs <sup>b</sup>	DPV	8.74 (1.8–32)	1800	Vitamin C tablet	[10]
3D GF/CuO nanoflowers <sup>c</sup>	Amperometric	2.060 (0.43–200)	430	–	[24]
Screen-printed graphene	DPV	0.393 (4–4500)	950	Human urine	[25]
Graphene ceramic composite electrode	Amperometric	6.06 (3–84)	820	orange juice urine sample	[26]
Nanocomposite/FTO <sup>d</sup>	DPV	– (0.006–0.265)	1.05	Human Urine	[27]
MoS <sub>2</sub> /rGO hybrid nanocomposite	DPV	0.12 (12–5402)	72	Human serum	[28]
Graphene anchored with Pd–Pt Nanoparticles	DPV	0.077 (40–1200)	610	Human serum and urine	[29]
$\beta$ -CD/rGO/SPE <sup>e</sup>	DPV	– (200–2000)	67	Human serum	[30]
Alumina Nano Fibers modified by graphene foliates (ANF-C300)	DPV	0.308 (1–60)	8586	Human Urine	This work
Alumina Nano Fibers modified by graphene foliates (ANF-C700)	DPV	1.06 (1–60)	117	Human Urine	This work

rGO reduced graphene oxide

<sup>a</sup> Three-dimensional graphene hydrogel and gold nanoparticles nanocomposite

<sup>b</sup> Few-layered epitaxial graphene nano walls

<sup>c</sup> 3D graphene foams decorated by CuO nano flowers

<sup>d</sup> Patterned fluorine doped tin oxide

<sup>e</sup> Conductive  $\beta$ -cyclodextrin polymer on reduced graphene oxide modified screen-printed electrode

standard addition method. Prior to the measurements, urine samples were diluted in a 1:10 ratio with 0.1 M phosphate buffer (pH = 7.0) and used without any additional treatment. The analytical results are summarized in Table 2. The recovery rates ranged from 98% to 104% with RSD less than 3.6% shows the potential application of the synthesized electrode for analytical determination of AA in biological samples.

## Conclusions

In summary, a network of graphene-decorated oxide ceramic nanofibers with tailored graphitic edges exposure has been produced by using a single-step hot-wall catalyst-free route of chemical vapor deposition of carbon onto the surface of  $\gamma$ -alumina nanofibers and used as a sensor for detection of ascorbic acid for the first time. Well-defined oxidation peaks with low anodic potentials and high peak currents have been attributed to the excellent electronic conductivity, large electroactive area and fast heterogeneous electron transfer capability. The electrode with  $50 \pm 10$  foliates density per micron of nanofiber length (ANF-C700) has demonstrated superior electrocatalytic performance towards ascorbic acid with fairly large peak currents as compared with material of lower density of foliated (ANF-C300) or glassy carbon electrode. Electrochemical measurements revealed a high sensitivity and selectivity, comparable linear ranges, and an excellent stability for ANF-C700 electrode material in analysis of ascorbic acid in the presence of interfering species such as dopamine and uric acid. Cost-effectiveness of electrode preparation combined with excellent electrochemical characteristics makes the developed material a promising candidate for designing an electrochemical sensor for simultaneous determination of the biological molecules in different samples.

**Acknowledgements** This research was supported by the Estonian Research Council under the personal grant PUT1063 (I. Hussainova). The authors also acknowledge Estonian Ministry of Higher Education and Research under Projects IUT19-29 and IUT19-28, the European Union through the European Regional Development Fund, Project TK141 and ERA.NET RUS PLUS Project Flexapp (ETAG15028).

**Compliance with ethical standards** The authors declare that they have no competing interests.

## References

- Gan T, Hu S (2011) Electrochemical sensors based on graphene materials. *Microchim Acta* 175:1–19
- Zhu Q, Bao J, Huo D, Yang M, Hou C, Guo J, Chen M, Fa H, Luo X, Ma Y (2017) 3D graphene hydrogel – gold nanoparticles nanocomposite modified glassy carbon electrode for the simultaneous determination of ascorbic acid, dopamine and uric acid. *Sensors Actuators B Chem* 238:1316–1323
- Allen MJ, Tung VC, Kaner RB (2009) Honeycomb carbon: a review of graphene. *Chem Rev* 110:132–145
- Li F, Li J, Feng Y, Yang L, Du Z (2011) Electrochemical behavior of graphene doped carbon paste electrode and its application for sensitive determination of ascorbic acid. *Sensors Actuators B Chem* 157:110–114
- Lei C-X, Hu S-Q, Gao N, Shen G-L, Yu R-Q (2004) An amperometric hydrogen peroxide biosensor based on immobilizing horseradish peroxidase to a nano-Au monolayer supported by sol-gel derived carbon ceramic electrode. *Bioelectrochemistry* 65:33–39
- Tadayon F, Vahed S, Bagheri H (2016) Au-Pd/reduced graphene oxide composite as a new sensing layer for electrochemical determination of ascorbic acid, acetaminophen and tyrosine. *Mater Sci Eng C* 68:805–813
- Mei LP, Feng JJ, Wu L, Chen JR, Shen L, Xie Y, Wang AJ (2016) A glassy carbon electrode modified with porous Cu<sub>2</sub>O nanospheres on reduced graphene oxide support for simultaneous sensing of uric acid and dopamine with high selectivity over ascorbic acid. *Microchim Acta* 183:2039–2046
- Wu F, Huang T, Hu Y, Yang X, Ouyang Y, Xie Q (2016) Differential pulse voltammetric simultaneous determination of ascorbic acid, dopamine and uric acid on a glassy carbon electrode modified with electroreduced graphene oxide and imidazolium groups. *Microchim Acta* 183:2539–2546
- Kazemi SH, Mohamadi R (2013) Electrochemical fabrication of a novel conducting metallopolymer nanoparticles and its electrocatalytic application. *Electrochim Acta* 109:823–827
- Kumar Roy P, Ganguly A, Yang W-H, Wu C-T, Hwang J-S, Tai Y, Chen K-H, Chen L-C, Chattopadhyay S (2015) Edge promoted ultrasensitive electrochemical detection of organic bio-molecules on epitaxial graphene nanowalls. *Biosens Bioelectron* 70:137–144
- Li J, Xie J, Gao L, Li CM (2015) Au nanoparticles–3D graphene hydrogel nanocomposite to boost synergistically in situ detection sensitivity toward cell-released nitric oxide. *ACS Appl Mater Interfaces* 7:2726–2734
- Xu J, Wang Y, Hu S (2017) Nanocomposites of graphene and graphene oxides: synthesis, molecular functionalization and application in electrochemical sensors and biosensors. A review. *Microchim Acta* 184:1–44
- Aghayan M, Hussainova I, Gasik M, Kutuzov M, Friman M (2013) Coupled thermal analysis of novel alumina nanofibers with ultra-high aspect ratio. *Thermochim Acta* 574:140–144
- Ivanov R, Mikli V, Kübarsepp J, Hussainova I (2016) Direct CVD growth of multi-layered graphene closed shells around alumina nanofibers. *Key engineering materials*. Trans Tech Publ 674:77–80
- Ivanov R, Hussainova I, Aghayan M, Drozdova M, Pérez Coll D, Rodríguez MA, Rubio Marcos F (2015) Graphene-encapsulated aluminium oxide nanofibers as a novel type of nanofillers for electroconductive ceramics. *J Eur Ceram Soc* 35:4017–4021
- Marinčić L, Soeldner JS, Colton CK, Giner J, Morris S (1979) Electrochemical glucose oxidation on a platinumized platinum electrode in Krebs ringer solution. *J Electrochem Soc* 126:43–49
- Cai W, Lai T, Du H, Ye J (2014) Electrochemical determination of ascorbic acid, dopamine and uric acid based on an exfoliated graphite paper electrode: a high performance flexible sensor. *Sensors Actuators B Chem* 193:492–500
- Hussainova I, Ivanov R, Stamatina SN, Anoshkin IV, Skou EM, Nasibulin AG (2015) A few-layered graphene on alumina nanofibers for electrochemical energy conversion. *Carbon* 88:157–164
- Stamatina SN, Hussainova I, Ivanov R, Colavita PE (2016) Quantifying graphitic edge exposure in graphene-based materials and its role in oxygen reduction reactions. *ACS Catal* 6:5215–5221
- Taleb M, Nerut J, Tooming T, Thomberg T, Lust E (2016) Oxygen electroreduction on platinum nanoparticles activated electrodes deposited onto D-glucose derived carbon support in 0.1 M KOH. *J Electrochem Soc* 163:F1251–F1257

21. Shang NG, Papakonstantinou P, McMullan M, Chu M, Stamboulis A, Potenza A, Dhessi SS, Marchetto H (2008) Catalyst-free efficient growth, orientation and biosensing properties of multilayer graphene nanoflake films with sharp edge planes. *Adv Funct Mater* 18:3506–3514
22. Bard AJ, Faulkner LR (2001) *Fundamentals and applications: electrochemical methods*, 2nd edn. Wiley, New York
23. Luo R, Zhang W, Cheng W, Zhao D, Li Y, Lin X, Dong F, Ding S (2013) A novel electrochemical immunosensor for detection of angiotensinII at a glass carbon electrode modified by carbon nanotubes/chitosan film. *Int J Electrochem Sci* 8:3186–3196
24. Ma Y, Zhao M, Cai B, Wang W, Ye Z, Huang J (2014) 3D graphene foams decorated by CuO nanoflowers for ultrasensitive ascorbic acid detection. *Biosens Bioelectron* 59:384–388
25. Ping J, Wu J, Wang Y, Ying Y (2012) Simultaneous determination of ascorbic acid, dopamine and uric acid using high-performance screen-printed graphene electrode. *Biosens Bioelectron* 34:70–76
26. Mohammad-Rezaei R, Razmi H, Jabbari M (2014) Graphene ceramic composite as a new kind of surface-renewable electrode: application to the electroanalysis of ascorbic acid. *Microchim Acta* 181:1879–1885
27. Puangjan A, Chaayasith S, Wichitpanya S, Daengduang S, Puttota S (2016) Electrochemical sensor based on PANI/MnO<sub>2</sub>-Sb<sub>2</sub>O<sub>3</sub> nanocomposite for selective simultaneous voltammetric determination of ascorbic acid and acetylsalicylic acid. *J Electroanal Chem* 782:192–201
28. Xing L, Ma Z (2016) A glassy carbon electrode modified with a nanocomposite consisting of MoS<sub>2</sub> and reduced graphene oxide for electrochemical simultaneous determination of ascorbic acid, dopamine, and uric acid. *Microchim Acta* 183:257–263
29. Yan J, Liu S, Zhang Z, He G, Zhou P, Liang H, Tian L, Zhou X, Jiang H (2013) Simultaneous electrochemical detection of ascorbic acid, dopamine and uric acid based on graphene anchored with Pd–Pt nanoparticles. *Colloids Surf B: Biointerfaces* 111:392–397
30. Qin Q, Bai X, Hua Z (2016) Electropolymerization of a conductive  $\beta$ -cyclodextrin polymer on reduced graphene oxide modified screen-printed electrode for simultaneous determination of ascorbic acid, dopamine and uric acid. *J Electroanal Chem* 782:50–58

# Curriculum vitae

## Personal data

Name: Masoud Taleb  
Date of birth: 19.09.1985  
Place of birth: Zanjan, Iran  
Citizenship: Iranian

## Contact data

E-mail: masoud.taleb@taltech.ee  
Phone: +372 58249601

## Education

2014–2018 Tallinn University of Technology—PhD  
2012–2014 Tallinn University of Technology—MSC  
2004–2008 Tehran University—BSC  
2000–2004 High school

## Language competence

English: Fluent  
Estonian: Elementary  
German: Intermediate  
Persian: Mother Tongue  
Turkish: Mother Tongue

## Professional employment

2014–2018 Researcher in Tallinn University of Technology  
2012–2014 Member of PEMFC research group in Tartu University, Estonia  
2011–2012 Technical supervisor at Asia Mining Development Executives  
(maintenance, repair and stock replenishment unit)

# Elulookirjeldus

## Isikuandmed

Nimi: Masoud Taleb  
Sünniaeg: 19.09.1985  
Sünnikoht: Zanjan, Iran  
Kodakondsus: Iraani

## Kontaktandmed

E-post: masoud.taleb@taltech.ee  
Telefon: +372 58249601

## Hariduskäik

2014–2018 Tallinna Tehnikaülikool—PhD  
2012–2014 Tallinna Tehnikaülikool—MSC  
2004–2008 Teherani Ülikool—BSC  
2000–2004 Keskkharidus

## Keelteoskus

English: Kõrgtase  
Estonian: Kõrgtase  
German: Keskmine  
Persian: Emakeel  
Turkish: Emakeel

## Teenistuskäik

2014–2018 Tallinna Tehnikaülikooli teadur  
2012–2014 Tartu Ülikooli PEMFC uurimisgrupi liige  
2011–2012 Aasia Mäetööstuse Arendusjuhid (hooldus-, remondi- ja varude täiendamise üksus), tehniline juhendaja